

# For Reference

---

NOT TO BE TAKEN FROM THIS ROOM

# For Reference

NOT TO BE TAKEN FROM THIS ROOM

Ex LIBRIS  
UNIVERSITATIS  
ALBERTAEISIS







THE UNIVERSITY OF ALBERTA

Mass Spectrometric Investigation of Gas Phase  
Hydration Equilibria  
Involving

- (a) Hydration of the Halide Negative Ions
- (b) Hydration of the Hydroxide, Nitrogen  
Dioxide and Oxygen Negative Ions
- (c) Hydration of the Proton

by



Mohammed Reza Arshadi

A THESIS

SUBMITTED TO THE FACULTY OF GRADUATE STUDIES  
IN PARTIAL FULFILMENT OF THE REQUIREMENTS FOR THE DEGREE  
OF DOCTOR OF PHILOSOPHY

Department of Chemistry

Edmonton, Alberta

Fall, 1969



UNIVERSITY OF ALBERTA

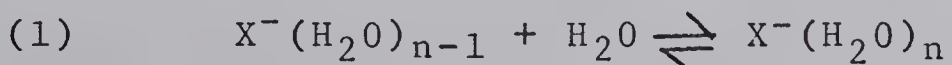
FACULTY OF GRADUATE STUDIES

The undersigned certify that they have read, and  
recommend to the Faculty of Graduate Studies for acceptance,  
a thesis entitled MASS SPECTROMETRIC INVESTIGATION OF THE  
GAS PHASE HYDRATION EQUILIBRIA (a) Hydration of the Halide  
Negative Ions, (b) Hydration of the Hydroxide, Nitrogen  
Dioxide and Oxygen Negative Ions, (c) Hydration of the Proton  
submitted by Mohammed Reza Arshadi in partial fulfilment  
of the requirements for the degree of Doctor of Philosophy.



ABSTRACT

The gas phase hydration of the halide negative ions was studied by means of a specially designed mass spectrometer which is capable of operating at an ion source pressure as high as 10 torr. By the determination of the equilibrium constants for the general reaction (1)



at various temperatures the thermodynamic values of  $\Delta H^\circ_{n-1,n}$ ,  $\Delta G^\circ_{n-1,n}$  and  $\Delta S^\circ_{n-1,n}$  were determined. The values of n, the number of water molecules around the negative ion, ranged from 1 to 5 for  $F^-$ ; 1 to 4 for  $Cl^-$  and  $Br^-$ ; and 1 to 3 for  $I^-$ . In addition to the halide negative ions, the gas phase hydration of  $O_2^-$ ,  $OD^-$  and  $NO_2^-$  was also studied. The  $\Delta H^\circ_{n-1,n}$ ,  $\Delta G^\circ_{n-1,n}$ ,  $\Delta S^\circ_{n-1,n}$  were determined for  $OD^-$  with n=1 to n=5 and for  $O_2^-$  with n=1 to n=3. However, the study of the  $NO_2^-(H_2O)_n$  was carried out at only one temperature (292°K), therefore, only  $\Delta G^\circ_{n-1,n,292}$  with n from 2 to 4 could be calculated.

A theoretical calculation of the potential energies of cluster  $X^-(H_2O)_n$  is presented. This calculation was based on the various electrostatic energies involved between the central ion and the ligand molecules as well as those among the ligand molecules. A qualitative agreement was observed between the potential energies  $\Delta E_{n-1,n}$



calculated and  $\Delta H_{n-1, n}^\circ$  obtained experimentally. The entropy values,  $\Delta S_{0,1}$  for reaction (1) were calculated theoretically and are compared with the experimental values.

From the results of this work and the study of the gas phase hydration energies carried out by other workers in this laboratory, a comparison is made between the hydration of the positive and negative ions. Our studies indicate that the initial hydration steps are more favorable for positive ions. However, as more water molecules are added to the clusters, negative ion hydration becomes more favorable. The trend in our data supports the single ion hydration energies obtained from the Randles free energies of hydration.



ACKNOWLEDGEMENTS

Sincere appreciation and gratitude is due Dr. P. Kebarle for his kind guidance and advice. The co-operation of Dr. J. Scarborough who worked jointly with the author in the study of the gas phase hydration of proton is also acknowledged.

I wish to thank Dr. R. Yamdagni for programming the theoretical calculations, Mr. William Paisley for his technical assistance during the study of  $I^-$  hydration and other members of the mass spectrometry group for their valuable suggestions during the course of this study.

The encouragement and understanding of my wife, Mehri, is sincerely appreciated. Her care in typing the manuscript was invaluable.

I am grateful for the financial assistance rendered by the University of Alberta during the academic year and support by the Canadian National Research Council during the summer months.



TABLE OF CONTENTS

	<u>Page</u>
Abstract . . . . .	i
Acknowledgements . . . . .	iii
List of Figures . . . . .	viii
List of Tables . . . . .	xi
1. <u>INTRODUCTION</u>	
1.1 Scope of Present Study . . . . .	1
1.2 Production of Negative Ions . . . . .	2
A. Electron Capture . . . . .	2
B. Pair Production . . . . .	4
1.3 A Survey of the Previous Work . . . . .	6
A. Hydration of Protons . . . . .	8
B. $O_2^+ n$ Clusters . . . . .	9
C. $N_4^+$ Clusters . . . . .	10
D. $N_2O_2^+$ System . . . . .	11
E. $O_4^-$ System . . . . .	11
F. Gas Phase Hydration of Alkali Ions . .	12
G. $NH_4^+ (NH_3)_n$ . . . . .	12
1.4 Purpose of the $X^-(H_2O)_n$ Study . . . . .	13
1.5 Application of Mass Spectrometric Study of Ion Clusters . . . . .	13
2. <u>EXPERIMENTAL</u>	
2.1 General Description . . . . .	17



	<u>Page</u>
2.2 Alpha Source Mass Spectrometer . . . . .	18
2.3 Electron Beam Mass Spectrometer . . . . .	22
2.4 Gas Handling Plant . . . . .	22
2.5 Electron Gun . . . . .	26
2.6 Ion Source . . . . .	29
2.7 Ion Accelerating Tower . . . . .	33
2.8 Mass Analysis and Ion Current Detection . .	36
2.9 Vacuum Chamber . . . . .	37
2.10 Experimental Procedure . . . . .	41
 <b>3. PRODUCTION OF IONS AND SAMPLING</b>	
3.1 Production of Halide Negative Ions . . . . .	45
3.1a Production of $I^-$ . . . . .	47
3.1b Production of $Br^-$ . . . . .	48
3.1c Production of $Cl^-$ . . . . .	48
3.1d Production of $F^-$ and $OD^-$ . . . . .	49
3.2 Production of $O_2^-$ and $NO_2^-$ . . . . .	52
3.3 Ion Sampling . . . . .	54
3.3a Equilibrium Condition in the Ion Source	54
3.3b Relation of the Ion Current to the Ion Concentration . . . . .	57
(i) Discrimination in Transport through the Ion Source . . . . .	57
(ii) Discrimination in Passage through Exit Slit . . . . .	57



(iii) Discrimination due to Stripping	
Outside of Ion Source . . . . .	58
(iv) Discrimination in Mass Analyzer	
Tube . . . . . . . . . . . . . . .	58
(v) Discrimination in the Ion Current	
Detection System . . . . . . . . .	59

#### 4. RESULTS AND DISCUSSION OF HYDRATION OF HALIDE

##### NEGATIVE IONS, X<sup>-</sup>

4.1 Introduction and Thermodynamic Relations .	61
4.2 Presentation of the Results and General	
Discussion . . . . . . . . . . . . . . .	62
4.3 Calculation of Electrostatic Potential	
Energy of the Negative Ion Cluster . . . .	79
4.4 Comparison of Calculated and Experimental	
Hydration Energies . . . . . . . . . . .	97
4.5 Calculation of the Entropy Change $\Delta S_{0,1}^\circ$ .	109
4.6 Gas Phase Solvation of OH <sup>-</sup> by Hydrogen	
Halides . . . . . . . . . . . . . . . . .	121
4.7 Ion-Molecule Reactions Involved in the	
Production of Negative Ions, X <sup>-</sup> . . . .	122
4.8 Equilibrium Distribution of X <sup>-</sup> (H <sub>2</sub> O) <sub>n</sub> .	126
4.9 Comparison of Gas Phase Hydration Energies	
for Positive and Negative Ions . . . . .	126



<u>Table</u>		<u>Page</u>
5-2	Thermodynamic Values for the Gas Phase Hydrat-	
	tion of $OD^-$ . . . . .	145
5-3	Thermodynamic Values for the Gas Phase Hydrat-	
	tion of $O_2^-$ . . . . .	153
5-4	Relative Abundances of $O_2^-(H_2O)_n$ . . . . .	154
6-1	Thermodynamic Values for the Gas Phase Solva-	
	tion of Proton . . . . .	165



LIST OF FIGURES

<u>Figure</u>		<u>Page</u>
2-1	Ion Source of Alpha Source Mass Spectrometer	19
2-2	Main Component of the Electron Beam . . . . .	23
2-3	Gas Handling Plant . . . . . . . . . . . . . .	24
2-4	Electron Gun . . . . . . . . . . . . . . . . .	27
2-5	Ion Source . . . . . . . . . . . . . . . . .	30
2-6	Ion Accelerating Tower . . . . . . . . . . .	34
2-7	Counts/Second Versus SEM Voltage . . . . .	38
2-8	Main Vacuum Chamber . . . . . . . . . . .	39
4-1 to 4-16	Log $K_{n-1,n}$ for the Gas Phase Hydration of Halide Negative Ions, at Various Temperatures, Versus Pressure of $H_2O$ . . . . .	63 to 78
4-17 to 4-20	Van't Hoff-Type Plots of the Equilibrium Constants, $K_{n-1,n}$ , for Gas Phase Hydration of Halide Negative Ions . . . . .	84 to 87
4-21	Relative Distribution of Hydrates $X^-(H_2O)$ at 1 torr Water Pressure and $292^\circ K$ . . . . .	88
4-22	$H_2O$ "Point Charge" Model Used in Theoretical Calculation . . . . .	90
4-23	Square Root of Repulsion Coefficient "A" for Noble Gases Versus Atomic Radii . . . . .	96







<u>Figure</u>	<u>Page</u>
5-7 Van't Hoff-Type Plots of $K_{n-1,n}$ for the Gas Phase Hydration of $OD^-$ . . . . .	144
5-8 Plots of $\log K_{n-1,n}$ for the Gas Phase Hydratation of $O_2^-$ , at Various Temperatures, Versus Pressure of $H_2O$ . . . . .	150 to 151
5-12 Van't Hoff-Type Plots of $K_{n-1,n}$ for the Gas Phase Hydration of $O_2^-$ . . . . .	152
6-1 Plots of $\log K_{n-1,n}$ for the Gas Phase Solvation of Proton, at Various Temperatures Versus Pressure of $H_2O$ . . . . .	158 to 162
6-6 Van't Hoff Plots of Equilibrium Constants for the Gas Phase Hydration of Proton . . .	164
6-7 Relative Concentrations of Clusters $H^+(H_2O)_n$ Versus Pressure . . . . .	166
6-8 Plots of $\log \Delta H_{n-1,n}^\circ$ Versus $n-1,n$ for the Gas Phase Solvation of Proton . . . . .	168



## LIST OF TABLES

<u>Table</u>	<u>Page</u>
2-1 Ion Accelerating Tower Potentials . . . . .	35
3-1 A typical Spectrum of $F^-(D_2O)_n$ . . . . .	51
4-1 Thermodynamic Values for the Gas Phase Hydratation of the Halide Negative Ions . . . . .	80
4-4 . . . . .	83
4-5 Coefficient "A" for Repulsion Term $(A/R^{12})$ between two atoms of the Noble Gases . . . . .	95
4-6 Comparison of Calculated and Experimental Values of Change of Energies for Cluster $X^-(H_2O)_n$ with $n$ . . . . .	98
4-7 Change of Absolute Values of $(\Delta E_{0,1})_{\text{sym}}$ with 5% change in ionic radii . . . . .	108
4-8 Moments of Inertia and $X^--OH_2$ Equilibrium Distance . . . . .	112
4-9 Force Constants, Vibrational Frequencies for $X^-(H_2O)$ . . . . .	118
4-10 Theoretical and Experimental Entropy Change $\Delta S_{0,1}$ . . . . .	119
4-11 Enthalpy Change for Reaction $OH^- + HX = OH^-(HX)$	123
4-12 Total Hydration Energies of Halide and Alkali Metals Ions . . . . .	130
5-1 Equilibrium Constants and Corresponding $\Delta G_{n-1,n}^\circ$ for $NO_2^-(H_2O)_n$ . . . . .	137



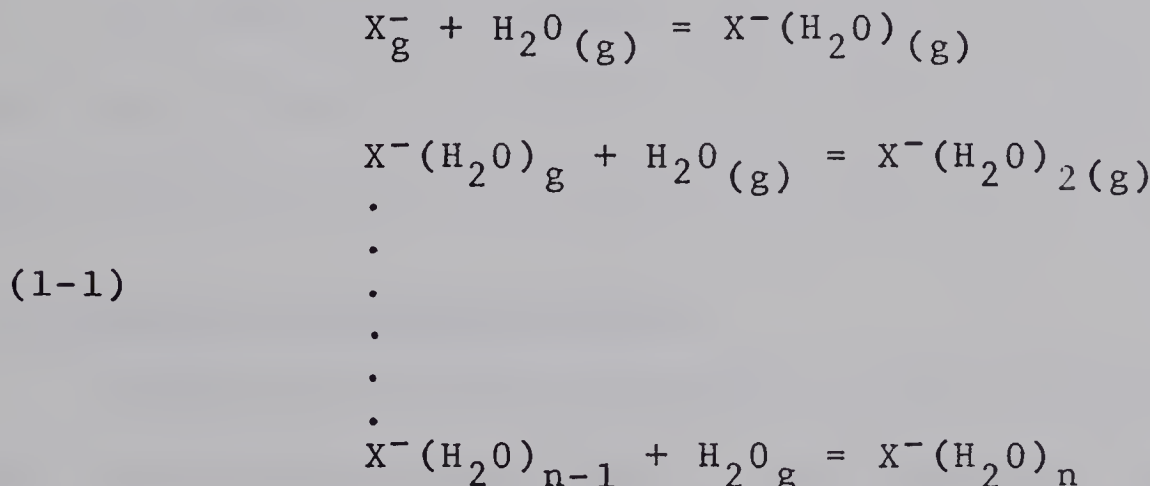
<u>Table</u>	<u>Page</u>
5-2 Thermodynamic Values for the Gas Phase Hydrat-	
tion of $OD^-$ . . . . .	145
5-3 Thermodynamic Values for the Gas Phase Hydrat-	
tion of $O_2^-$ . . . . .	153
5-4 Relative Abundances of $O_2^-(H_2O)_n$ . . . . .	154
6-1 Thermodynamic Values for the Gas Phase Solva-	
tion of Proton . . . . .	165



## INTRODUCTION

### 1.1 Scope of Present Study

The present work is mostly concerned with the study of the attachment reactions between the halide negative ions and water molecules in the vapour phase. This investigation was carried out in the ion source of a specially designed mass spectrometer. The temperature of the ion source could be varied from room temperature ( $25^{\circ}\text{C}$ ) to  $500^{\circ}\text{C}$ . The equilibrium constants for the attachment reactions of the type:



were determined, at different ion source temperatures, by the following relation:

$$\text{K}_{n-1, n} = \frac{P_{\text{X}^-(\text{H}_2\text{O})_n}}{P_{\text{X}^-(\text{H}_2\text{O})_{n-1}}} \cdot \frac{1}{P_{\text{H}_2\text{O}}} \tag{1-2}$$

where  $P_{\text{X}^-(\text{H}_2\text{O})_{n-1}}$  is the pressure of the reacting ion and  $P_{\text{X}^-(\text{H}_2\text{O})_n}$  that of the product.  $P_{\text{H}_2\text{O}}$  is the partial pressure of water in the ion source. The pressure ratio of the ions was taken as equal to the ratio of the intensities



of the respective ions, recorded by the mass spectrometer. The standard free energy of the reactions (1-1) can be calculated by the following equation:

$$\Delta G^\circ_{n-1,n} = -RT \log_e K_{n-1,n}$$

where R is the universal gas constant, T is the absolute temperature and  $K_{n-1,n}$  is equilibrium constant. From the study of the equilibrium constant at various temperatures,  $\Delta H^\circ_{n-1,n}$  could be calculated and  $\Delta S^\circ_{n-1,n}$  was determined from

$$\Delta G^\circ_{n-1,n} = \Delta H^\circ_{n-1,n} - T\Delta S^\circ_{n-1,n}$$

In addition to halide negatives the  $O_2^-$ ,  $OD^-$  and  $NO_2^-$  also were studied and their thermodynamic properties  $\Delta G^\circ_{n-1,n}$ ,  $\Delta H^\circ_{n-1,n}$  and  $\Delta S^\circ_{n-1,n}$  were determined similarly.

## 1.2 Production of Negative Ions

Negative ions are produced in the ion source of the mass spectrometer ordinarily by two distinct processes: (A) electron capture and (B) ion pair production.

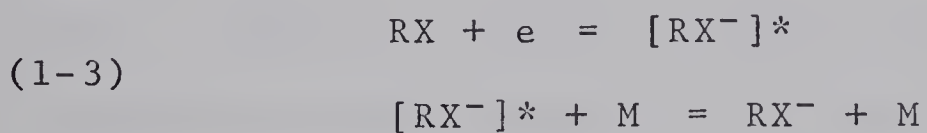
### A. Electron Capture Process

When a beam of electrons or some other ionizing media such as alpha particles or protons are passed through a gaseous medium, collisions between the gas molecules and the electron beams will take place. These collisions can result in the ionization of some of the gaseous molecules. This process can be represented as





The secondary electrons produced by the above process can undergo further collisions and subsequently ionize more molecules. Finally when these secondary electrons have lost most of their energy and have become thermalized, some of them may be captured by the gas molecules. The molecular negative ion which is formed can be stabilized either by radiating its excess energy or by losing it through collisions with other molecules (third body collision)



The appearance potential (the minimum electronic energy for production of the ion) of the ion  $RX^-$  is

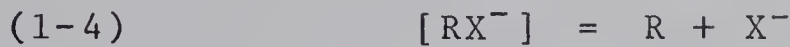
$$AP(RX^-) = EE + EA(RX)$$

where  $EE$  is the excess energy of  $RX^-$  and  $EA(RX)$  is the electron affinity of  $RX$ . As it is observed from equation (1-3), the rate of formation of the negative ion  $RX^-$  depends on the availability of a third body,  $M$ , thus, initially it will be proportional to the pressure of the gas. However, as the gas pressure is increased a value would be reached above which the rate will become pressure independent. It can be shown (1) that this critical value is the pressure at which the average time,  $t_s$ , taken by the excited ion  $[RX^-]^*$  to transfer its excess energy to another



molecule, becomes equal to the average life time,  $t_d$ , of the ion against dissociation.

If the negative ion  $RX^-$  could not stabilize itself either through collisions with other molecules or emission of radiation, it would return to its original state  $RX$ , by releasing the captured electron, or dissociate to a negative ion  $X^-$  and a free radical  $R$



The appearance potential of  $X^-$  by process (1-4) is given by



$D(R-X)$  is dissociation energy of  $RX$ ,  $EA(A)$  electron affinity of  $X$  and  $EE$  is the excess energy. The bond dissociation energy  $D(R-X)$  for most molecules is about 3 to 5 eV and the electron affinities for most atoms are between 1.5 to 3.5 eV, thus  $AP(X^-)$  is in the range of 0.5 to 4 eV.

### B. Pair Production

Negative ions can also be produced by an ion pair production such as



In this process the electron serves simply as a source of energy, therefore, other ionizing media such as alpha particles or protons can also initiate this process.



In the ion pair process, the molecule RX, through absorption of energy from the ionizing media, is raised to an excited state  $[RX]^*$  and then dissociates into a positive and a negative ion



The ions  $R^+$  and  $X^-$  can be either in their normal ground state or in an excited state. This process differs from the dissociative attachment in the products of the dissociation as well as the effect of the energy of the ionizing electron. The dissociative capture of an electron can only take place if the electron energy is within a narrow range, usually from 0.5 to 5 eV (1). Ion pair production on the other hand is not restricted to a small energy range, as long as the ionizing media has an energy equal or greater than the appearance potential of  $X^-$ , the process (1-6) can take place. The appearance potential of  $X^-$ ,  $AP(X^-)$  for the ion pair production is given as

$$(1-7) \quad AP(X^-) = D(R-X) + I(R) + EA(A) + EE$$

where  $I(R)$  is the ionization potential of R and other terms have been defined previously. Again a rough estimate of appearance potential  $AP(X^-)$  can be made by applying the data given in dissociative attachment process (1-5) and noticing that the first ionization potentials of most atoms lie between 6 and 15 eV. Thus, equation (1-7) would give



a value of 6 to 13 eV for  $AP(X^-)$ .

### 1.3 A Survey of the Previous Work

The knowledge of the existence of the ions, composed of clusters or group of molecules, in the gas phase dates back to the beginning of this century. Rutherford and Thomson (2) discovered that the mobilities of the ions were lower than the values predicted by the kinetic theory. They attributed this deviation to the formation of the ion clusters. Thus the ion cluster theory was born. According to this theory the charge on the ion would attract the neutral molecules so strongly that a bond is formed between the central ion and the surrounding molecules. As the result of this bonding, there will be an increase in the mass and the size of the ions, which will cause a decrease of the ion mobility. The condition for the stability of these clusters was set as follows (2): Since a cluster is subjected to repeated collisions with the gas molecules, it could be stable only if its potential energy were greater than thermal energy. The potential energy of the central ion - ligands system is the result of the polarization interaction between an ion and a neutral molecules. Mathematically this is expressed (3) by:

$$\frac{(D-1)e^2}{12\pi Pr^4} > 1$$

here D is the diffusion constant of the gas, r is the



distance of the closest approach of the ion and neutral molecule,  $P$  is pressure of the gas and  $e$  in the electronic charge.

A second theory, to explain the discrepancy between the theoretical and the experimental values of ion mobility, was put forward by Sutherland and Wellisch (2) independently. This theory which later on became known as "small ion theory" assumes that the increased size of the clustered ions is not the major factor in retarding the ionic motion through the gas, but the motion is retarded by momentum transfer as the result of the electrical forces between the ions and neutral molecules. Although it is the general belief today that the polarization scattering is mostly responsible for the lowering of the mobility (4), ions do form clusters when the conditions are right. Munson and Hoselitz, for instance, have obtained evidence of the attachment of inert gas atoms to lithium ion. They have shown (5) that, the clusters  $\text{Li}^+(\text{Xe})_n$  and  $\text{Li}^+(\text{Kr})_n$  are formed at room temperature with values of  $n$  ranging from one to two. Munson and Tyndall in their experimental measurements of the mobility of alkali ions (6) also observed evidence of formation of  $\text{Li}^+(\text{H}_2\text{O})_n$  with  $n$  as large as six at room temperature.

Although, there were some studies of the gas phase cluster formation made in early 1930, by mass spec-



tographic method (7), the vigorous work on this subject did not start until early 1960. In the following a brief review of the recent works is given.

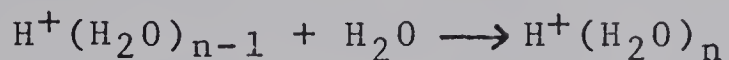
#### A. Hydration of Proton

The system  $H^+(H_2O)_n$  has been studied by a number of investigators. Beckey (8), for instance, observed cluster  $H^+(H_2O)_n$  up to  $n=10$ . Furthermore he obtained the value of 4 Kcal/mole for  $\Delta H_{1-2}$  and  $\Delta H_{2-3}$ . Knewstubb and Sugden (9) in a mass spectrometric study of ionization in flame, observed the ion  $H_3O^+$  as well as  $NH_4^+$  and  $NO^+$ . The first two of these also occurred in hydrated form up to 4 molecules of  $H_2O$ .

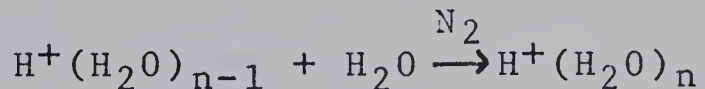
They concluded that these hydrated ions were formed, to a large extent, in the cooler part of the flame system. In a later study, Knewstubb and Tickner (10) observed the  $H_3O^+(H_2O)_n$  from  $n=0$  to  $n=6$  in glow discharges. They concluded that their results indicated an exceptional stability of the ion  $H_3O^+(H_2O)_3$  and stated that there might be two hydration shells for  $H_3O^+$  the first one containing three molecules of water. This, however, is in contradiction with what was observed in this laboratory. The hydration of proton was studied here in an alpha irradiated ion source by J. Scarborough and this author and in a proton beam mass spectrometer by S. K. Searles and A. Zolla (11). Our results, which will be presented in a



later chapter, did not indicate any discontinuity in exothermicity of the reaction



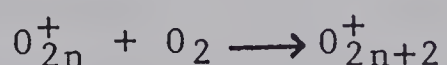
which is essential for the theory for the exceptional stability of the ion  $\text{H}_3\text{O}^+(\text{H}_2\text{O})_3$ . More recently the  $\text{H}^+(\text{H}_2\text{O})_n$  system was also investigated by F. H. Field (12) and his results are in excellent agreement with Kebarle et al (11). A. Good and D. Durden and P. Kebarle (13) have made a kinetic study of hydration of proton. Employing a quadrupole mass spectrometer, they have determined the rate constants for the forward reactions



for  $n=2$  to  $n=4$ . With the aid of the equilibrium constant determined previously (11), they were able to calculate also the rate constant of the reverse reactions.

#### B. $\text{O}_{2n}^+$ Clusters

Yang and Conway (14) (15) have studied mass spectrometrically the system



for  $n=1$  to 4. They found that the higher clusters are too unstable to be the dominant species of the series  $\text{O}_{2n+2}^+$  in the lower region of the ionosphere. From a plot of the



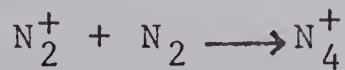
equilibrium constant,  $K_p$  versus  $\frac{1}{T}$  they determined the  $\Delta H^\circ$  for the above reactions. Their results are as follows



The reaction  $O_2^+ + O_2 \longrightarrow O_4^+$  has also been studied by D. Durden, P. Kebarle and A. Good (16) over a temperature range of 295-350°K. These authors' value for  $\Delta H_{2-4}^\circ$  is in good agreement with the result obtained by Yang and Conway.

### C. $N_4^+$ Clusters

The attachment reaction



has been studied extensively (17, 18, 19). Varney (19) studied the extent of the dissociation of  $N_4^+$ , from the change of ion mobility with variation of the field strength to the pressure ratio ( $E/P^\circ$ ), in a drift field tube. He calculated the equilibrium constant for the above reaction. By relating the ion temperature,  $T_i$ , to the field strength

$$T_i = T_{\text{gas}} + \Theta E/P^\circ$$

where  $\Theta$  is a constant; from a plot of the equilibrium constants versus  $1/T_i$  he estimated a value of 0.50 eV for the



dissociation energy,  $D(N_2-N_2^+)$ .

D.  $N_2O_2^+$  System

Equilibrium constant for the reaction



have been determined mass spectrometrically by Janik and Conway (20). On the basis of the observed value of -5.6 Kcal/mole for  $\Delta H_{\text{reac.}}$ , they have concluded that the equilibrium ratio of the [60]/[32] peak could not be  $[(NO)_2^+]/[O_2^+]$ . According to these authors the reaction



is endothermic by  $22 + D(NO-NO^+)$  Kcal.

E.  $O_4^-$  System

Conway and Nesbitt (21) have studied the formation of  $O_4^-$  in 6-12 torr of  $O_2$  gas irradiated by 2-ci tritium source with the subsequent mass analysis. From the equilibrium constants for reaction

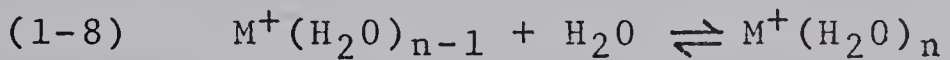


it was deduced that  $\Delta H^\circ_{298} = -13.55$  Kcal/mole. Voshall, Pack and Phelps (22), on the basis of the negative ion mobilities in pure  $O_2$  near  $80^\circ K$  concluded that  $D(O_2-O_2^-) = 1.4 \pm 0.5$  Kcal/mole. This value has been questioned by Conway and Nesbitt on the ground of the uncertainty involved in the calculation and non-equilibrium conditions in the system.



#### F. Gas Phase Hydration of Alkali Ions

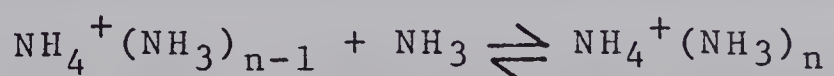
The gas phase hydration of alkali metals have been studied in this laboratory by S. K. Searles, I. Dzidic and P. Kebarle (24,35). The alkali metal ions were produced by thermoionic emission from a platinum filament which was located in a housing attached to the ion source. These ions were hydrated by drifting through the water vapour which was present in the ion source as well as the filament housing. The equilibrium constants for reaction



were determined at different temperature and thus  $\Delta H^\circ$ ,  $\Delta G^\circ$ ,  $\Delta S^\circ$  were obtained by the method explained earlier. These authors have also calculated, semi-empirically, the hydration energies of formation of these clusters by considering the net electrostatical forces involved and obtained relatively good agreement between the calculated and experimentally determined values of the heat of hydration of the reaction (1-8).

#### G. $NH_4^+(NH_3)_n$

The study of  $NH_4^+(NH_3)_n$  system was also undertaken in this laboratory extensively (25,35) and the thermodynamic values for the reactions:



have been determined.

In addition to the works cited above, there have been a number of other studies of ion-cluster formation,



both here in this laboratory and by other investigators, which cannot be dealt with in more detail here. Among these are the competitive solvation of protons by  $H_2O$  and  $CH_3OH$  (26), of  $NH_4^+$  by  $NH_3$  and  $H_2O$  (25) and flowing after-glow kinetic study of  $N_n^+$  where  $n=6$  to 9 at  $82^\circ K$  (32).

#### 1.4 Purposes of the $X^-(H_2O)_n$ Study

As can be seen from the above discussion, most of the previous work dealt with positive ion clusters. The present study was undertaken to obtain some comparative data for negative ion clusters and thus complement the gas solvation studies which have been taking place in this laboratory for the past few years. The choice of hydration of the halide negative ions was somewhat natural. Water is the most common solvent and halide ions have been the subject of interest in physical chemistry throughout the years. Moreover, the relative ease of production of halide negative ions in the ion source of a mass spectrometer makes them a good steppingstone for further study of other negative ion-solvent interactions.

#### 1.5 Application of Mass Spectrometric Study of Ion Clusters

Before leaving this chapter, it is appropriate to mention in a few words about the importance of ion cluster studies and their applications in the other fields of chemistry and physics. The role of clusters in



ion mobility work has already been mentioned. The importance of ion clusters in radiation chemistry was realized already a few decades ago when Lind (27) put forward his theory about ion molecule complexes. According to Lind's theory, an ion can attract one or two molecules through induced polarization and hold them until neutralized by an oppositely charged ion. The heat of neutralization and the close proximity of ions and attached molecules would promote chemical reaction, polymerization, decomposition etc. Later on this theory was over-shadowed by the free radical theory of Eyring, Hirschfelder and Taylor (28). The E. H. T. Theory postulates that the reaction of single ions and free radicals and molecules is more probable than large ion cluster reaction. The products of the neutralization of ions or ion clusters and also the products of dissociation of excited molecules may be free radicals or atoms which can initiate chain reactions and thus improve the yield (27).

Early in the 1950's, however, Lind's theory gained additional support when it was shown, by mass spectrometric work that long lived complex ions are formed by ions and neutral molecules (29). Recently, in a study of the radio-lysis of ethanol vapour, Bansal and Freeman (30) have attributed the decrease of acetaldehyde and hydrogen



yields with increasing dose to the scavenging of the electrons by acetaldehyde with ultimate production of  $(CH_3CHO^-)_n C_2H_5OH$ . Also the formation of  $H^+(C_2H_5OH)_m$  and  $NH_4^+(C_2H_5OH)_n$  have been postulated by the same authors.

Formation of ion clusters in the D region of the ionosphere has been confirmed by the investigation of Narcisi and Bailey (31). In experiments carried out by rocketborne quadrupole mass spectrometers, they have observed heavy positive ions with mass numbers greater than 45 amu. Some of these ions have been attributed to hydrate ion clusters. Also they have reported that the cluster  $H_3O^+(H_2O)$  appeared to be a dominant positive ion at an altitude of 60 to 80 Km. The "D region simulation" flowing afterglow experiment by Ferguson et al (32) have proved the formation of the hydrated clusters  $H_3O^+(H_2O)_n$ , in the ionosphere, with n as large as 6. Primary negative ions also may form clusters with neutral molecules in D region. Formation of clusters such as  $O_2^-(H_2O)_n$ ,  $NO^-(H_2O)$  and  $CO_4^-$  have been postulated (33). The diurnal variation in the electron density of D regions has been attributed to certain negative ion molecule reactions including cluster formation (33). Thus we can conclude that the importance of the process of ion-cluster formation cannot be overemphasized, if a full understanding of the chemical composition of the



ionosphere and the ion molecule reaction involved and the related phenomena is desired.

Another interesting application of cluster ions has been recently considered by Doyle and Caldwell (34). According to these authors, the removal of certain molecular contaminants from manned space cabin atmosphere can be accomplished by injection of some stable ions into the contaminated atmosphere and allowing them to react with the polar contaminants to form stable clusters. These clusters can then be collected at an appropriate electrodes. The only theoretical complication involved is the competition of innocuous polar constituents of the atmosphere, especially water vapour, with the contaminants to form the clusters. Therefore, only certain compounds such as alcohols, amines and acids are collectable by this method. One way which has been suggested (34) is to remove most of the water vapour and then inject the ions. Alternately, since the mixture of the ions, water vapour, and oxygen constitutes an oxidizing atmosphere, an attempt can be made to fragment or oxidize those neutral molecular species that would not be able to compete in clustering reactions to the polar species that could be clustered.



## 2 EXPERIMENTAL

### 2.1 General Description

The gas phase solvation study by means of a mass spectrometer involves the production of the solvated species  $X^-A_n$ ,  $X^-A_{n+1}$ , etc. in a field free ion source and the measurement of their relative concentrations. The clusters,  $X^-A_n$ , are produced by the interaction of some ionizing media such as an electron beam or alpha particles with suitable compound containing X, in the presence of a polar compound A. The measurement is performed by bleeding a sample of the gas into the main vacuum chamber of the mass spectrometer. There, the ions present in the gas are captured, accelerated by the electric field of the mass spectrometer and then mass analyzed. After mass analysis the ion current is amplified and detected.

Certain modifications have to be made in a conventional mass spectrometer in order to make it applicable for solvation studies. Most of these modifications apply to the ion source of the mass spectrometer. In order to assure the achievement of equilibrium in the ion source, the ion source has to be able to handle pressures of the order of 5 to 10 torr. This condition, in turn, requires that the electron beam, which is used for ionizing the gas, must be generated in the region outside of the ion source. It is also necessary that the attachment reactions be carried



out in a field free region. Therefore, the repeller voltage, which is an essential part of the conventional mass spectrometer, has to be eliminated from the ion source of the mass spectrometer used in the solvation studies. In order that the high pressure of the ion source does not interfere with the performance of the mass spectrometer, a high capacity pumping speed system is required. Differential pumping between the main chamber and the mass analyser tube is also desirable.

A conventional mass spectrometer already present in this laboratory was modified for the purpose of studying the gas phase hydration of the halide negative ions. Since the investigation of the gas phase solvation of proton and a portion of the negative ions study was performed by the alpha source mass spectrometer, this instrument will be discussed in brief first.

## 2.2 Alpha Source Mass Spectrometer

This instrument has been in operation in this laboratory for several years, and descriptions concerning its design and construction have been given in several publications (11, 25, 26). Therefore, only those features pertinent to the present work will be discussed here.

The ion source of this instrument is shown in figure (2-1). A mixture of the carrier gas and the compounds required was passed through the ion source, where



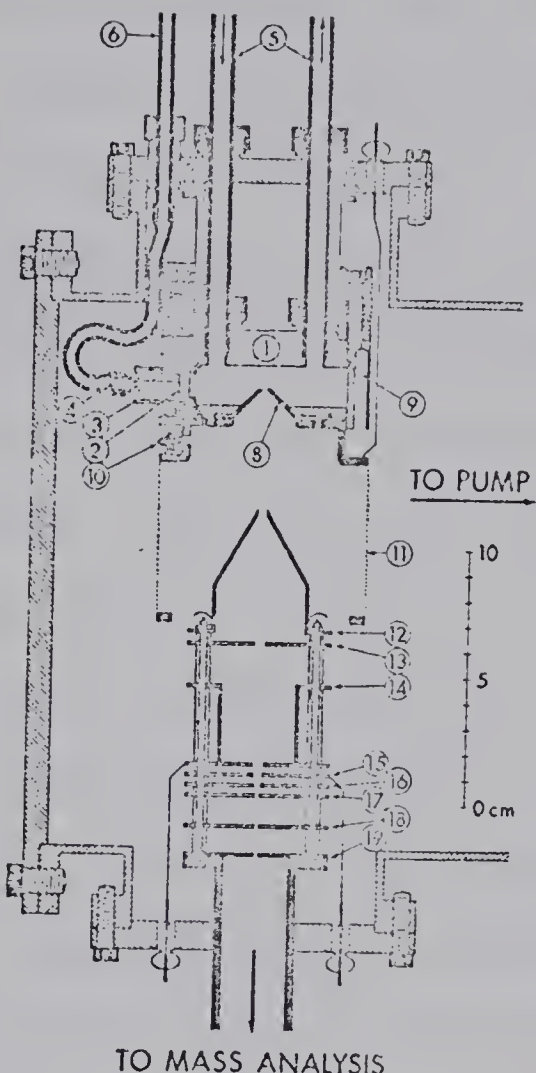


Figure 2-1: Ion Source and Electrode System: (1) Ion Source, (2) Alpha Source carrying polonium Disk, (3) Alpha Source Container with stainless Foil Window, (4) Stainless-Steel Porous Plug, (5) Gas Supply and Flow System, (6) Pressure Equalization, (7) Electrical and Thermal Insulator, (8) Cone Carrying Metal Foil Leak, (9) Heater and Thermocouple Wells, (10) Auxiliary Electron Gun, (11)-(19) Electrodes.



it was irradiated by a 200 m-C. polonium 210 source. This polonium 210 alpha source was contained in a removable compartment. The alpha rays entered the ion source through a three micron thick nickel foil, which separated the ion source from the polonium 210 compartment.

In the primary study of the halide negative ions as well as proton-water attachment reactions, all the runs were made with a continuous flow of the gaseous mixture through the ion source. The flow was used to provide gas mixing, scavenging of impurities out of ion source, and constant water pressure in the ion source. For this purpose the ion source was provided with an inlet and an outlet tubes figure (2-1, item 5). The linear flow through the ion source was approximately 20 cm/sec. This corresponded to a gas residence time in the irradiated volume of about 0.1 second. The ion residence time in the same volume was estimated to be about 1 milli-second (11), thus the gas flow could not affect the ion residence time.

The ion source could be heated by means of heater windings mounted around the ion source. The maximum working temperature of the ion source was restricted to 150°C. This was due to the direct contact of the polonium source with the ionization chamber and the fear of rapid spreading of the polonium which could occur above this temperature. The ionization chamber could also be cooled below room temperature by circulating cold nitrogen gas through the copper tubing



which was silver soldered around the ion source. Thus experiments could be performed at temperatures from  $-40^{\circ}\text{C}$  to  $150^{\circ}\text{C}$ . As will be explained later, this temperature range was not wide enough for the complete study of the halide negative ions.

The gas handling plant and flow system of the alpha source mass spectrometer were identical with the electron beam mass spectrometer to be described in detail in later sections.

After being irradiated inside the ion source a part of the ion-gas mixture effused into the electrode chamber, through the ion exit leak. In order to assure that the ion cluster would not undergo any cooling due to the adiabatic expansion past the exit leak, measurements were carried out only at conditions of molecular flow i.e. at conditions where the mean free path of the gas molecules and the ion-clusters was larger than the dimension of the ion exit slit. For the pressure range used in these studies a slit of 10 microns width fulfilled this requirement. This was proven by varying the slit size and observing its effect on the distribution of the detected ion-clusters.

In the electrode chamber the ions were accelerated and mass analyzed by a  $90^{\circ}$  sector mass spectrometer. The detection of the ion current was accomplished by a Bendix M-306 electron multiplier.



### 2.3 Electron Beam Mass Spectrometer

The alpha source mass spectrometer had certain drawbacks which made it inadequate for the complete study of the halide negative ions. Thus while temperatures up to 500°C were required for this study, the ion source of this instrument could not be heated above 150°C without endangering the polonium 210 alpha source. Also while the work on the hydration of proton and the halide ion was undertaken by this author with the alpha mass spectrometer, a pulsed electron beam mass spectrometer for high ion pressure studies had been developed by D. A. Durden and P. Kebarle of this laboratory. This pulsed high pressure mass spectrometer has been described elsewhere (67). Since the pulsed electron beam high pressure model seemed to offer a number of advantages also for the present study, it was decided to equip a second mass spectrometer with the pulsed electron beam high pressure source. The main components of this instrument are shown in figure (2-2). They are gas handling plant, ion source, electron gun, mass analysis and detection units and high capacity vacuum system.

### 2.4 Gas Handling Plant

The gas handling plant is shown in figure (2-3). It consisted mainly of a large glass bulb (4 litre), with the proper valves and connections to let gas, at desirable flow rate, pass through the ion source of the mass spec-

21. Cylinder entrance
22. First cylinder
23. Second cylinder
24. Cylinder exit
25. First deflection half plate
- 25a. Second deflection half plate
26. Mass analysis slit flange
27. Mass analyzer tube



Figure 2-2

A. Electron Gun

1. Filament
2. Draw out
3. Extractor
4. First focussing and accelerating electrode
5. Second focussing and accelerating electrode
6. Third focussing and accelerating electrode
7. Horizontal deflection half plates
8. Vertical deflection half plates
9. Shielding cylinder

B. Ion Source

10. Copper Jacket
11. Electrostatic Shield
12. Electron entrance slit flange
13. Electron trap flange
14. Ion exit slit cone
15. Gas inlet
16. Kovar seal flange
17. Stainless steel support
18. Ceramic Spacer

C. Ion Accelerating Tower

19. First cone
20. Second cone

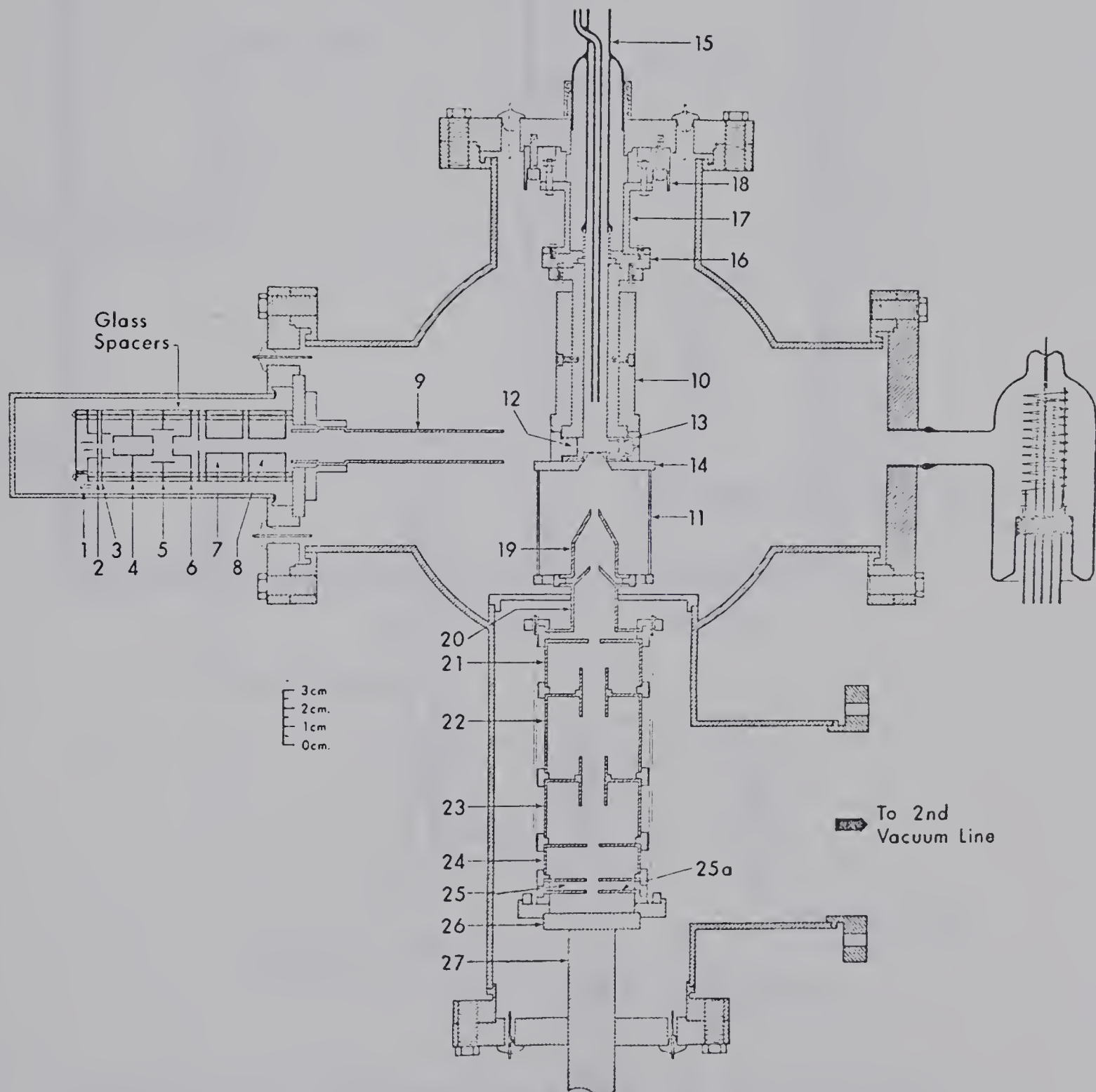


Figure 2-2: Main Components of the Electron Beam Mass Spectrometer: Ion Source, Electron Gun, Ion Accelerating Tower.



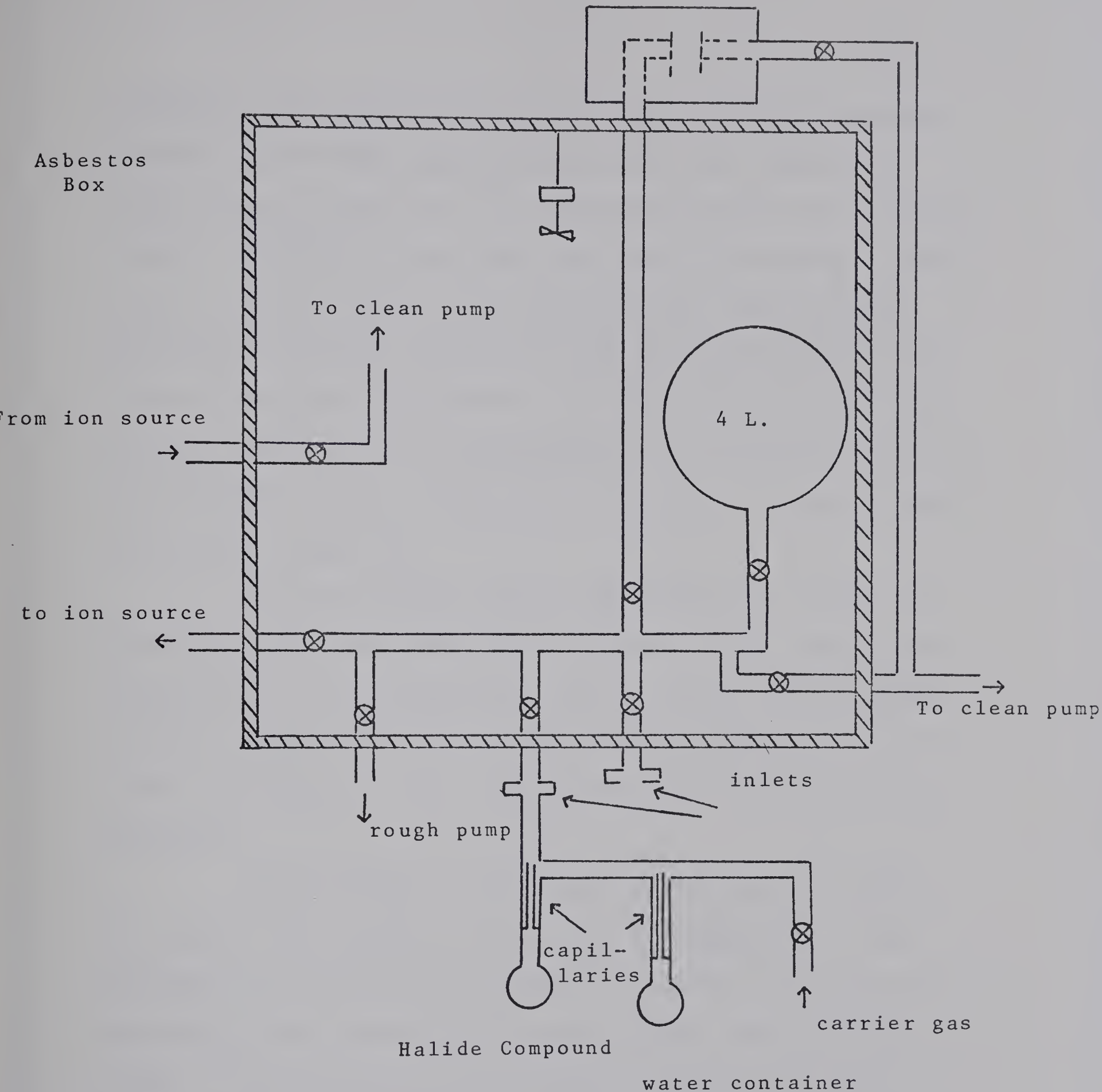


Figure 2-3: Gas Handling Plant for Introduction  
of Gases into the Ion Source



trometer. It could be evacuated by two different pumping systems. The rough pumping system was used whenever a large amount of gas was to be removed from the gas handling plant. The clean vacuum line was used for removing a small amount of gas from the ion source and the inlet system. Moreover, the clean vacuum line was also used as the flow outlet during the experiment. The flow of the carrier gas and the compounds to be investigated was conducted from the gas handling plant, through the ion source, and out through the clean vacuum line.

All the valves and the main manifold of the gas handling plant were made from stainless steel. The inside diameter of the main manifold and the glass tubing connecting the various part of the gas handling system and the ion source was about 1.5 cm. The valves were all 1/2 inch in diameter.

The pressure in the gas handling plant and the ion source was measured by an Atlas MCT manometer. This manometer was calibrated by means of a wide U tube mercury manometer and a cathetometer prior to the start of this study. The calibration was checked, during this study, from time to time to assure the accuracy of the pressure measurement. The entire gas handling plant was enclosed in an asbestos board chamber which could be thermostated up to 150°C. The inlet and outlet gas line, connecting the



gas handling plant to the ion source, could also be heated to 150°C by means of heating tape.

## 2.5 Electron Gun

The electron gun is shown in figure (2-4). The electrons, emitted from the filament [1] were passed through small hole (1/16 inch) at the centre of the draw out electrode [2]; then they were accelerated slightly by the field between the draw out and the extractor electrodes [3]. The major acceleration and focussing occurred by three accelerating and focussing electrodes [4,5,6]. The horizontal and the vertical deflection of the beam was obtained by the two sets of deflection half plates [7,8]. After emerging from the second set of deflection half plates, the beam passed through a shielding cylinder [9] and entered the ion source through the electron entrance slit. The electron gun was designed and constructed to operate for both positive and negative ions study. For this work when negative ions were studied and the ion source was at -2000 volts, the potential at the different electrodes were as follows: the filament was at -4000 volts, the draw out potential was about 10 to 20 volts positive with respect to the filament. The potential of the extractor plate could be varied from -4000 to -3800 volts. The first and the third focussing electrodes were at -2000 volts and the second focussing electrode potential could be varied from -4000 volts to



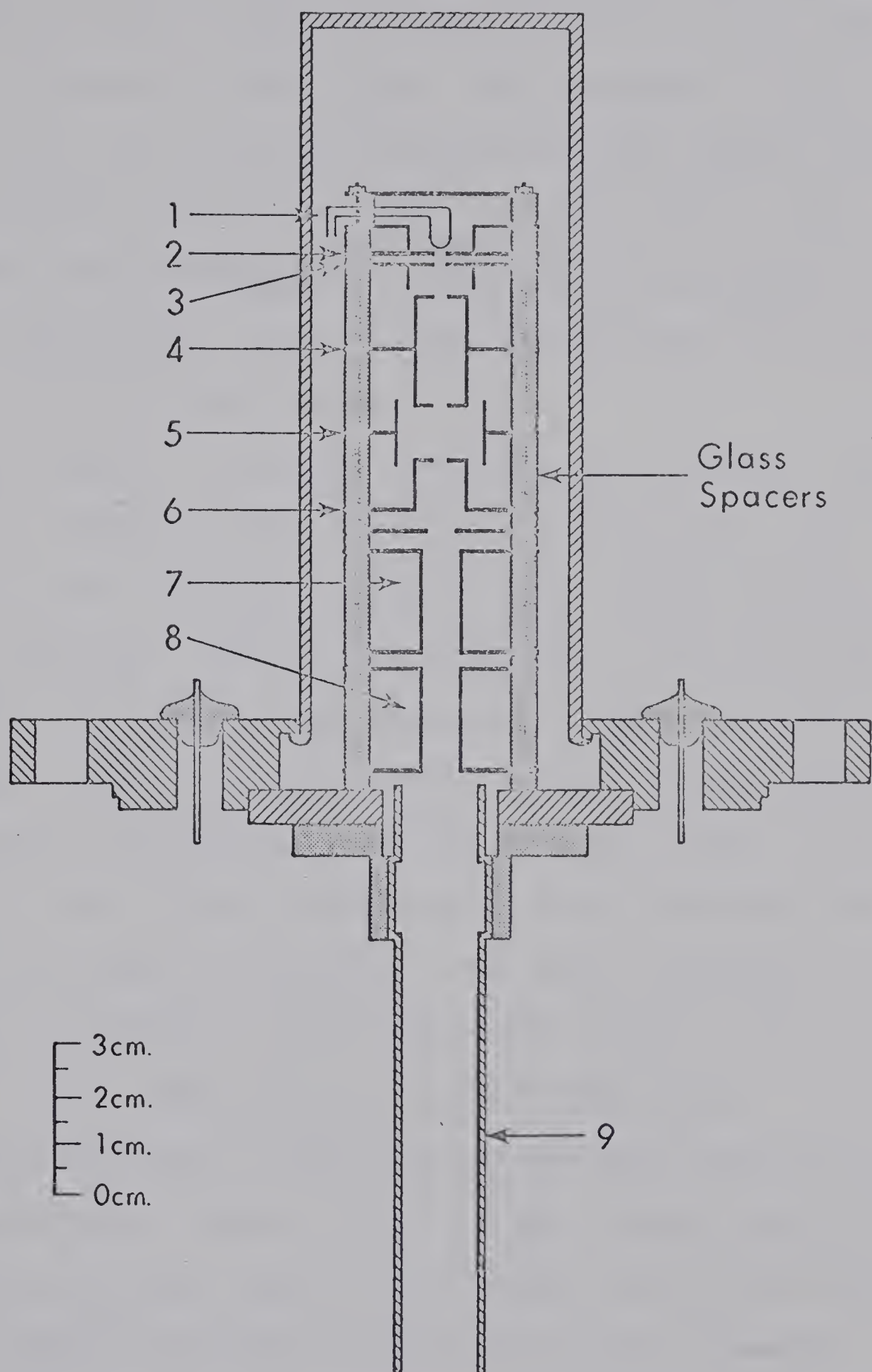


Figure 2-4: Electron Gun Numerical Legends are give on  
Page Opposite to Figure (2-2).



-3000 volts. The first vertical and the first horizontal half plates as well as the shielding cylinder were at the ion source potential, -2000 volts. The potential of the second vertical and horizontal deflection half plates could be independently varied from -2000 to -1800 volts. Thus, the electrons were generated at -4000 volts, accelerated by a field of 2000 volts, focussed, and entered the ion source with 2000 electron-volts energy.

To assure the proper focussing of the beam, there was a plate located in the front of the ion source entrance slit, coated with a mixture of phosphorus, sodium silicate and sodium chloride. This plate contained a 1/8 inch hole coaxial with the electron entrance slit. Prior to each experiment the electron beam was deflected out of the central hole, properly adjusted and focussed to a spot with a diameter of the order of two millimeters, then deflected back to the central hold of the plate. The total emission current from the filament was 200 micro-amps and the trap current was  $1 \times 10^{-8}$  ampere in an ordinary experiment.

The filament of the electron gun was heated by a direct current power supply. The voltage across the filament was two to three volts, the filament current was from 5.2 to 4.2 amperes depending on the age of the filament. The electron current was automatically controlled by using a saturable transformer filament regulator which controlled



the filament heating current through the total emission from filament. Originally, pure tungsten ribbon was used as the material for the filament. This, however, proved unsatisfactory, since the life time of the filament was very short when oxygen was used as carrier gas. Finally, a thoriated iridium filament was used. This filament proved to be very satisfactory since it was inert to both oxygen and water vapour.

In order to prevent the interference of the mass spectrometer magnetic field with the performance of the electron gun, the electron gun was equipped with a magnetic shield. The shield was made from the "Netic and Co-netic Alloys" obtained from the Magnetic Shield Division of Perfection Mica Company of Bensenville, Illinois. These alloys were rolled into cylinders and were mounted on the electron gun housing.

Originally, the electron gun was designed such that the electron beam could be pulsed for ion pulsing experiments. The electron beam pulsing was to be accomplished by applying pulses from a generator to the electron deflection plates [7] or [8]. However, no pulsing experiments were attempted in this work.

## 2.6 Ion Source

The ion source is shown in figure (2-5). It was machined from non-magnetic stainless steel. It consisted



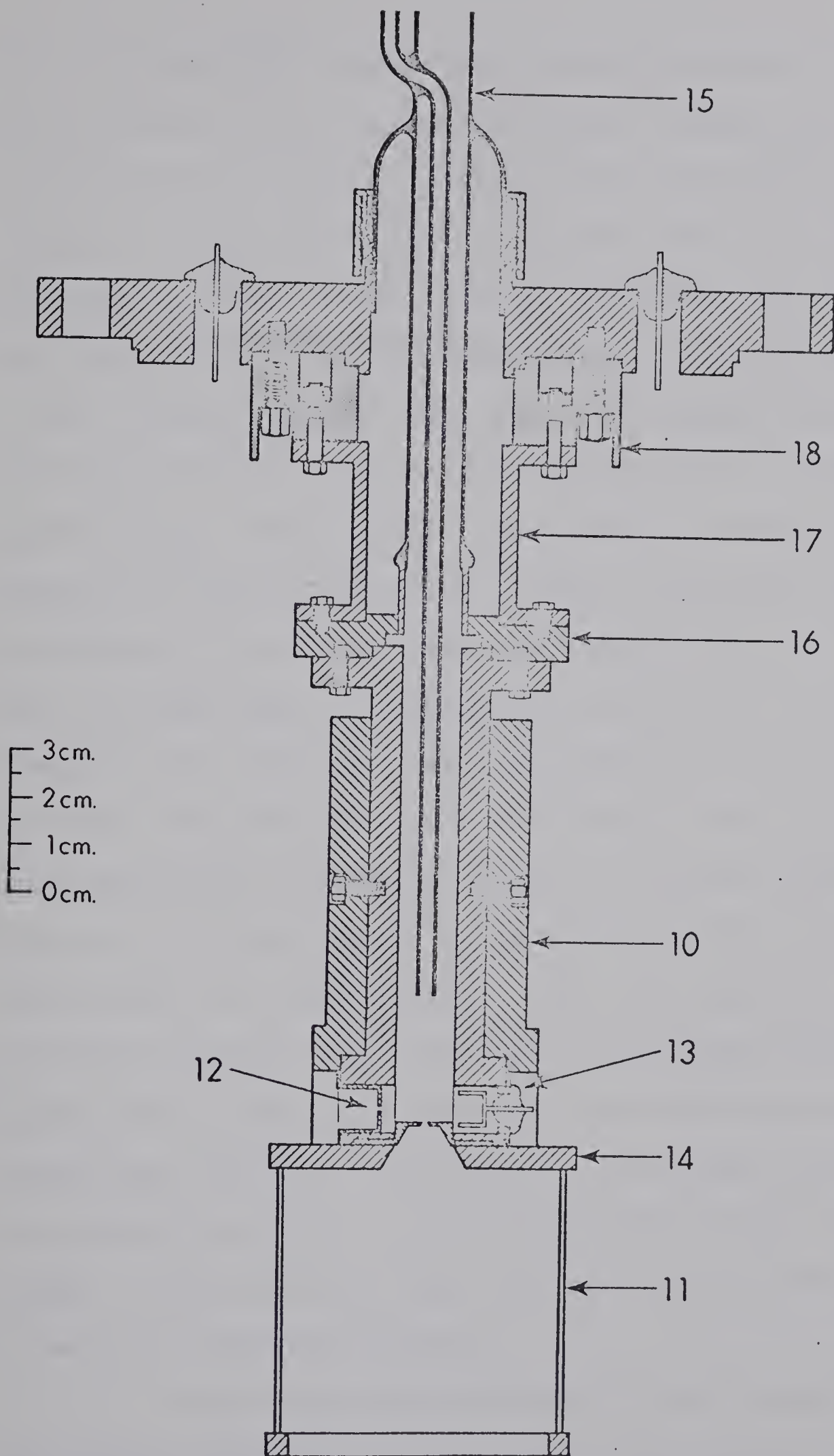


Figure 2-5: Ion Source Numerical Legends are explained in the Page Opposite to Figure (2-2).



of a cylindrical chamber with inside diameter of 1/2 inch. In the lower part of the ion source a channel was bored perpendicular to the main axis of the ion source. A small flange carrying the electron entrance slit was located in one side of this channel and the electron trap flange in the other side. The electron entrance slit was welded on a "hat shaped" flange, [12] and this flange was sealed onto the ion source by four 1-72 stainless steel screws and a gold O-ring. The electron trap assembly consisted of a flange [13] which contained a kovar electrical feed through. A Faraday cup electron trap was mounted on this feed through. This cup was made of non-magnetic stainless steel. The electron trap assembly was also sealed to the ion source by four 1-72 screws and a gold O-ring. The ion exit slit was mounted on a cone [14] which in turn was bolted to the bottom of the ion source by four 1-72 stainless steel screws and sealed by a gold O-ring. Both, ion exit slit and the electron entrance slit were made by welding stainless steel razor blade edges to a circular tantalum disc which was 0.030 inch thick and contained a 2 mm centre hole. These tantalum discs were in turn spot welded to the respective cones. Both, ion exit slit and electron entrance slit were 2 mm long and 0.015 mm wide.

The connections between the ion source and the gas inlet system were provided by two concentric tubes [15].



The gas entered the ion source through the outer tubing and left the ion source through the inner tubing. The concentric tubes were sealed to a flange by a kovar seal and this flange [16] was mounted on the top of the ion source and sealed in place by a set of six screws and a gold O-ring.

For the purpose of heating, the ion source was enclosed in a heating jacket [10]. This jacket was machined from copper and it was divided into two half cylinders. Each half was secured to the ion source by means of a screw. The jacket was slotted and an electrical heater was placed in these slots. The heater consisted of 28 gauge nichrome wire inserted into fused silica insulators. There were a total of six fused silica insulators and each one had six bores. Each insulator was fitted into one of the slots on the copper jacket. The heater voltage was supplied by a variac and the temperature was controlled by manual setting of the heater voltage. The copper jacket and the heater were surrounded by a stainless steel thermal shield which was supported by two screws going through to the copper jacket. To minimize the heat lost by radiation, the entire ion source assembly was surrounded by another stainless steel radiation shield.

The temperature of the ion source was measured by means of an iron-constantan thermocouple. The thermocouple was placed in a well drilled in the wall of the ion



source to a depth of 3/8 inch, and was located next to the ion exit slit.

To provide a controlled electric field between the ion source and the first cone of the ion accelerating tower, an electrostatic shield [11] was mounted below the source. This shield was fabricated from metallic mesh of high transparency and extended from the ion exit slit cone of the ion source to the second cone of the ion accelerating tower.

The entire ion source assembly was mounted on a cylindrical stainless steel support [17] which in turn was mounted on a machined ceramic (super-mica spacer) [18]. The spacer was mounted on the vacuum chamber port flange. The electrical connections to the ion source were made by 10 electrical feed-throughs which were soldered on the port flange.

## 2.7 Ion Accelerating Tower

The ion accelerating tower is shown in figure (2-6). Ions diffusing out of the ion exit slit of the ion source were accelerated and focussed on the mass analyzer entrance slit by the ion accelerating tower. This stepwise acceleration of the ions was carried out by the successive electrodes of the ion accelerating tower. The approximate voltages of the ion accelerating tower electrodes are shown in table (2-1). The last electrode before mass analyzer tube consisted of two half plates. One of these half plates



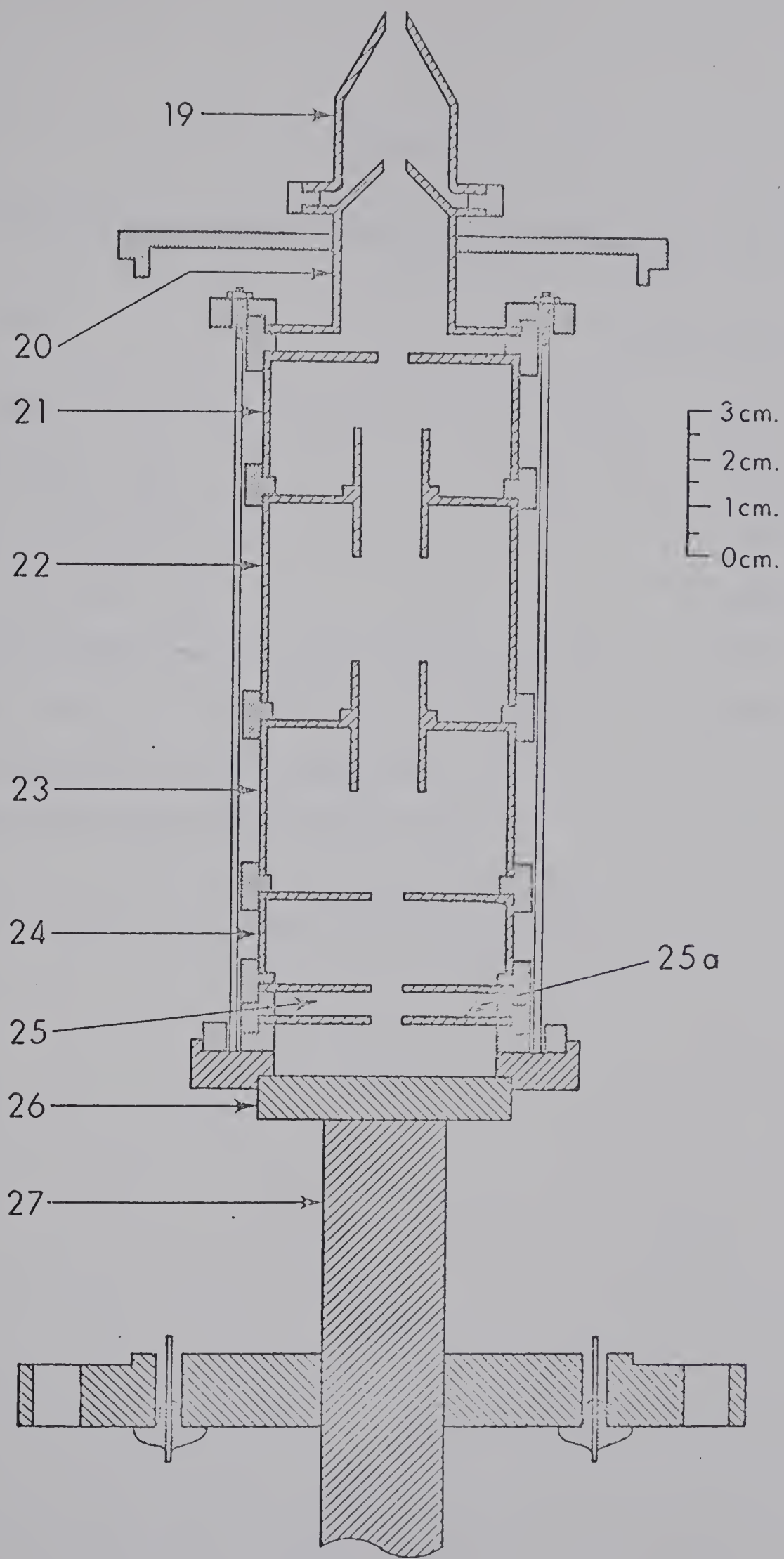


Figure 2-6: Ion Accelerating Tower. Numerical Legends are explained on the Page Opposite to the Figure (2-2).



Table 2-1

## Ion Accelerating Tower Potentials For Negative Ion Study

Electrode*	Potential, Volts
First Cone, 19	-1874
Second Cone, 20	-1702
Cylinder Entrance, 21	-1786
First Cylinder, 22	-1006
Second Cylinder, 23	-1207
Cylinder Exit, 24	-1274
First deflection half plate, 25	0
Second deflection half plate, 25a	-49

\*Numbers refer to figures (2-2) and (2-6).



was at ground potential, and the potential of the other one could be varied from ground to -400 volts. It was intended to use this electrode for pulsing of the ion beam. However, the pulsing capability of the mass spectrometer is to be developed in future work in this laboratory. In the present experiments, the potential of this half plate was kept slightly negative, about -20 to -50 volts, for optimum operating condition.

## 2.8 Mass Analysis and Ion Current Detection

After acceleration the ions were magnetically mass analyzed in a 90°, 15 cm radius tube. Differential pumping was applied to the analyzer tube and thus the pressure in the tube was about ten times lower than that of the main vacuum chamber. Mass scanning was obtained by changing the magnetic field at a constant accelerating voltage. Mass determination was obtained by a Hall probe (manufactured by F. W. Bell Inc., Columbus, Ohio) which was located in the magnetic field just next to the analyzer tube. A constant voltage of 14 volts was applied across the primary circuit of the Hall probe and the induced voltage in the secondary circuit was measured by a Hewlett Packard digital voltmeter. Prior to these studies the Hall probe was calibrated for both positive and negative ions by working with gases which provided ions of known mass to charge ratio. Although the Hall voltage changed with room



temperature, the calibration remained valid within one mass unit for the mass range of 15 to 70 and within two mass unity for the range 70 to 200.

After mass analysis the ion current was amplified by a 17 stage secondary electron multiplier (SEM). The first dynode was slightly above ground voltage (about 50 volts), the last dynode was at +3200 volts and the SEM collector plate was at +3500 volts. The SEM output, was connected, through a capacitor, to a pulse counting system consisted of a preamplifier, amplifier, discriminator unit, manufactured by Johnston Laboratories Inc., Model PAD-1. The amplified pulses coming out of this unit were counted by a "Hamner Electronic Model N730" counter. The noise level of the counting circuit was approximately 20 counts per second. Figure (2-7) represent a plot of the counter output versus the SEM voltage.

## 2.9 Vacuum Chamber

The main vacuum chamber was built from 8 inch stainless steel pipe [figures (2-2) and (2-8)]. In addition to the top entrance, there were four entrances or ports provided for the chamber. To each port another piece of 4 inch stainless steel pipe was welded and each one was provided with a flange. The orientation of the different component of the mass spectrometer was as follows: the ion source was mounted on entrance [1], figure (2-8), the



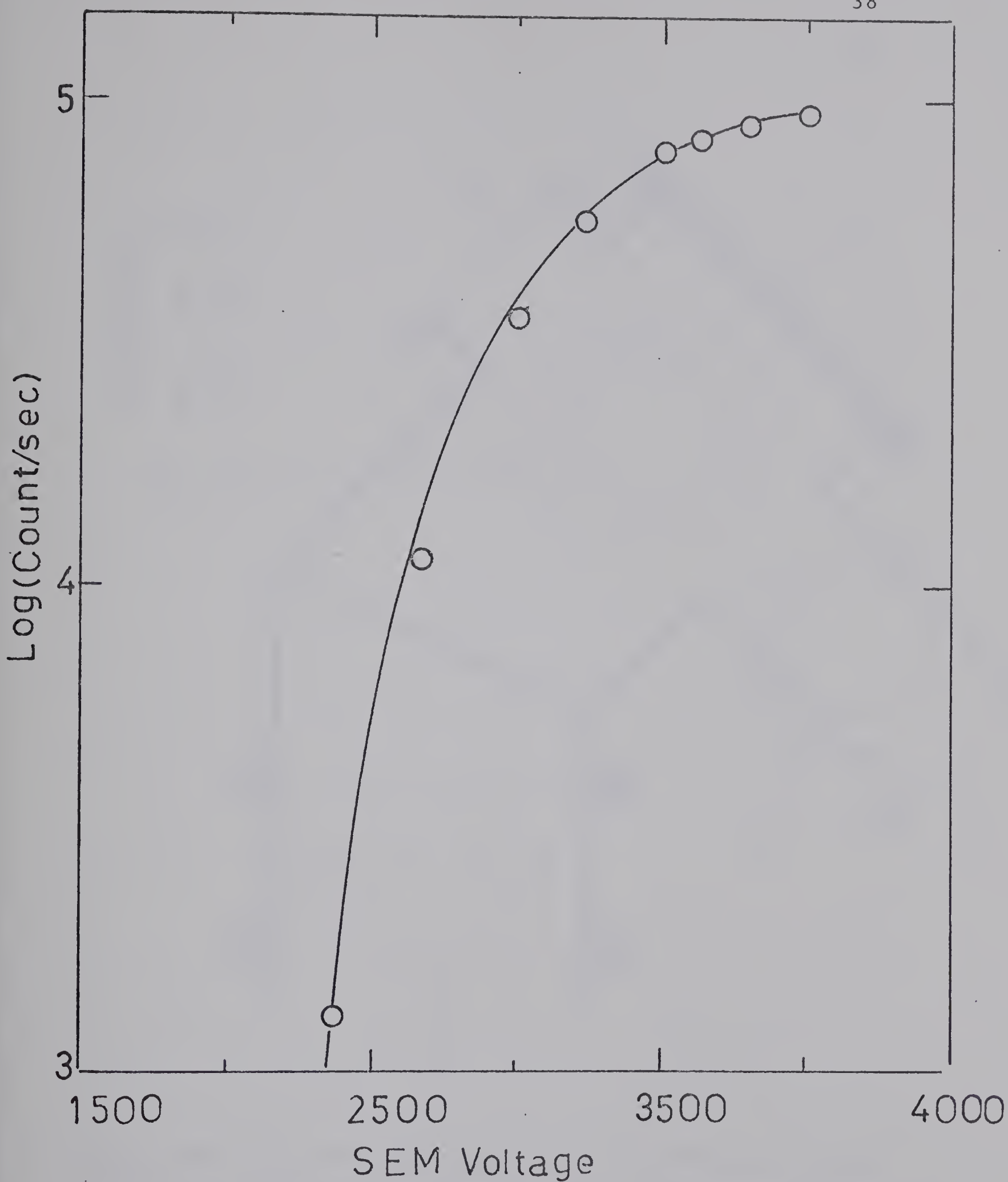


Figure 2-7: Counts/Second as a Function of Voltage Across Secondary Electron Multiplier.



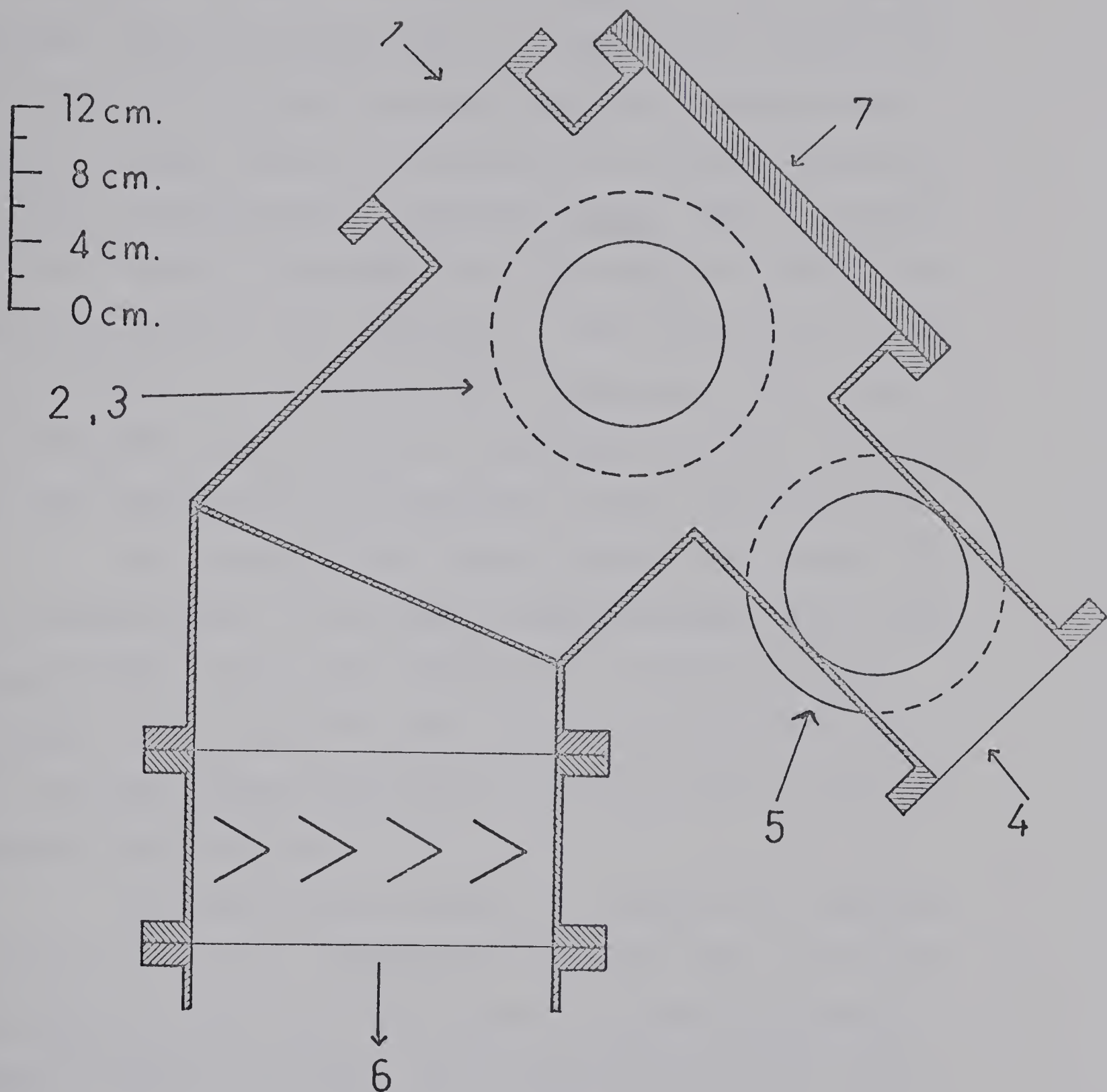


Figure 2-8: Main Vacuum Chamber, 1) Ion Source Flange, 2) Electron Gun flange, 3) Ionization Gauge, 4) Mass Analyzer Tube flange, 5) To Second Vacuum Line 6) Main Diffusion Pump, 7) The Top Entrance.



electron gun on [2] the ionization gauge on [3], and mass analyzer tube on entrance [4]. In addition to these, the 4 inch pipe on the mass analyzer side was provided with another flange, which was connected to a 4 inch "National Research Corporation" oil diffusion pump. This auxiliary vacuum line was to evacuate the mass analyzer tube and the detection part of the instrument. The top entrance of the vacuum chamber was covered with a plexiglass lead. The use of plexiglass lead instead of stainless steel was necessary for the observation and adjustment of the electron beam.

The bottom of the vacuum chamber was welded, at a 45 degree angle, to another 8 inch stainless steel pipe, figure (2-8). This port was fitted, by means of proper flanges, to the top of a water cooled optical baffle of the type 506 Chevron Cryo-baffle, manufactured by National Research Corporation.

The main vacuum chamber was pumped by a National Research Corporation "VHS6-184" diffusion pump. The pumping speed at the top of the baffle was given by manufacturer as 1100 litres/sec. The conductance of the 8 inch pipe from the baffle to the ion source exit slit was obtained from the graph in reference (69), and was also about 1100 litres/sec. The pumping speed,  $S$ , just outside of the ion exit slit can be calculated from the equation:

$$\frac{1}{S} = \frac{1}{F} + \frac{1}{S_p}$$



where  $S_p$  is the pumping speed at the top of the baffle, and  $F$  is the conductance of the 8 inch stainless steel pipe. Using the values given above for  $S_p$  and  $F$ , a value of 550 litres/sec is obtained for  $S$ . The conductance of the ion exit slit and the electron entrance slit of the ion source can be calculated from equation (2-1), if we assume molecular flow through both slits.

$$(2-1) \quad F = \frac{\bar{V}}{4} A$$

$F$  is the conductance of the slit,  $\bar{V}$  is the average linear velocity of the gas through the slit and  $A$  is the area of the slit. For air at  $300^{\circ}\text{K}$ ,  $\bar{V}$  is equal to  $4.70 \times 10^4 \text{ cm/sec}$  (68). The total area of the two slits is  $6 \times 15^4 \text{ cm}^2$ , thus,  $F$  is calculated to be 7.0 cc/sec. From the value of the conductance of the slits, the pumping speed outside of the ion source and the ion source pressure, the pressure outside of ion source in the main vacuum chamber can be calculated by the equation:

$$S.P_{\text{chamber}} = F.P_{\text{i.s.}}$$

The calculated value for the pressure in the main vacuum chamber, when the ion source pressure was two torr, is  $2.5 \times 10^{-5}$ . The observed reading from the Veeco ionization gauge was  $5 \times 10^{-5}$  torr, which is of the same magnitude.

## 2.10 Experimental Procedure

The investigation of the halide negative ions



was carried out at ion source temperatures from 25 to 500°C. Whenever the experiment was to be performed at an elevated temperature, the voltage of the ion source heater was adjusted, at least, five hours in advance. Ordinarily, the ion source heater was set for the desired temperature the night before the experiment was to be carried out, so that the ion source temperature equilibrated by the morning.

For the experiments in which oxygen was used as carrier gas, the water vapour was supplied to the gas stream through a capillary by means of small bulb containing liquid water. The rate of flow of water vapour through the capillary was regulated by controlling the temperature of liquid water and thus the water vapour pressure in the bulb. This was done by placing the water container in a constant temperature bath and adjusting the temperature of the bath, for a particular partial pressure of water. The partial pressure of water in the gas stream was determined by the weight loss of the water container during the experiment and the flow rate of the carrier gas. The flow rate was determined by means of a calibrated flowmeter which was installed in the gas line. Assuming that the water-oxygen mixture obeyed the ideal gas law, the partial pressure of water is given by

$$P_{H_2O} = \frac{P_{\text{total}} \cdot W_{H_2O}}{W_{H_2O} + (W_{\text{oxygen}}) 18/32}$$

where  $P_{\text{total}}$  is the ion source pressure,  $P_{H_2O}$  is the partial



pressure of water,  $W_{H_2O}$  and  $W_{oxygen}$  are the weight loss of water and the weight of oxygen passing through the ion source per unit time, respectively.

The halide compound to be studied was also added to the gas stream, through a capillary. The partial pressure of the halide compound in the ion source was adjusted to be between 30 to 100 microns. In most cases this was done by the proper selection of the capillary and having the halide compound container at room temperature. In those instances where this procedure was not applicable due to the limitation of the capillary size, the compound to be studied was cooled, by means of a mini-freezer. Most of the experiments were carried out with a carrier gas pressure of 4 torr, although pressures up to 8 torr were used in some cases.

In those experiments where no carrier gas was used, the water pressure was measured directly with the Atlas MCT manometer. Experiments were run with water pressure of one to four torr. After the water pressure and the partial pressure of the halide compound were adjusted to the desired values, the gas stream was allowed to run through the ion source for approximately 30 minutes. After this time interval, the electron beam was turned on, adjusted and focussed properly, the ion source, SEM and magnet high voltages were also turned on and adjusted. To assure that



the emission has reached a constant value, the system was allowed to run for another fifteen minutes before a complete spectrum of the mass range pertinent to the halide ion under consideration was taken and studied. From these spectra, the equilibrium constants, for the reactions which were taken place in the ion source at that particular temperature, were determined. For each temperature, several runs were made at different partial pressures of water in the ion source. The temperature of the ion source was checked before and after each run. The variation of the ion source temperature during each run was about two degrees at the high temperature ( $200-500^{\circ}\text{C}$ ) and about one degree at temperatures below  $200^{\circ}\text{C}$ .



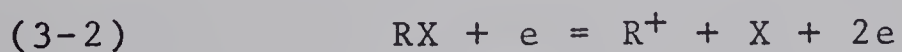
### 3 PRODUCTION OF IONS AND SAMPLING

#### 3.1 Production of Halide Negative Ions

At the normal operating condition of a conventional mass spectrometer, where ionizing electrons of 50-75 eV are employed and the gas pressure is less than  $10^{-4}$  torr, the predominant products of the electron impact ionization of a molecule, RX, are a positive ion and a secondary electron



or



Thus the probability for production of negative ions by electron impact, through dissociative electron capture (3-3) or pair production (3-4), is generally two orders of magnitude smaller than that of positive ions (36)



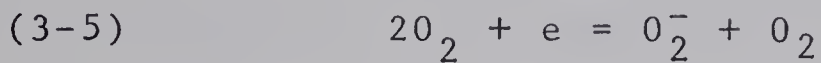
However, at high ion source pressure (above 1 torr), as in this work, negative ions can be produced in abundance approaching that of the positive ions by "three body" capture of the low energy or thermalized electrons



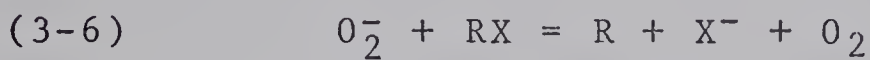
In the first part of this work, oxygen was used



as a carrier gas. In this case the thermal electrons were captured by the oxygen molecules according to the reaction (3-5)



Then they were transferred to the halogen being studied, through negative ion molecule reactions of the type (3-6)



where RX is a suitable compound of the halogen. Reaction (3-6) can occur in the ion source of a mass spectrometer, only if the electron affinity of the halogen is greater than the sum of the electron affinity of oxygen molecule and the bond energy,  $D(R-X)$ . The electron affinities of halogens are about 70-85 Kcal/mole (48) and  $EA(O_2) = 10$  Kcal/mole (38); therefore, only halogen compounds with  $D(R-X)$  below 60 Kcal/mole can be used as a source of  $X^-$ . Moreover, since the life time of the ionic species,  $O_2^-$ , is of the order of 1 to 2 milli-seconds, only fast ion molecule reactions of the type (3-6) can be used. In other words, the reaction time of (3-6) has to be short enough so that the electron transfer is completed before the ion is lost by some other processes like collisions with the walls, neutralization by positive ions, etc.

The use of carrier gas was essential for the part of this work which was carried out with the alpha source



mass spectrometer. This was due to the low sensitivity of that instrument especially for ion source pressures below 1 torr. With the electron beam mass spectrometer, where the problem of low sensitivity was no longer present, it was found more convenient to abandon the oxygen gas and use a flow of pure water vapour. In this case, although the exact process by which  $X^-$  was produced is not known, it is believed that the thermal electrons were captured by molecule RX followed by its dissociation to R and  $X^-$ .

In the following section the production of halide negative ions  $I^-$ ,  $Br^-$ ,  $Cl^-$  and  $F^-$  will be discussed individually. However, a more detailed discussion of reactions involved will be given after the results of this work have been presented in the next chapter.

### 3.1a Production of $I^-$

The iodide ion was produced from the compound  $CH_3I$ . This compound was supplied to the gas stream through a capillary, from a small glass container. The conductance of the capillary was so selected that the resulting pressure of methyl iodide in the ion source was about 30 to 50 microns. The methyl iodide used was Eastman Chemical reagent grade. No attempt was made to purify it any further. The spectra obtained by our instrument did not show any peaks which could be attributed to the impurities in methyl



iodide. In addition to the peaks due to  $I^-(H_2O)_n$ , some very small peaks were observed which could always be traced back to  $Cl^-$ . It is believed that impurities producing the chloride ion were present in our apparatus from the previous work and could not be completely removed by baking out.

### 3.1b Production of $Br^-$

The compound used in the production of bromide ion was  $CH_2Br_2$ . As in the case of  $CH_3I$ , the bromide compound was introduced into the ion source from a glass container through a capillary. By proper adjustment of the temperature of methyl dibromide container and the size of the capillary, the partial pressure of  $CH_2Br_2$  in the ion source was regulated to be about 50 microns. The methyl dibromide used was spectroscopic grade and was obtained from Eastman Chemical.

### 3.1c Production of $Cl^-$

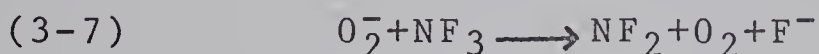
The chloride ion was produced by addition of  $CCl_4$  to the oxygen stream or to the water vapour whenever oxygen was not used. The chloride ion could also be obtained from  $CH_3Cl$  or  $CH_2Cl_2$ . Some peaks corresponding to the attachments of chloride ions to  $CH_3Cl$  or  $CH_2Cl_2$  were also observed, but the intensities of these peaks were very low in comparison to those due to  $Cl^-(H_2O)_n$ . This was due to the low concentration of  $CH_3Cl$  which was about



100 microns. The carbon tetrachloride used in this experiment was Eastman Chemical reagent grade.

### 3.1d Production of $F^-$ and $OD^-$

The fluoride ion was produced by the addition of 30 to 50 microns of  $NF_3$  to the oxygen stream. Reese and Dibeler (37) have observed the ion  $F^-$  with near 0-Volt appearance potential, in the electron impact study of  $NF_3$ . In the present study, reaction (3-7) was probably involved



In the study of the hydration of fluoride ions, the effect of chloride ion impurity was very serious. This was mostly due to the correspondence of the mass of  $^{37}Cl-(H_2O)_n$  with the mass of the series  $F^-(H_2O)_{n+1}$ . This difficulty was successfully eliminated by the use of deuterium oxide instead of water. Upon replacing of water with  $D_2O$  a new series of peaks corresponding to  $OD^-(D_2O)_n$  was observed. This observation was confirmed when the ion source temperature was raised above  $350^\circ C$  and the peak at mass number 18 was detected. It is believed that the following process is involved in the production of  $OD^-$ :



This postulate was supported by the observation of some small peaks (less than 4% of total ionization) corresponding to



$F^-(DF)_n$  and  $F^-(DF)_n(D_2O)_m$ . Since  $NF_3$  was purified by fractional distillation at  $150^{\circ}K$ , it was very unlikely that the hydrogen fluoride entered into the system with nitrogen trifluoride gas. A typical spectrum of the fluoride ion study is given in table (3-1). This spectrum was taken at ion source temperature of  $409^{\circ}C$  and deuterium oxide pressure of 3.5 mm Hg. The impurities referred to in this table are  $Cl_{35}^-$ ,  $Cl_{37}^-$  peaks along with some unknown peaks at mass number 26 and 43 and 62. The peak at 26 could be due to  $CN^-$ , and the one at 62 due to  $OCN^-(D_2O)$ . A trace of mass 42 ( $OCN^-$ ) was observed later at higher ion source temperatures. The peak at mass number 43 could not be identified at all.

Referring back to series  $OD^-(D_2O)_n$ , it should be mentioned that the ions  $OH^-(H_2O)_n$  were not observed in the study of  $Br^-$  and  $I^-$  hydration. Since the series  $OH^-(H_2O)_n$  appears at the same mass numbers as  $^{35}Cl^-(H_2O)_{n-1}$ , it cannot be said definitely whether this series was present when the  $Cl^-$  hydration was studied or not. But the isotope ratio of  $^{37}Cl^-(H_2O)_{n-1}$  to  $Cl_{35}^-(H_2O)_{n-1}$  did not indicate the presence of  $OH^-(H_2O)_n$ .

Although the exact process of production of  $OD^-$  ion cannot be determined solely by this work, the consistency of the equilibrium constants (given in chapter 5) for attachment of  $OD^-$  to  $D_2O$  indicates that the equilibrium



Table 3-1

A typical Mass Spectrum of Fluoride Ion Hydration Study at  
 $409^{\circ}\text{C}$  and  $P_{\text{D}_2\text{O}} = 3.50 \text{ mmHg}$

Ion	m/e	% of Total Ionization
$\text{OD}^-$	18	4.04
$\text{F}^-$	19	2.92
$\text{OD}^- (\text{D}_2\text{O})$	38	20.6
$\text{F}^- (\text{D}_2\text{O})$	39	56.0
$\text{F}^- (\text{DF})$	40	1.31
$\text{OD}^- (\text{D}_2\text{O})_2$	58	0.8
$\text{F}^- (\text{D}_2\text{O})_2$	59	3.9
$\text{F}^- (\text{D}_2\text{O}) (\text{DF})$	60	0.2
$\text{F}^- (\text{DF})_2$	61	0.90
Impurities	---	9.5



condition in our ion source was achieved.

### 3.2 Production of $O_2^-$ , $NO_2^-$

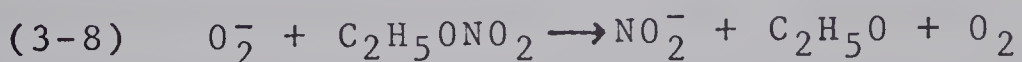
In addition to the halide negative ions and  $OD^-$ , the hydration of the ions  $O_2^-$ ,  $NO_2^-$ , was also studied. The study of the hydration of  $O_2^-$  was accomplished simply by adding known amounts of water to the oxygen stream. The major ions observed in the pure oxygen stream were  $O_2^-(H_2O)_n$ , although some small peaks due to the series  $O^-(H_2O)_n$  and  $O_3^-(H_2O)_n$  were also noticed. This observation confirmed our assumption that the majority of the negative ions produced in the ion source of both our mass spectrometers -- alpha source and electron beam system-- were due to thermal electrons with energy less than 3.5 eV, since the production of  $O^-$  requires electrons with energy higher than 3 eV (38).

In the study of  $NO_2^-$ , at first it was attempted to produce  $NO_2^-$  by the addition of nitrogen dioxide gas into the oxygen stream. However, this attempt proved unsuccessful. The series  $NO_2^-(H_2O)_n$  could not be observed, but instead the series  $NO_2^-(HNO_2)_n$  and  $NO_2^-(HNO_3)_n$  were seen, with the  $NO_2^-(HNO_2)_n$  being the major peaks. The presence of the series  $NO_2^-(HNO_2)_n$  and  $NO_2^-(HNO_3)_n$  could be attributed to the formation of  $HNO_2$  and  $HNO_3$  by the following reactions:





nitrogen oxide being present as impurity in  $\text{NO}_2$  gas. The identities of  $\text{NO}_2^-(\text{HNO})_n$  and  $\text{NO}_2^-(\text{HNO}_3)_n$  were established by replacing water with  $\text{D}_2\text{O}$  and observing the resulting mass shift in the clusters. When nitrogen dioxide was purified by low temperature distillation thus removing  $\text{NO}$ , the ions  $\text{NO}_2^-(\text{HNO}_2)_n$  were no longer the major series, they were overtaken by ions  $\text{NO}_2^-(\text{HNO}_3)_n$ . It was observed that the preferential attachment of  $\text{NO}_2^-$  to nitrous and nitric acid in place of water could occur even when no  $\text{NO}_2$  was added to the water-oxygen stream. In this case, the only possible source of  $\text{NO}_2^-$ ,  $\text{HNO}_3$ ,  $\text{HNO}_2$  was the minute quantities of these acids absorbed on the glass walls of the gas handling plant. Considering that the flow of gas through the ion source was over 300 cc/min and the partial pressure of water in the ion source was 100 microns, the equilibrium concentration ratio of nitrous and nitric acid to water could not possibly be over  $10^{-3}$ . Thus the  $\text{HNO}_3$  molecule attaches preferentially by a factor of at least 1000. Finally, the  $\text{NO}_2^-$  was successfully produced from  $\text{C}_2\text{H}_5\text{ONO}_2$ . Ethyl nitrate was added to the oxygen stream so that a partial pressure of approximately 100 microns of  $\text{C}_2\text{H}_5\text{ONO}_2$  was obtained. The reaction involved was possibly



The available thermochemical data:  $\text{EA}(\text{NO}_2) = 84 \text{ Kcal/mole}$



(48)  $EA(O_2) = 10 \text{ Kcal/mole}$  (38) and  $D(C_2H_5O - NO_2) = 36 \text{ Kcal/mole}$  (48) will give a value of  $-38 \text{ Kcal/mole}$  for the enthalpy change of the reaction (3-8).

### 3.3 Ion Sampling

There are two basic assumptions made in this work, and in fact, in any other mass spectrometry study of the gas phase solvation reactions;

- (a) equilibrium conditions prevail in the ion source,
- (b) ion currents recorded by the mass spectrometer are proportional to the concentration of the respective ions in the ion source.

#### 3.3a Equilibrium Condition in the Ion Source

The achievement of equilibrium in the ion source can be studied best by the investigation of the conditions of the ions from the time of their formation to the time of their departure from the ion source through the ion exit slit. After their production, in the ionization region of the ion source, some of the primary negative ions will diffuse out of this region. In their way towards the walls of the ion source where they are discharged, the primary ions will collide with the solvating molecules. Some of these collisions may result in the attachment of the ion to the neutral molecules thus forming ion-clusters. The ion-clusters can stabilize themselves by giving up their

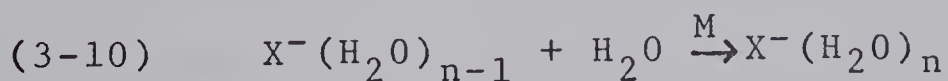


excess energy through collisions with other molecules (third body collisions). In order that equilibrium conditions prevail, this stabilization of ion clusters should be achieved and all reactions involved be completed before the ion clusters diffuse out of the ion exit slit.

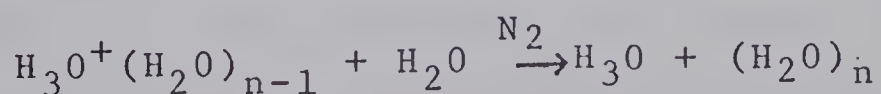
The time,  $t$ , necessary for the ions to travel the distance from the ionization region to the ion exit slit can be estimated by the approximate equation given below, which establishes a relationship between the time,  $t$ , required by a particle to diffuse the distance,  $d$  (39), and the diffusion coefficient,  $D$ .

$$(3-9) \quad t \approx \frac{d^2}{2D}$$

In the present case  $d$  is the distance from the electron beam plate to the ion exit slit and is equal to 4 mm,  $D$  is the diffusion coefficient of the ions through the gas and is taken as  $50 \text{ cm}^2/\text{sec}$  (39) for an ion source pressure of one mm Hg and a temperature of  $300^\circ\text{K}$ . Thus, the diffusion time  $t$  is calculated to be 1.6 milli-seconds. The half life of the attachment reaction



can be calculated, if we assume a value for the rate constant,  $K$ . The reaction



has been studied by A. Good, D. Durden and P. Kebarle (13)



kinetically. They found the third order rate constants to be around  $1 \times 10^{-27} \text{ cc}^2/\text{molecule}^2\text{-sec}$ . As an approximation, the same value can be assumed for the rate constant of the reaction (3-10). The half-life  $t_{1/2}$  is then given by

$$(3-11) \quad t_{1/2} = \frac{1}{1 \times 10^{-27} [\text{H}_2\text{O}]^2}$$

where  $[\text{H}_2\text{O}]$  is the concentration of water in the ion source, in molecules/cc. At an ion pressure of 1 mm Hg and a temperature of  $298^\circ\text{C}$ , the water concentration is equal to  $3 \times 10^{16}$  molecules/cc. Introducing this value, into equation (3-11), the half life comes out to about one microsecond. This is three order of magnitude smaller than the ion residence time calculated from equation (3-9).

The ion residence time calculated from equation (3-9) represents a statistical average value, thus it applies to ions with relatively high observed ion intensities. The equilibrium conditions, therefore, can be assumed only for the ions which are represented by a major peak in the spectra.

In addition to the diffusion process, the ions can be removed from the ion source by mass flow. It has been shown (35), however, that the mass flow does not become significant until about 1 mm from the exit slit. Thus starting from the electron beam, the ions are transported for the first 2 to 3 mm by diffusion and in the last one mm by mass flow.



### 3.3b Relation of the Ion Current to the Ion Concentration

From the time of their formation in the ion source to the time of their recording by the detection system, the ion-clusters are engaged in a number of processes. A few of these processes may discriminate against one or the other type of ions. Some of these discriminatory processes will be discussed below.

#### (i) Discrimination in Transport Through the Ion Source

The diffusion coefficient of an ion is inversely proportional to the square root of the mass of the ion (39). Therefore, one expects that the lighter ions would travel, through the ion source, faster and would reach the ion exit slit in a shorter interval than the heavier ions. Thus, the actual concentration of the ions with smaller mass would be less than what is represented by the recorded signal. In short, there would be a discrimination against the heavier ions by the diffusion process. However, since the average half life of the clustering reaction is short in comparison to the ion residence time of the ion, and a cluster,  $X^-(H_2O)_n$ , gains and loses water molecules at a fast rate; all the clusters would have the same average molecular weight and their diffusion coefficient would be equal.

#### (ii) Discrimination in Passage Through Exit Slit

The flow through the ion exit slit may also cause discriminations. If the width of the ion exit slit is much



larger than the mean free path of the ion cluster- water molecule collision, the condition of molecular flow would cease to exist. This will result in the cooling of the gas due to adiabatic expansion in vacuum and consequently, a trend towards heavier clusters would appear. For a slit of 10 microns, the maximum allowable pressure of the ion source is 6 mm Hg (11).

(iii) Discrimination due to Stripping Outside of Ion Source

If the pressure in the region just outside of the ion exit slit is high, some ion molecule collisions may take place in the vacuum region between the ion source exit slit and the first cone electrode. Due to the presence of the ion accelerating field, these collisions occur with kinetic energies much higher than thermal. As a result of these collisions, the heavier ion-clusters may dissociate. To avoid this handicap and also the effect of adiabatic expansion, discussed in previous section, almost all runs were made with the ion source pressure below 5 mm Hg.

(iv) Discrimination in Mass Analyzer Tube

In general, in a magnetic mass analyzer tube such as the one used in this work, any loss of ions due to elastic scattering, collisions with the wall, etc., will be the same for all ions. Consequently, we can assume that the effect of mass discrimination in the analyzer



tube was negligible.

(v) Discrimination in the Ion Current Detection System

It has been reported (40) that the emission of electrons from the cathode of the secondary electron multiplier (SEM), upon the impinging of the incoming ions, is dependent on the velocity of the ions as well as their chemical composition. Thus, the gain of the multiplier would not be the same even for two isobaric ions such as  $N^+$  and  $(CH_2)^+$  (41). The reason for this difference is that, the multi-atom ions may break up when they strike the surface of the SEM cathode and act as a group of particles instead of just one ion.

When a secondary electron multiplier is used for the counting ions, as in this work, it is the efficiency, not the gain, which is of prime concern. The efficiency is the ratio of the number of output pulses to the number of the incoming ions. Unfortunately, due to the low negative ion current ( $10^{-14}A$ ), it was not possible to measure the efficiency of the electron multiplier used in this work. However, S. K. Searles, while studying (35) the positive ions  $H^+(H_2O)_n$  and  $NH_4^+(NH_3)_n$ , determined the gain of a similar electron multiplier. He found that the maximum error introduced by the SEM discrimination in the ion-cluster measurements was about 20%. Considering the fact that the efficiency of an electron multiplier is not affected



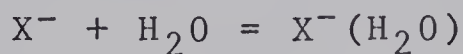
by the factors which cause mass discrimination as much as its gain, our maximum error due to the SEM discrimination should not be over Searles' value of 20%.



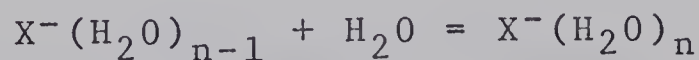
4 RESULTS AND DISCUSSIONS OF HYDRATION OF  
HALIDE NEGATIVE IONS,  $X^-$

4.1 Introduction and Thermodynamic Relations

After their formation, some of the halide negative ions diffuse out of the ionization region of the ion source and react with the water molecules and are converted to ion clusters,  $X^-(H_2O)_n$ , by the following sequence:



•  
•  
•  
•  
•



provided that the equilibrium is achieved in the ion source, the equilibrium constant can be calculated from

$$K_{n-1,n} = \frac{P_{X^-(H_2O)_n}}{P_{X^-(H_2O)_{n-1}} P_{H_2O}}$$

The partial pressure of  $H_2O$ ,  $P_{H_2O}$  is determined by direct pressure measurement or by the weight loss of water (see chapter 2) and the ratio

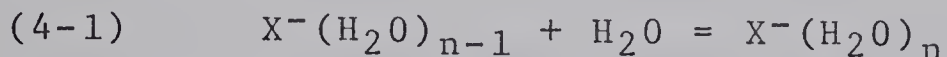
$$\frac{P_{X^-(H_2O)_n}}{P_{X^-(H_2O)_{n-1}}}$$

is assumed to be the same as the ratio of the ion currents



$$\frac{I_{X^-(H_2O)_n}}{I_{X^-(H_2O)_{n-1}}}$$

Determination of the equilibrium constants, at different ion source temperatures, will result in the calculation of the thermodynamic values  $\Delta H^\circ$ ,  $\Delta G^\circ$ ,  $\Delta S^\circ$  for the reaction



$\Delta H_{n-1,n}^\circ$  is determined from the plot of the equilibrium constant,  $K_{n-1,n}$ , versus reciprocal of temperature (in degrees Kelvin).  $\Delta G_{n-1,n}^\circ$  from

$$(4-2) \quad \Delta G_{n-1,n}^\circ = -RT \log_e K_{n-1,n}$$

where R is the universal gas constant,  $\Delta S_{n-1,n}^\circ$  is obtained from

$$(4-3) \quad \Delta S_{n-1,n}^\circ = \frac{\Delta H_{n-1,n}^\circ - \Delta G_{n-1,n}^\circ}{T}$$

#### 4.2 Presentation of the Results and General Discussion

The equilibrium constants obtained for the gas phase hydration of the fluoride, chloride, bromide and iodide ions are presented in figures (4-1) to (4-16). It can be seen that at any one temperature, the values of  $K_{n-1,n}$  are relatively constant, over the pressure range covered. This independency of  $K_{n-1,n}$  of water pressure indicates that, equilibrium conditions indeed prevailed in the ion source and no significant amounts of collisions occurred outside of the ion source.



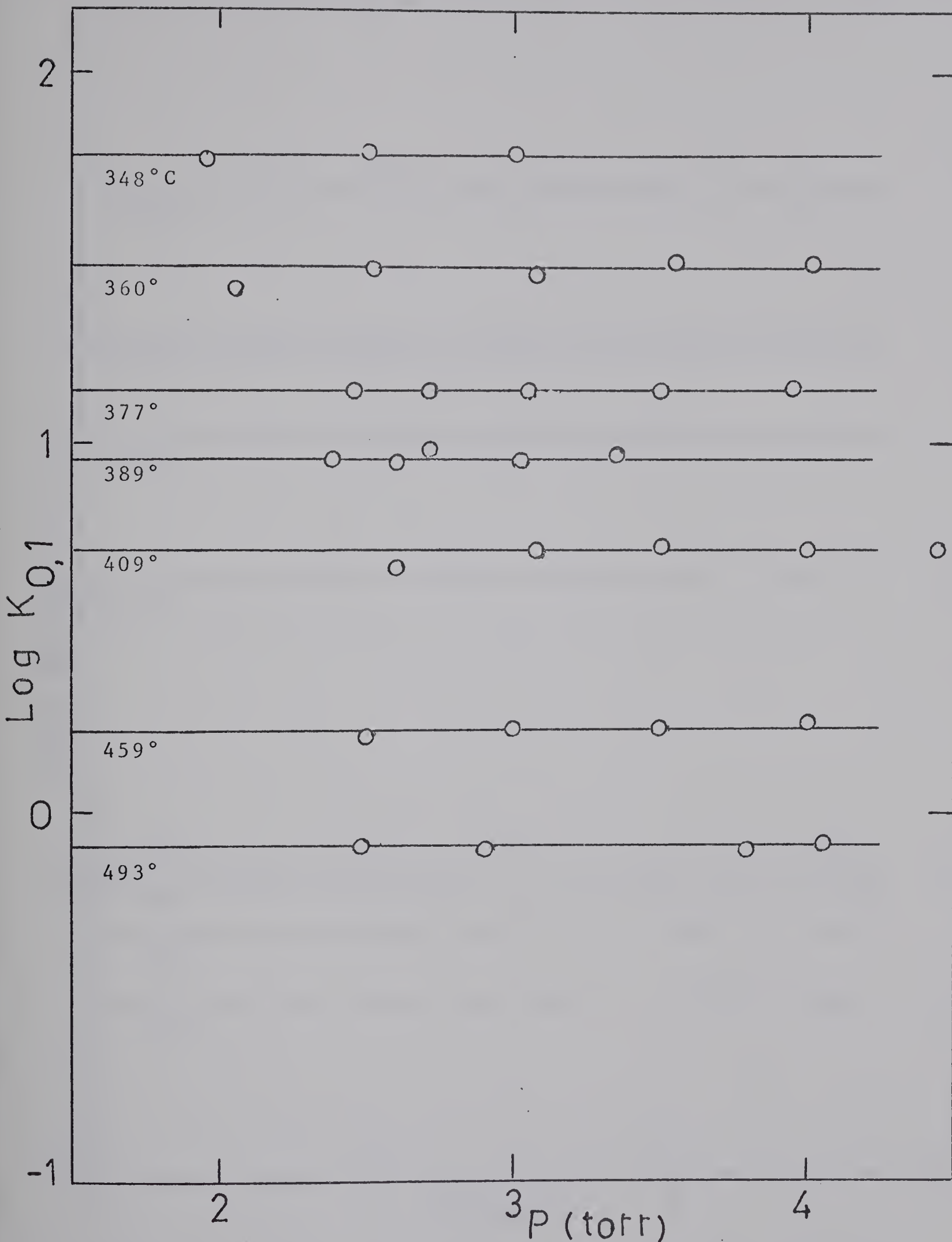


Figure 4-1: Plots of  $\text{Log } K_{0,1}$  for the Gas Phase Hydration of  $\text{F}^-$ , at Various Temperatures, Versus Pressure of  $\text{D}_2\text{O}$ .



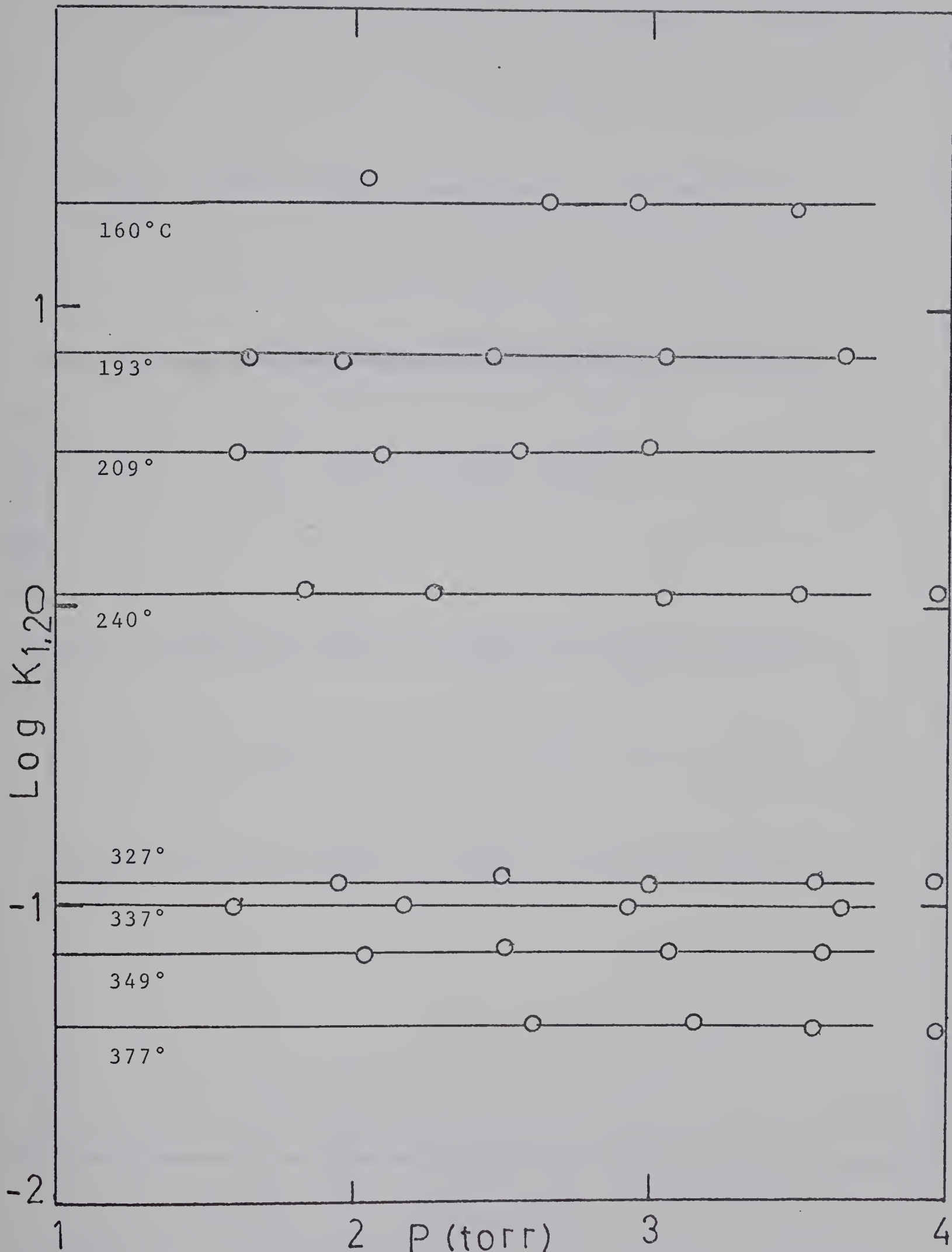


Figure 4-2: Plots of  $\log K_{1,2}$  for the Gas Phase Hydration of  $F^-$ , at Various Temperatures, Versus Pressure of  $D_2O$ .



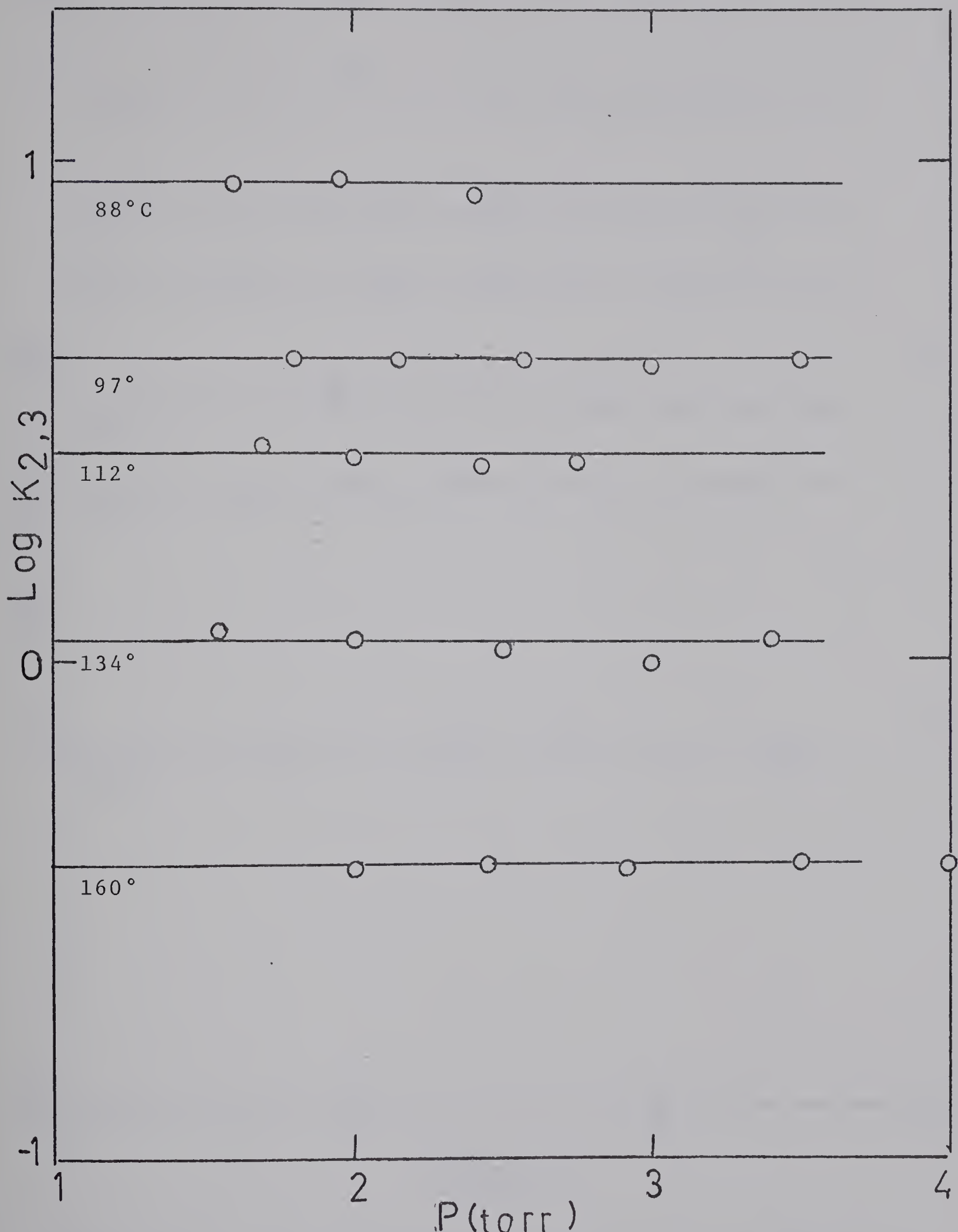


Figure 4-3: Plots of  $\text{Log } K_{2,3}$  for the Gas Phase Hydration of  $\text{F}^-$ , at Various Temperatures, Versus Pressure of  $\text{D}_2\text{O}$ .



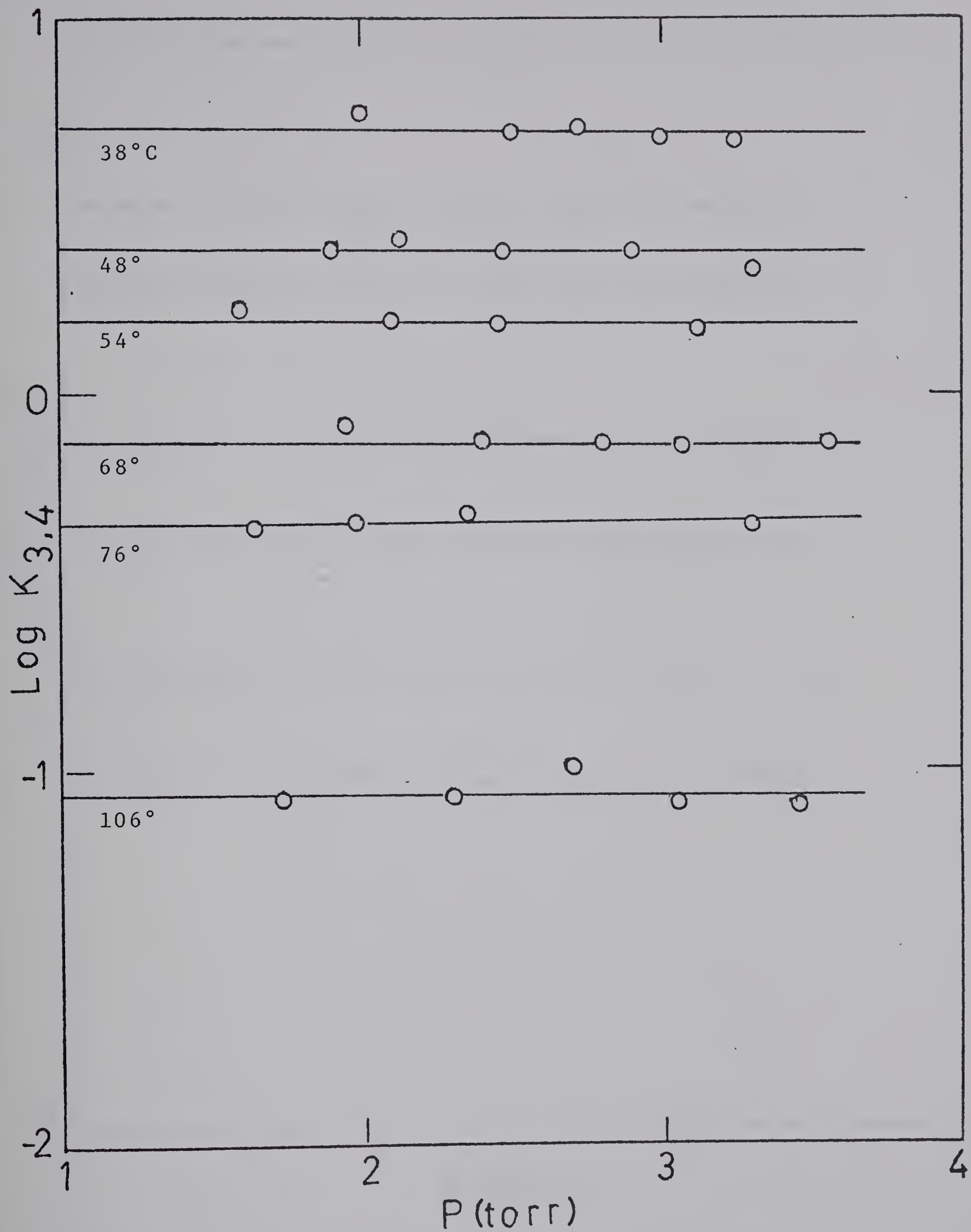


Figure 4-4: Plots of  $\text{Log } K_{3,4}$  for the Gas Phase Hydration of  $\text{F}^-$ , at Various Temperatures, Versus Pressure of  $\text{D}_2\text{O}$ .



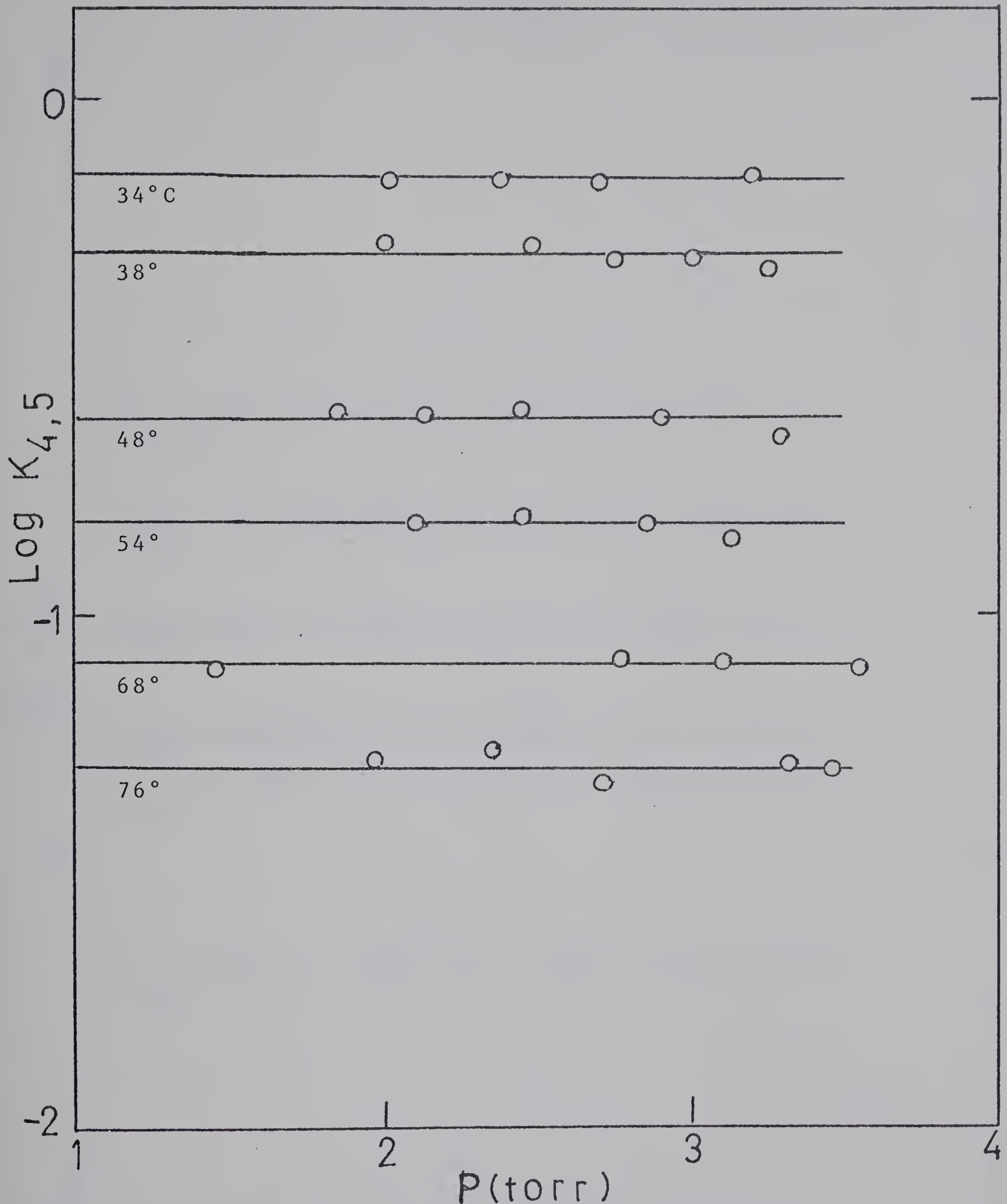


Figure 4-5: Plots of  $\text{Log } K_{4,5}$  for the Gas Phase Hydration of  $\text{F}^-$ , at Various Temperatures, Versus Pressure of  $\text{D}_2\text{O}$ .



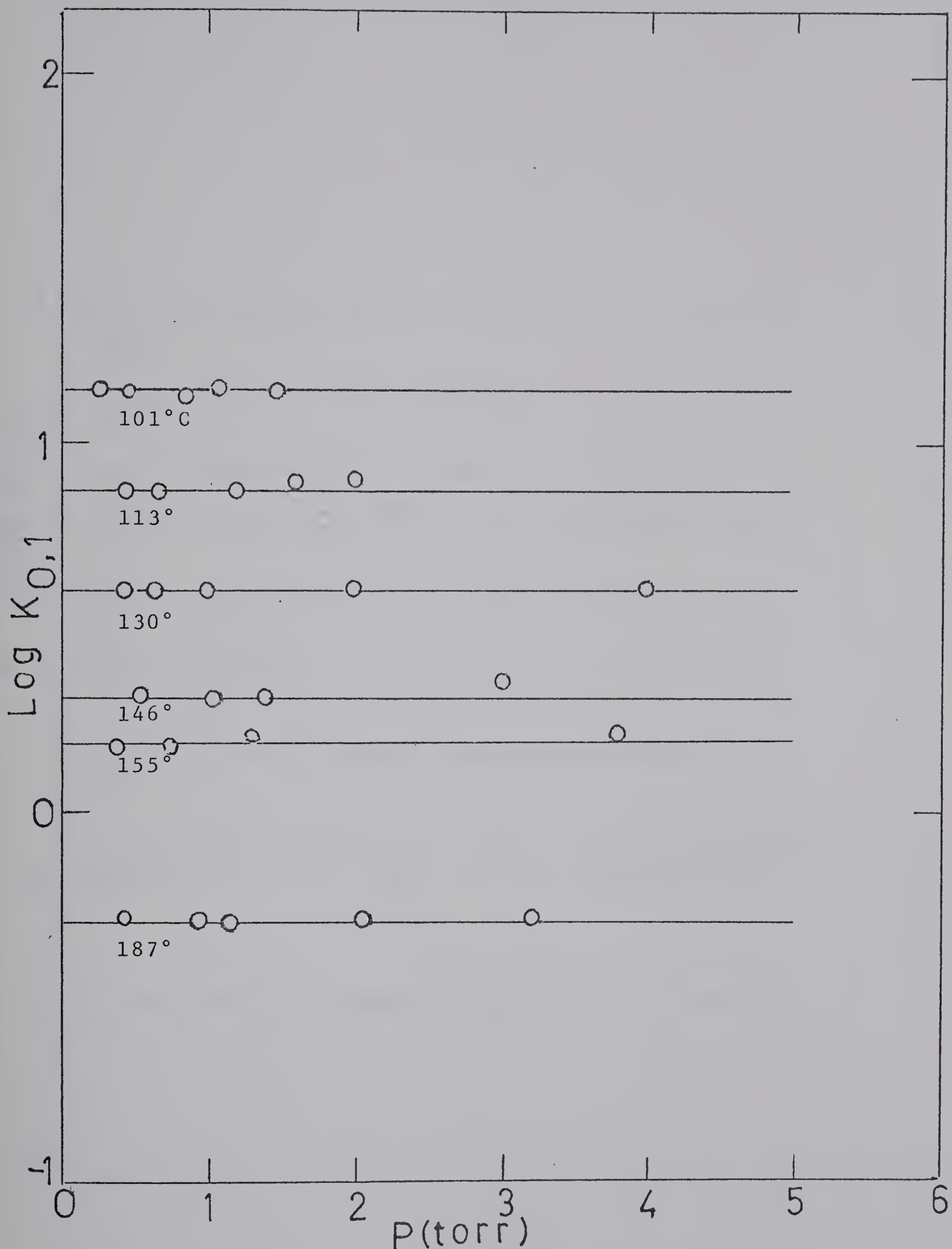


Figure 4-6: Plots of  $\log K_{0,1}$  for the Gas Phase Hydration of  $\text{Cl}^-$  at Various Temperatures, Versus Pressure of  $\text{H}_2\text{O}$ .



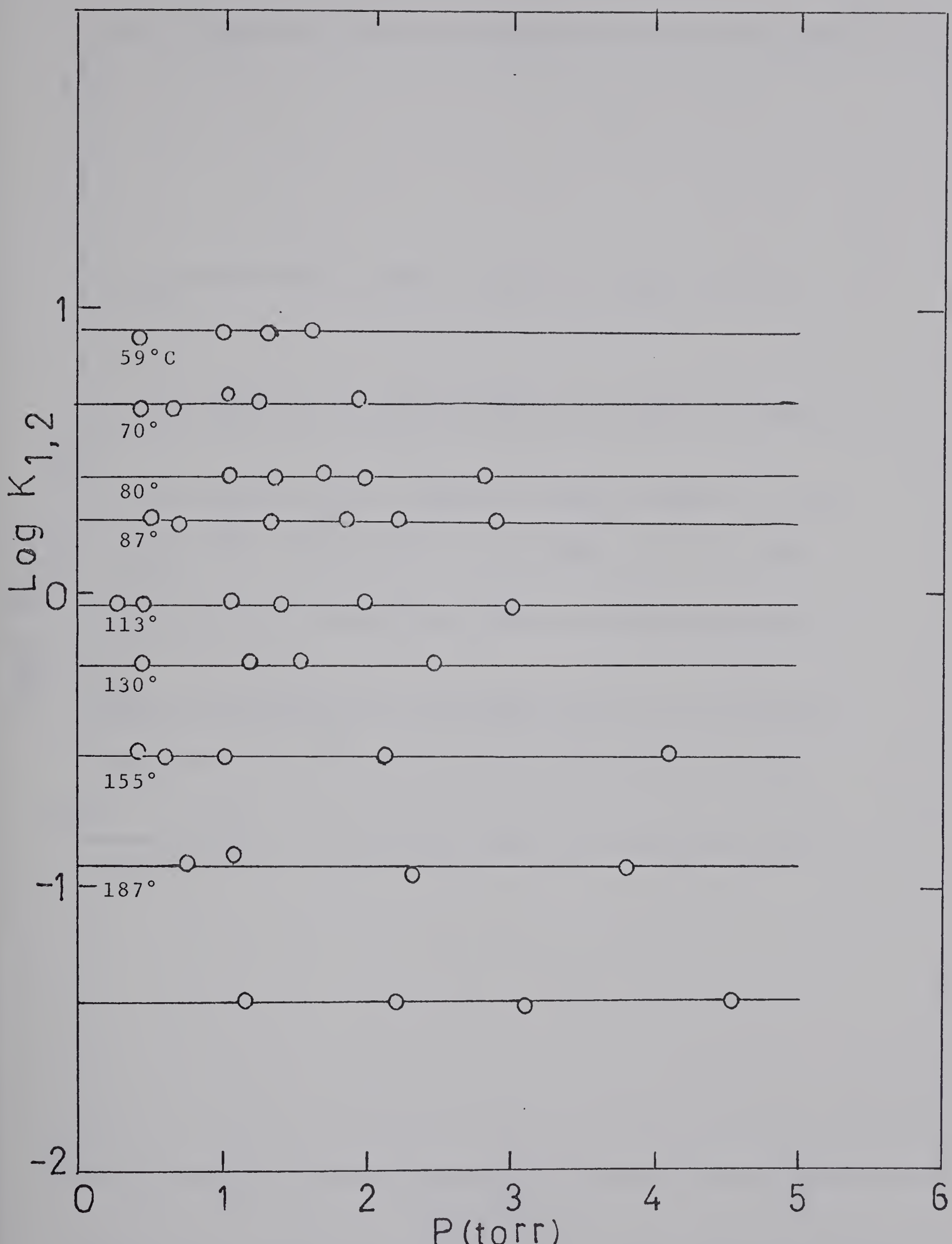


Figure 4-7: Plots of  $\log K_{1,2}$  for the Gas Phase Hydration of  $\text{Cl}^-$ , at Various Temperatures, Versus Pressure of  $\text{H}_2\text{O}$ .



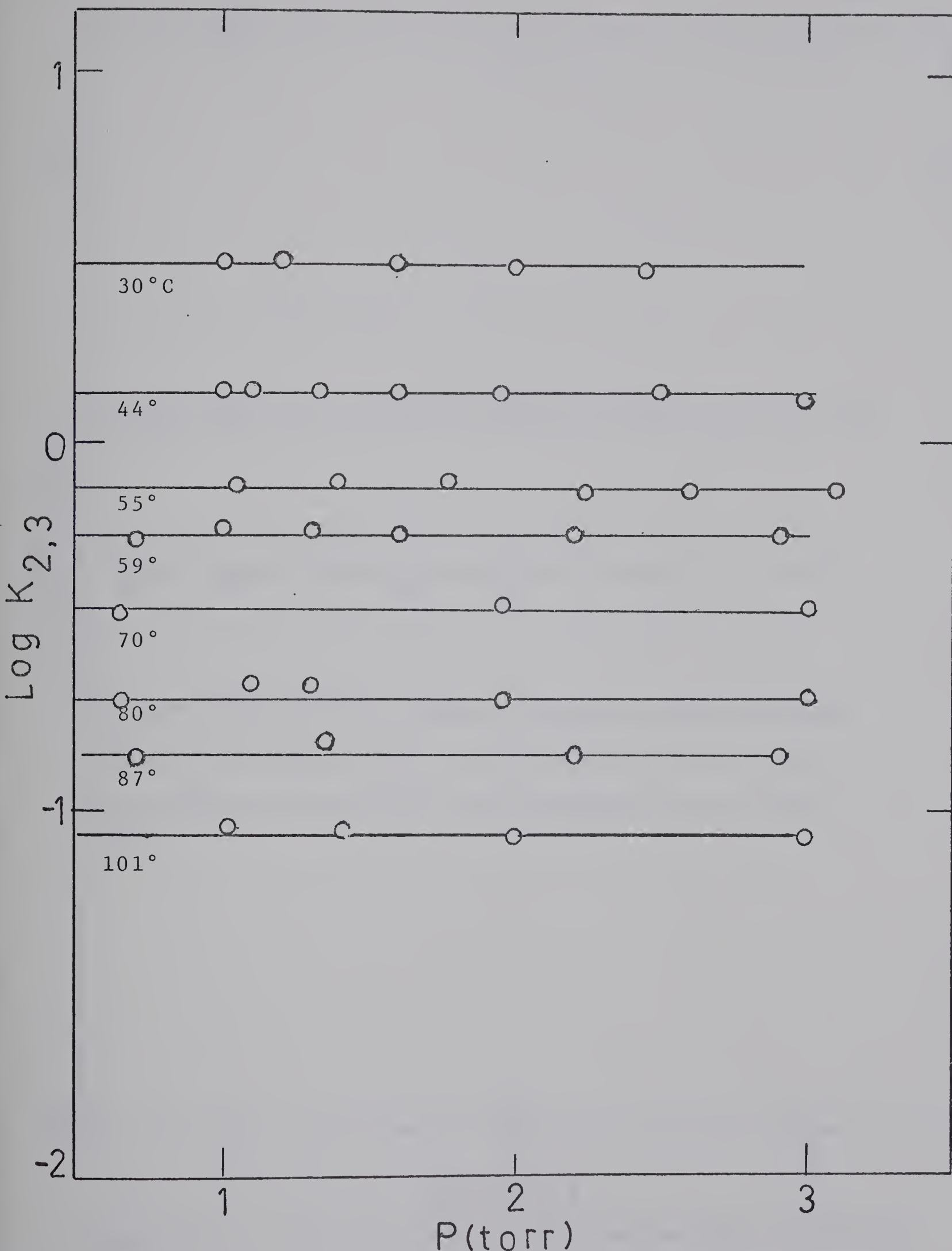


Figure 4-8: Plots of Log K<sub>2,3</sub> for the Gas Phase Hydration of Cl<sup>-</sup> at Various Temperatures, Versus Pressure of H<sub>2</sub>O.



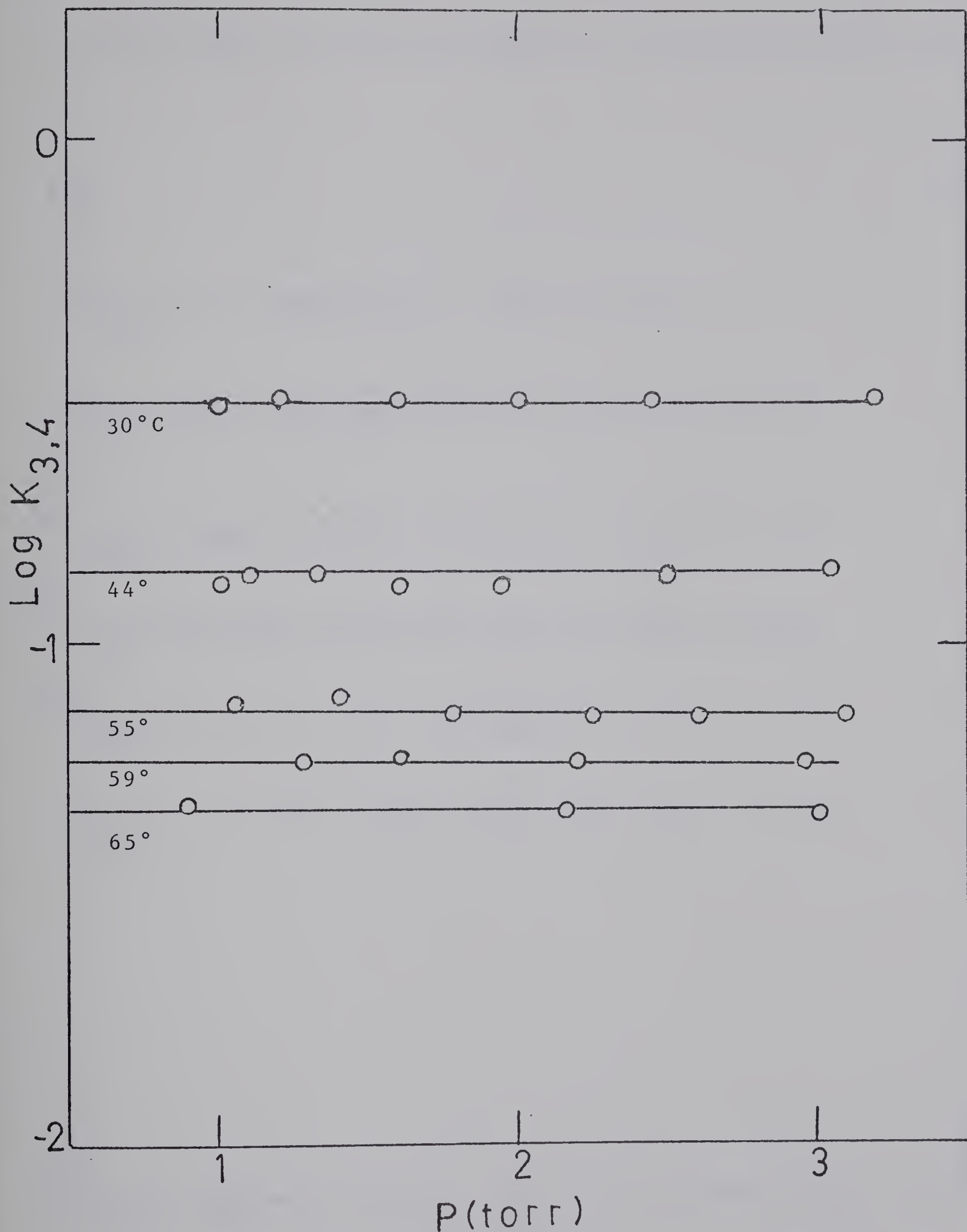


Figure 4-9: Plots of  $\text{Log } K_{3,4}$  for the Gas Phase Hydration of  $\text{Cl}^-$  at Various Temperatures, Versus Pressure of  $\text{H}_2\text{O}$ .



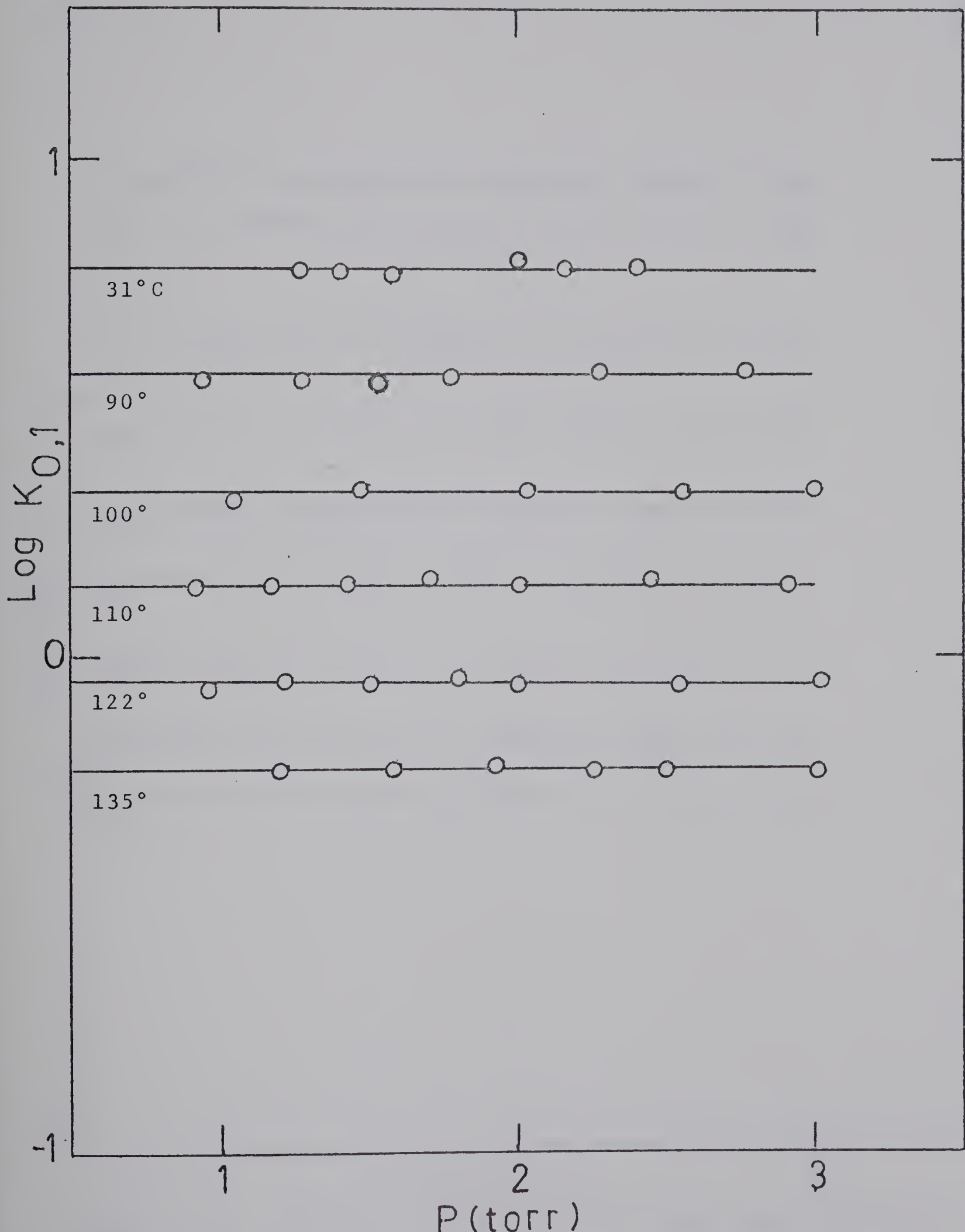


Figure 4-10: Plots of  $\text{Log } K_{0,1}$  for the Gas Phase Hydration of  $\text{Br}^-$ , at Various Temperatures, Versus Pressure of  $\text{H}_2\text{O}$ .



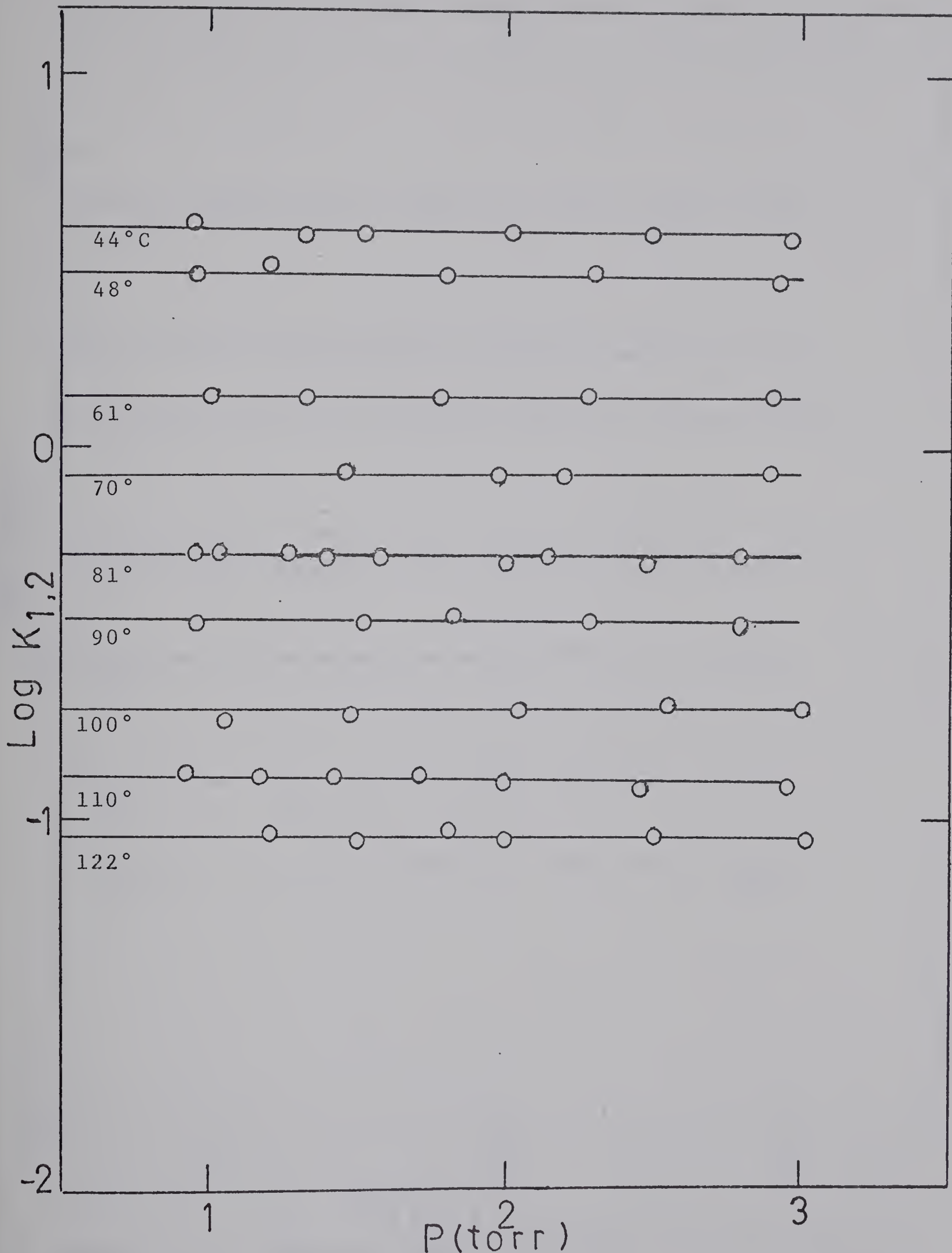


Figure 4-11: Plots of  $\text{Log } K_{1,2}$  for the Gas Phase Hydration of  $\text{Br}^-$  at Various Temperatures, Versus Pressure of  $\text{H}_2\text{O}$ .



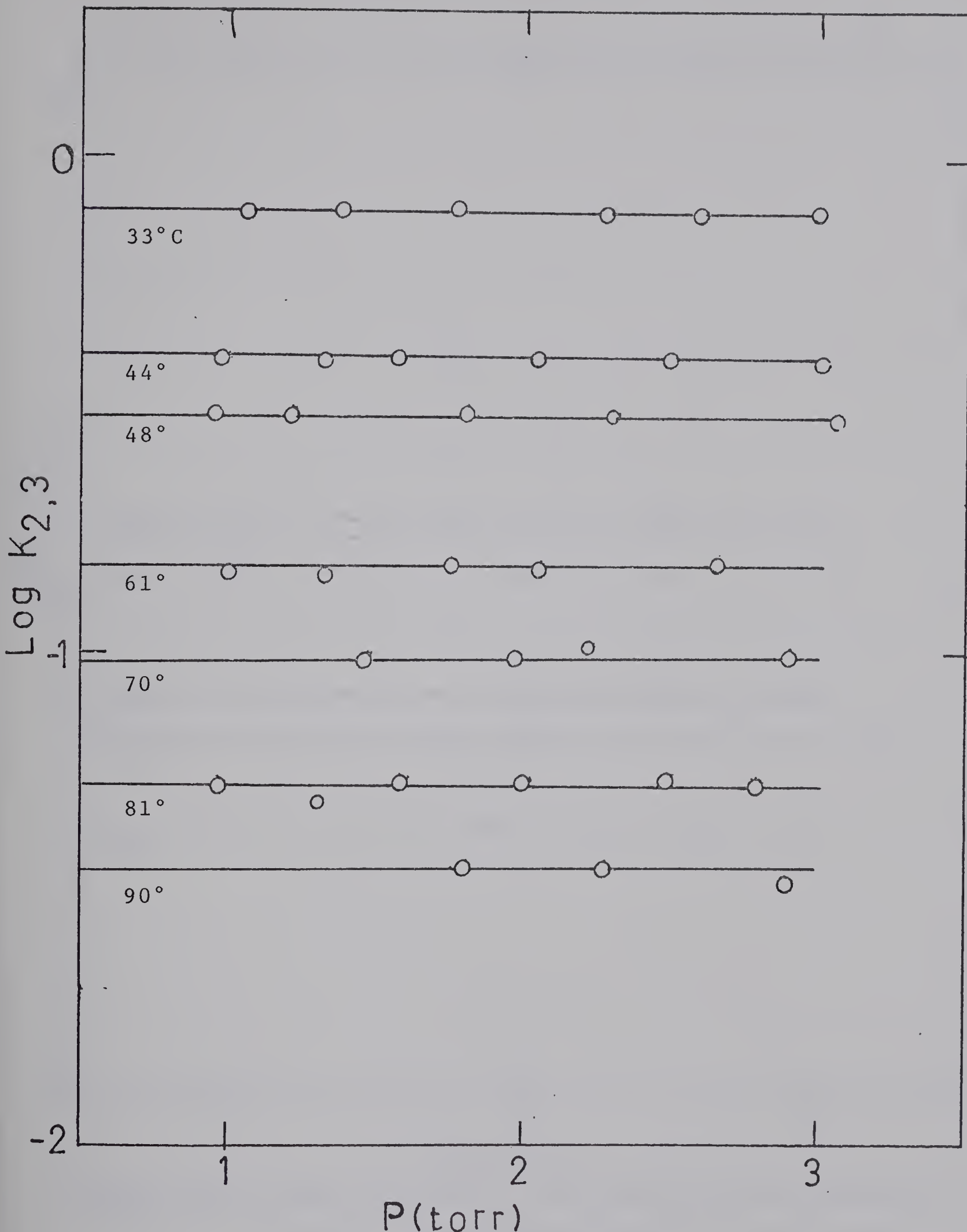


Figure 4-12: Plots of  $\text{Log } K_{2,3}$  for the Gas Phase Hydration of  $\text{Br}^-$  at Various Temperatures, Versus Pressure of  $\text{H}_2\text{O}$ .



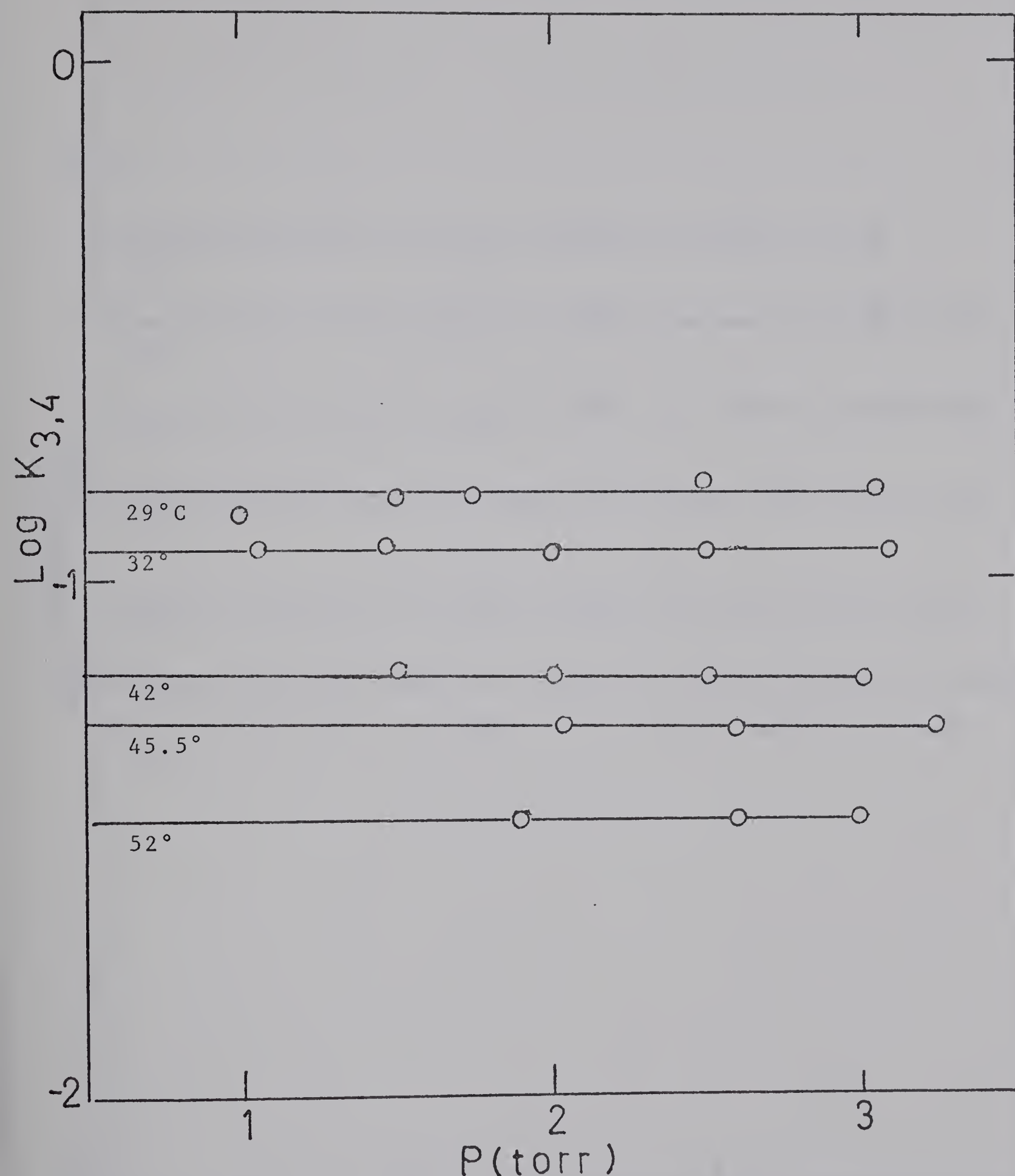


Figure 4-13: Plots of  $\log K_{3,4}$  for the Gas Phase Hydration of  $\text{Br}^-$ , at Various Temperatures, Versus Pressure of  $\text{H}_2\text{O}$ .



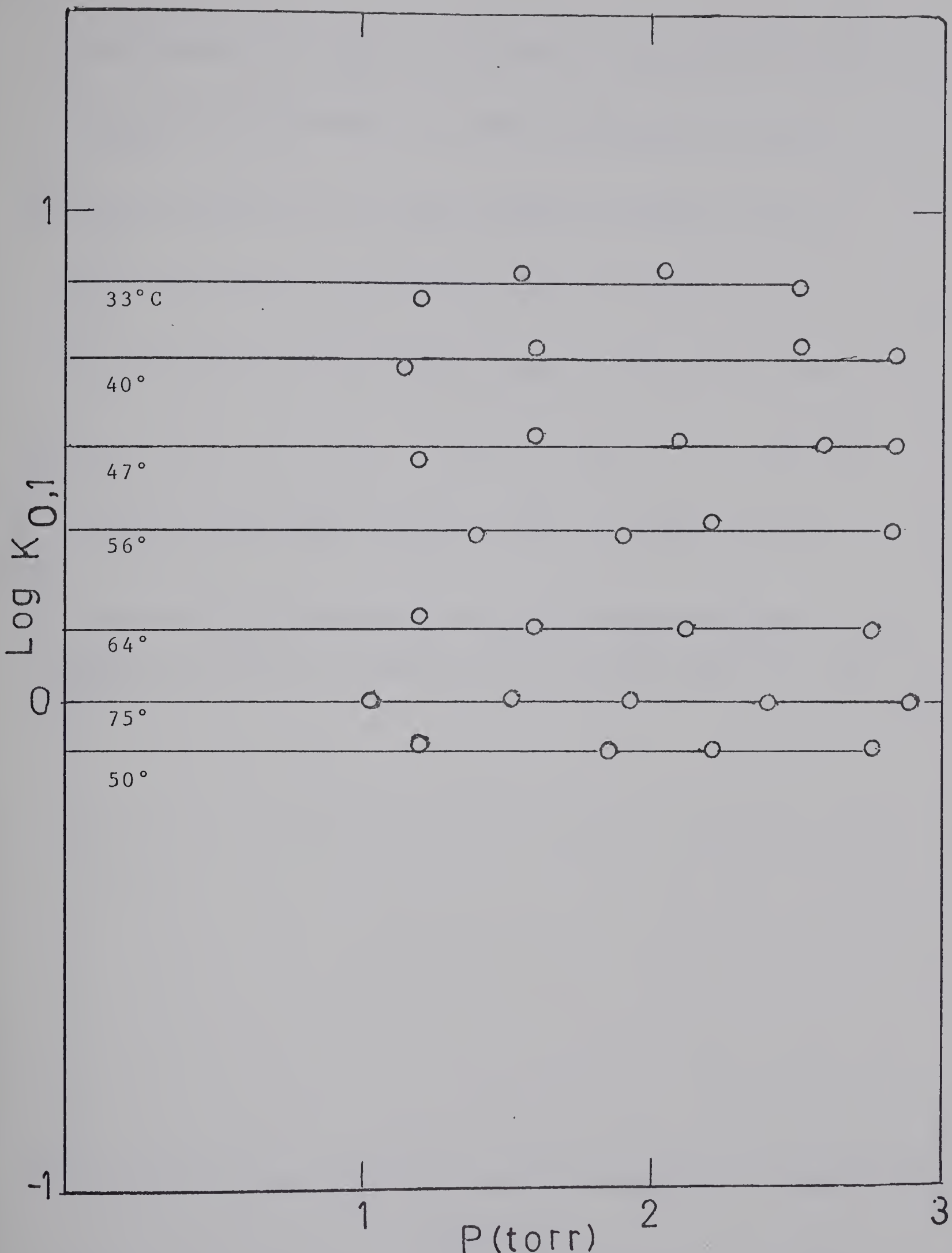


Figure 4-14: Plots of  $\text{Log } K_{0,1}$  for the Gas Phase Hydration of  $\text{I}^-$ , at Various Temperatures, Versus Pressure of  $\text{H}_2\text{O}$ .



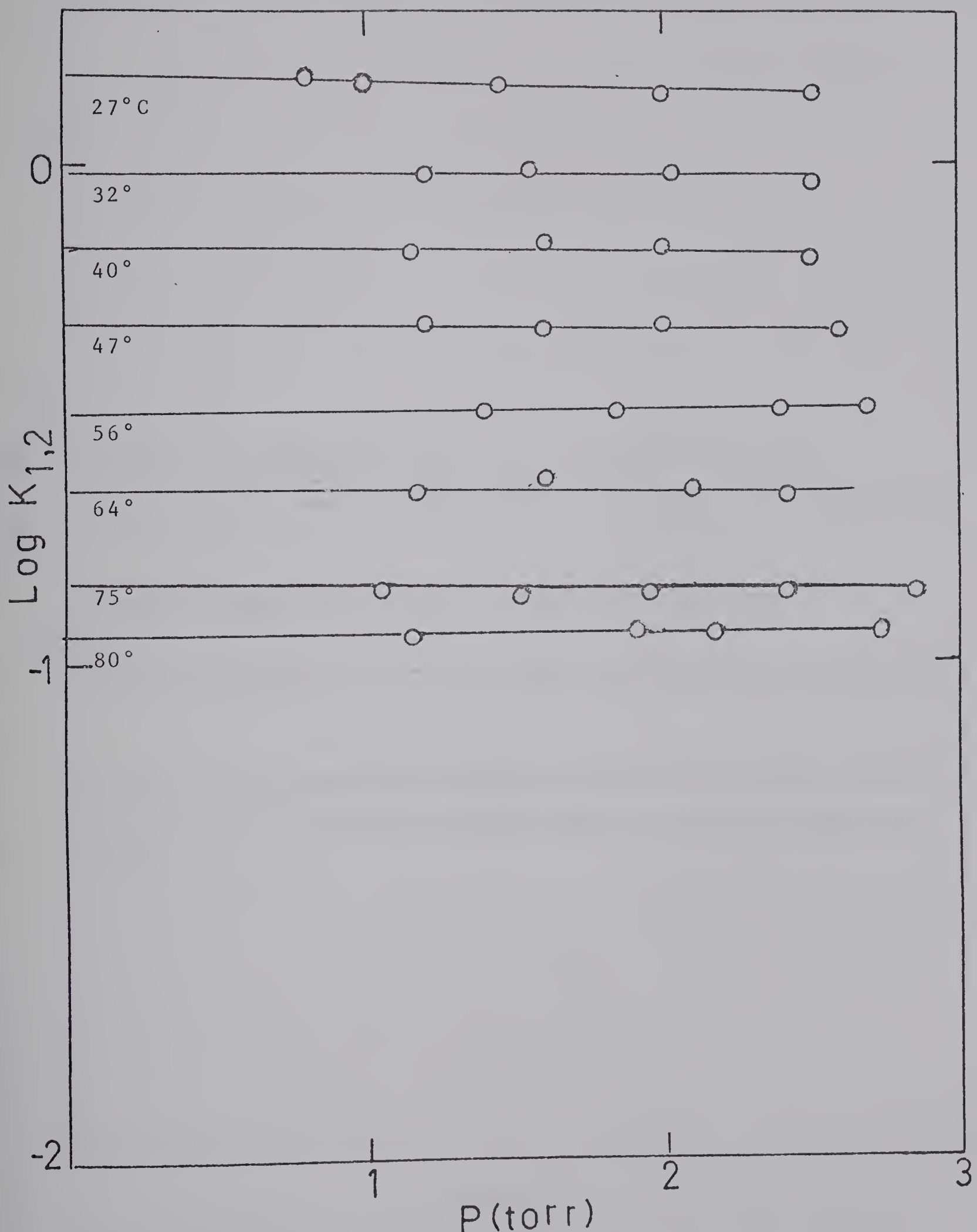


Figure 4-15: Plots of  $\log K_{1,2}$  for the Gas Phase Hydration of  $I^-$ , at Various Temperatures, Versus Pressure of  $H_2O$ .



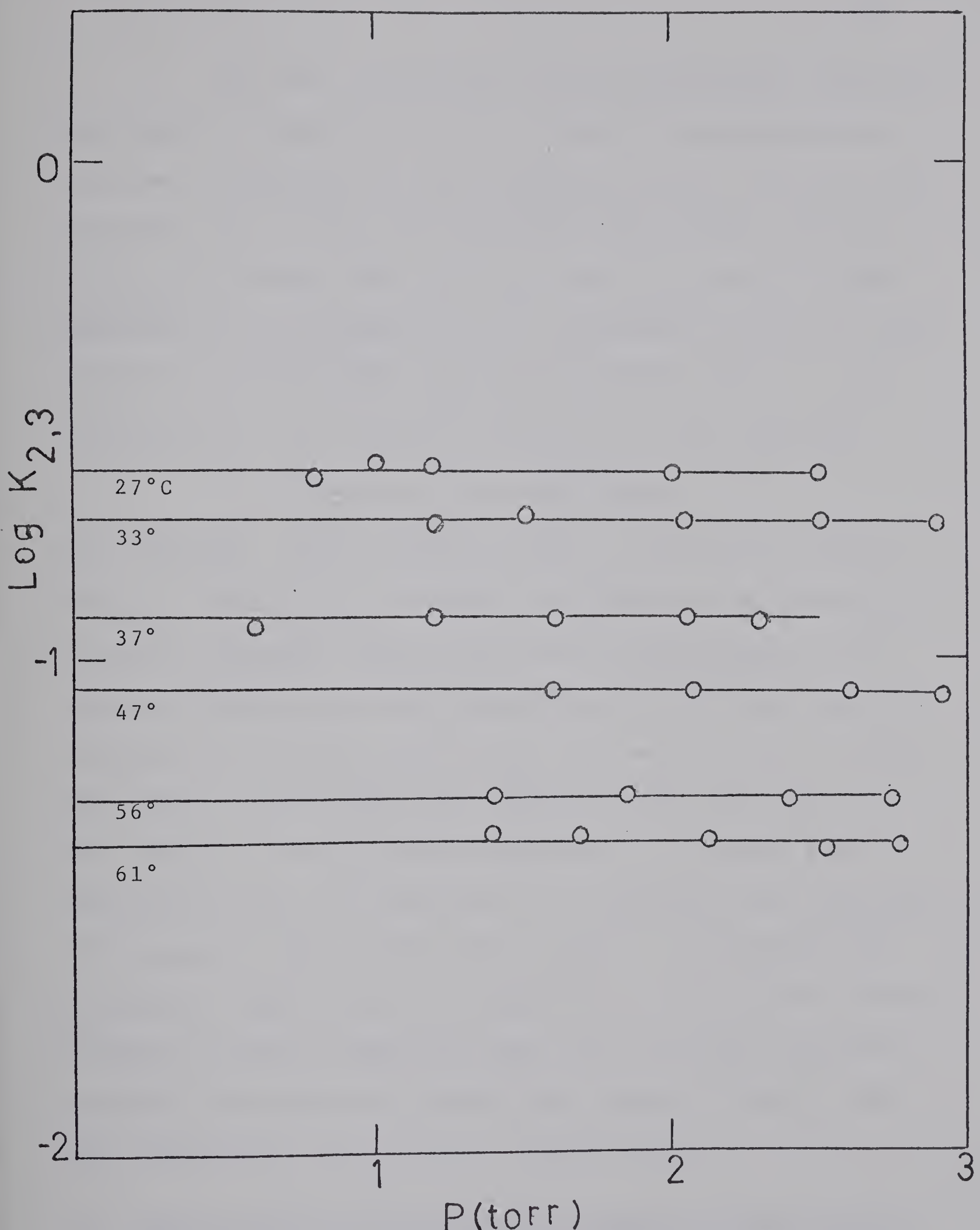


Figure 4-16: Plots of  $\text{Log } K_{2,3}$  for the Gas Phase Hydration of  $\text{I}^-$ , at Various Temperatures, Versus Pressure of  $\text{H}_2\text{O}$ .



The Van't Hoff plots of the equilibrium constants are shown in figures (4-17) to (4-20). The equilibrium constants presented in these figures are,  $K_{0,1}$  to  $K_{4,5}$  for fluoride,  $K_{0,1}$  to  $K_{3,4}$  for chloride and bromide, and  $K_{0,1}$  to  $K_{2,3}$  for iodide ion clusters. From the least squares treatment of the values of  $K_{n-1,n}$  measured at various pressures and temperatures, the slope of Van't Hoff line and, consequently, the change of enthalpy for the reaction



was obtained. These values of  $\Delta H_{n-1,n}^\circ$  as well as values of  $\Delta G_{n-1,n}^\circ$  and  $\Delta S_{n-1,n}^\circ$  at  $298^\circ K$  are presented in tables (4-1) to (4-4). In figure (4-21) the relative abundance of the cluster  $X^-(H_2O)_n$ , at the temperature of  $292^\circ K$  and one torr pressure, is plotted for  $F^-$ ,  $Cl^-$ ,  $Br^-$  and  $I^-$  ion clusters. This figure illustrates the effect of the ionic size on the extent of the gas phase hydration. As can be seen from this figure, as the size of the negative ion increases the number of water molecules attached to the halide ion decreases. Thus while it is possible to observe the cluster  $F^-(H_2O)_5$  at room temperature and one torr water pressure; in order to be able to observe the cluster  $I^-(H_2O)_5$ , the ion source has to be cooled to about  $250^\circ K$ .

#### 4.3 Calculation of Electrostatic Potential Energy of The Negative Ion Clusters

Theoretical electrostatic calculations of potential



Table 4-1

Experimental Thermodynamic Values for the Gas Phase Reaction



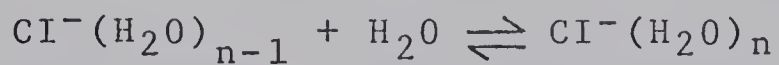
Reaction n-1, n	$-\Delta H_{n-1, n}$ Kcal/mole	$-\Delta G^\circ_{n-1, n} (298^\circ)$ Kcal/mole	$-\Delta S^\circ *_{n-1, n}$ e.u.
0, 1	23.3	18.1	17.4
1, 2	16.6	11.0	18.7
2, 3	13.7	7.64	20.4
3, 4	13.5	5.46	26.9
4, 5	13.2	4.07	30.68

\*Calculated for 298°K



Table 4-2

Experimental Thermodynamic Values for the Gas Phase Reactions



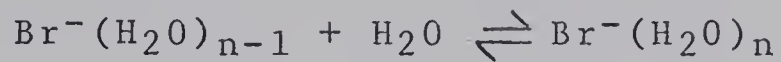
Reaction	$-\Delta H_{n-1,n}$ Kcal/mole	$-\Delta G_{n-1,n}^\circ (298^\circ)$ Kcal/mole	$-\Delta S_{n-1,n}^\circ$ e.u.
n-1, n			
0, 1	13.1	8.17	16.5
1, 2	12.7	6.49	20.8
2, 3	11.7	4.84	23.2
3, 4	11.1	3.42	25.8

\*Calculated for 298°K



Table 4-3

Experimental Thermodynamic Values for the Gas Phase Reaction



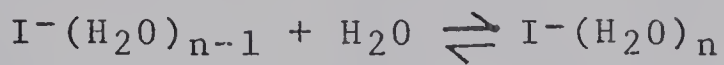
Reaction	$-\Delta H_{n-1,n}$	$-\Delta G_{n-1,n}^\circ (298^\circ)$	$-\Delta S_{n-1,n}^{\circ*}$
	Kcal/mole	Kcal/mole	e.u.
n-1, n			
0, 1	12.6	6.98	18.4
1, 2	12.3	5.48	22.9
2, 3	11.5	4.09	24.8
3, 4	10.9	2.91	26.8

\*Calculated for 298°K



Table 4-4

Experimental Thermodynamic Values for the Gas phase Reaction



Reaction n-1, n	$-\Delta H_{n-1, n}$ Kcal/mole	$-\Delta G^\circ_{n-1, n}$ (298) Kcal/mole	$-\Delta S^\circ_{n-1, n}^*$ e.u.
0, 1	10.2	5.4	16.3
1, 2	9.85	4.20	19.0
2, 3	9.40	3.08	21.3

\*Calculated for 298°K



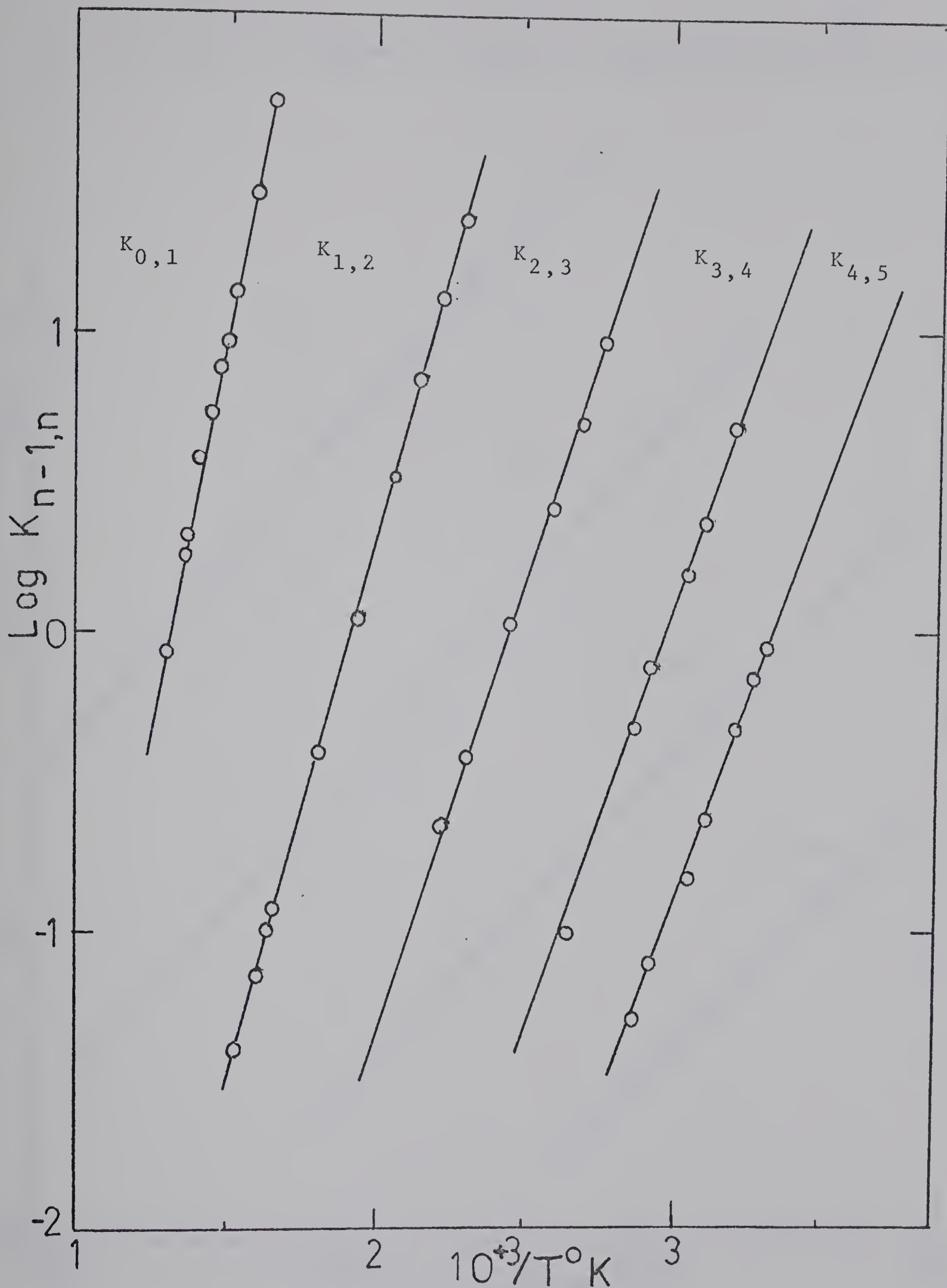


Figure 4-17: Van't Hoff-Type Plots of the Equilibrium Constants for the Gas Phase Hydration of  $\text{F}^-$ .



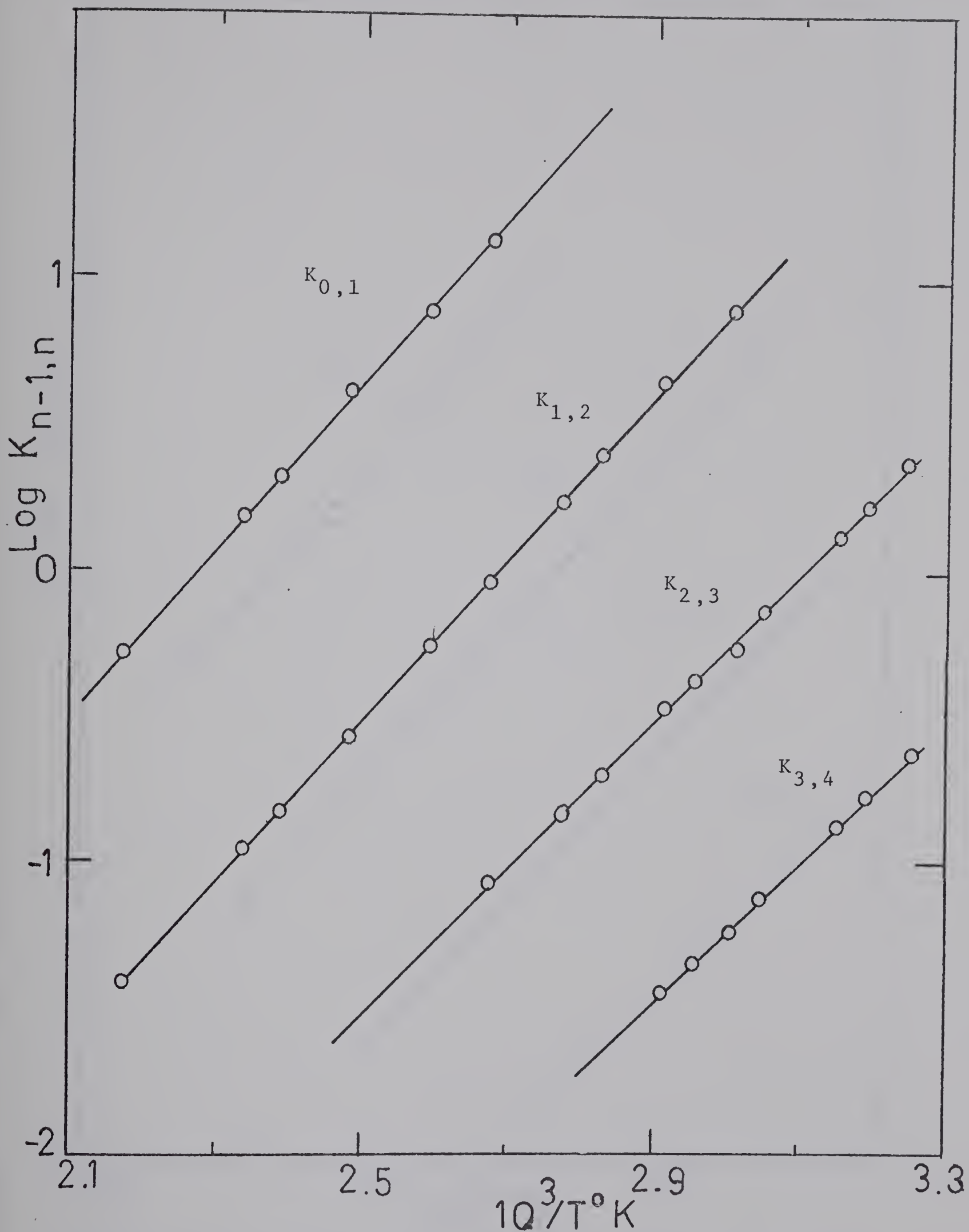


Figure 4-18: Van't Hoff-Type plots of the Equilibrium Constants,  $K_{n-1,n}$  for the Gas Phase Hydration of  $\text{Cl}^-$ .



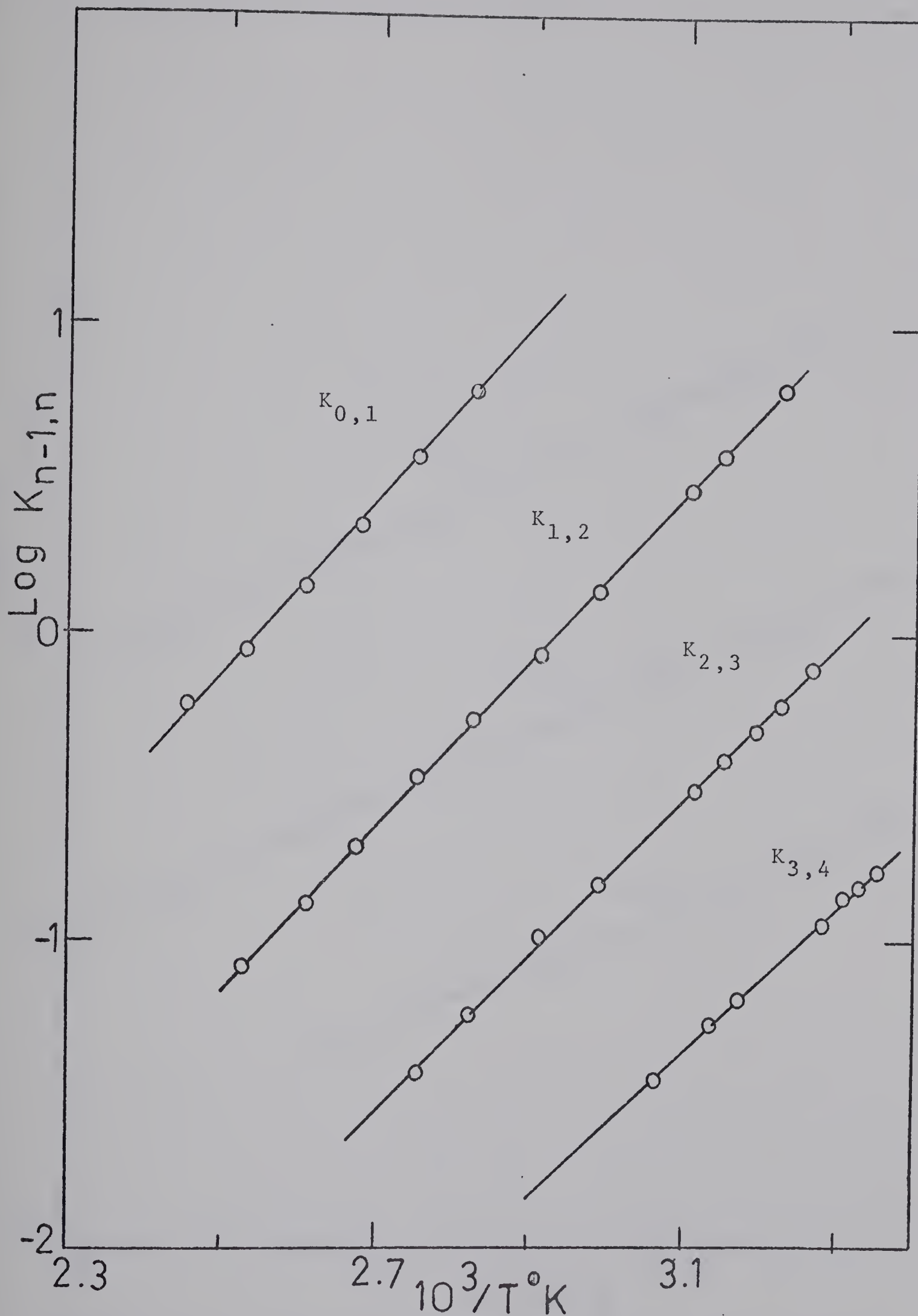


Figure 4-19: Van't Hoff-Type plots of the Equilibrium Constants,  $K_{n-1,n}$  for the Gas Phase Hydration of  $\text{Br}^-$ .



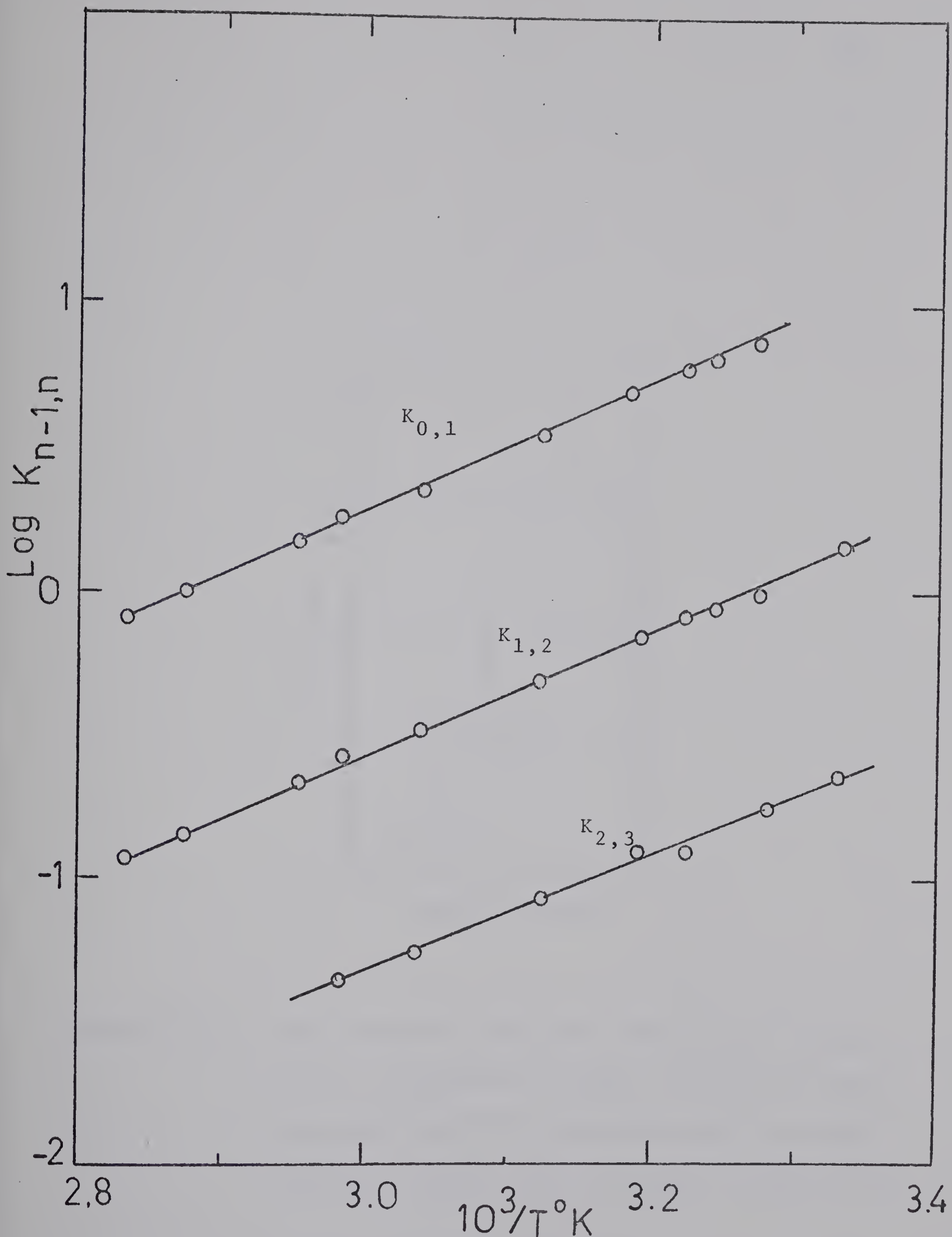


Figure 4-20: Van't Hoff-Type Plots of the Equilibrium

Constants  $K_{n-1,n}$  for the Gas Phase Hydration  
of  $\text{I}^-$ .



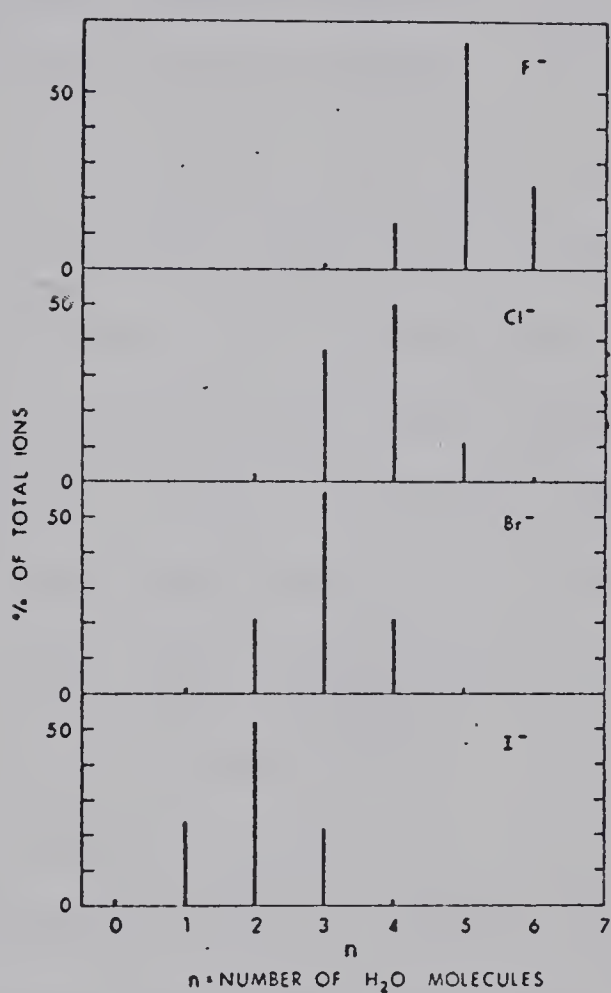


Figure 4-21: Experimentally Measured Equilibrium Distribution of Hydrates  $\text{X}^-(\text{H}_2\text{O})_n$  at one torr Water Pressure and 292°K, Showing Shift to Lower Hydration Number with Increase of Ionic Size.



energy of ion clusters have been carried out by a number of authors (34), (42), (43). Doyle and Caldwell (34) have applied this method to the system  $H_3O^+(H_2O)_n$ . Their calculation is based on a "point charge" model for water molecules. Thus they have assumed the electrostatic charges to be centered on the atomic nuclei of the water molecule, as it is shown in the figure (4-22). S. K. Searles (35) and I. Dzidic and P. Kebarle (24) have applied the same technique to calculate the potential energy of hydration of alkali positive ions. In the present work, Searles, Dzidic and Kebarle's method has been adopted for the calculation of potential energy of halide negative ions. It should be pointed out that these calculations are only approximations to the real bonding conditions and can not be expected to give accurate values of the actual energies involved. Nevertheless, reasonable conclusions can be drawn from a comparison of the results of this calculation with the experimental hydration energies.

In order to perform these calculation for negative ion hydration, we must select a reasonable "negative ion, water" configuration. There are two such configurations possible. In one, the negative ion,  $X^-$ , is located on the bisector of HOH angle ( $X^-$ — $\begin{smallmatrix} H \\ | \\ H \end{smallmatrix}$ —O) and in the other model, the negative ion is on the O-H bond axis ( $X^-$ —H— $\begin{smallmatrix} H \\ | \\ O \end{smallmatrix}$ ). The potential energy,  $E$ , relative to that of the



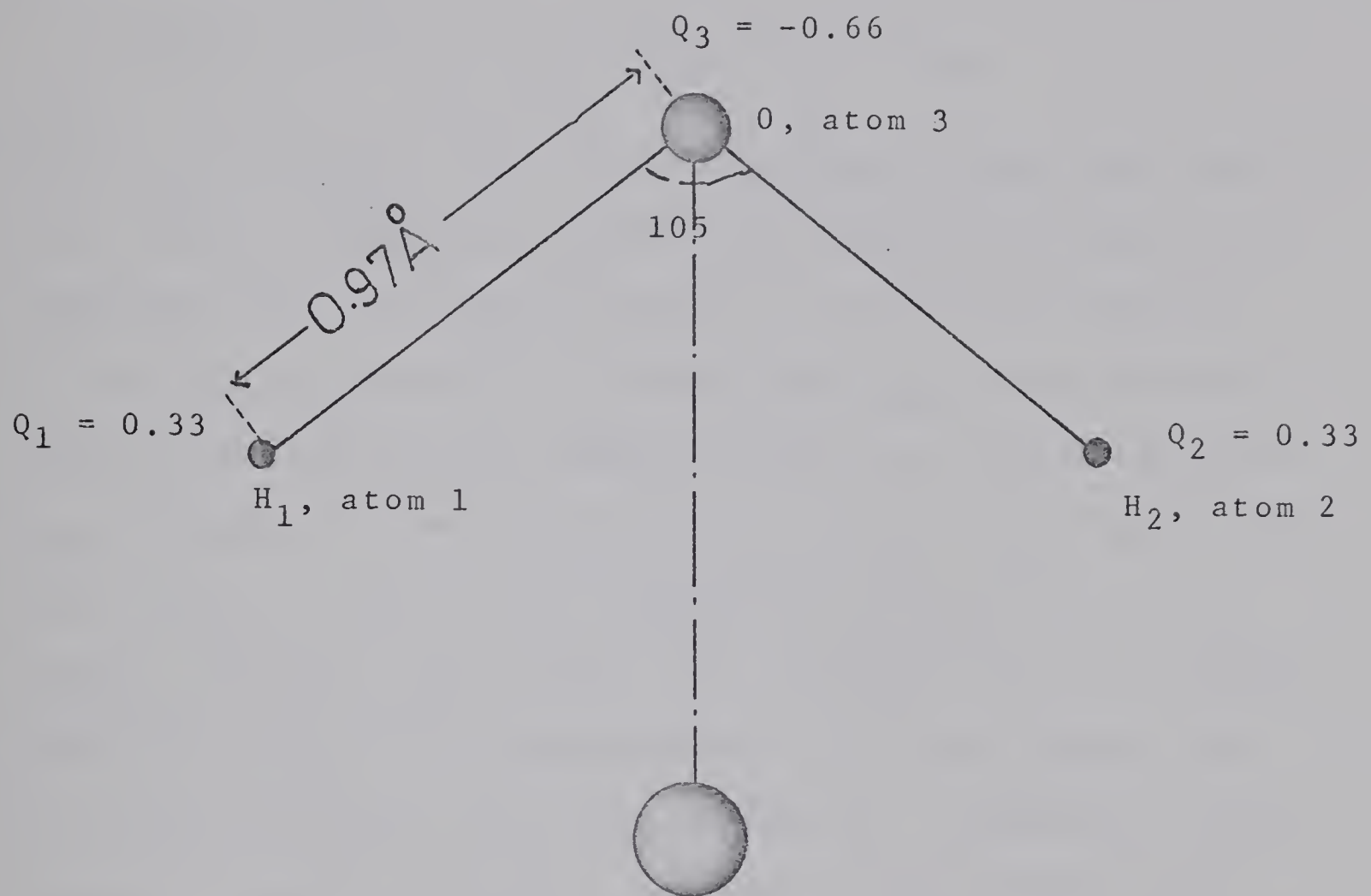


Figure 4-22: H<sub>2</sub>O "Point Charge" Model used in Theoretical Calculation.



halide and water molecules at infinity, of an ion cluster, can be written as

$$(4-4) \quad E = E_{ID} + E_{IP} + E_{DD} + E_{DS} + E_{RP}$$

Here  $E_{ID}$  represents the attraction energy between the central ion and the permanent dipole of the ligand molecules,  $E_{IP}$  represents the attraction energy due to the polarization of the ligand molecules by central ion,  $E_{DD}$  represents the dipole-dipole repulsion energy between the ligand molecules,  $E_{DS}$  represent the dispersion energy between the central ion and ligands as well as the dispersion energy between the various ligands, and finally,  $E_{RP}$  represents the ion-ligand repulsion energy. The dipole-dipole repulsion energy can be further divided into three components: permanent dipole-permanent dipole repulsion, induced dipole-induced dipole repulsion, and induced dipole-permanent dipole repulsion. The following equations were used (35), (37) to calculate the various contribution to the total energy:

Ion-Dipole

$$(4-5) \quad E_{ID} = \sum_{j=1}^n \sum_{i=1}^p \frac{(334)(Q_{ion})(Q_{i,j})}{R_{i,j}}$$

Ion Polarizability

$$(4-6) \quad E_{IP} = - \sum_{j=1}^n \sum_{i=1}^p \frac{(167)(Q_{ion})^2 \alpha_{i,j}}{R_{i,j}^4}$$

Permanent Dipole - Permanent Dipole

$$(4-7) \quad E_{PD} = \sum_{l=2}^n \sum_{i=1}^p \sum_{j=1}^{l-1} \sum_{k=1}^p \frac{(334)(Q_{i,j})(Q_{k,l})}{R_{i,j,k,l}}$$



Induced Dipole - Induced Dipole

$$(4-8) \quad E_{II} = \sum_{j=1}^{n-1} \sum_{m=j+1}^n \frac{14.397 \alpha_M^2 \epsilon^2}{R_{ion,j}^4 S_{j,m}^3} (1 + \cos^2 \theta_{j,m})$$

Induced Dipole - Permanent Dipole

$$(4-9) \quad E_{IPD} = \sum_{j=1}^{n-1} \sum_{m=j+1}^n \frac{28.794 P \alpha_M \epsilon}{R_{ion,j}^2 S_{j,m}^3} (1 + \cos^2 \theta_{j,m})$$

Dispersion

$$(4-10) \quad E_{DD} = \sum_{j=1}^{n-1} \sum_{m=j+1}^n \frac{17.28 \alpha_M^2 I_{PM}}{S_{j,m}^6}$$

$$+ \sum_{j=1}^n \frac{(34.56) \alpha_{ion} \alpha_M (I_{PI} \cdot I_{PM})}{R_{ion,j}^6 (I_{PI} + I_{PM})}$$

Ion-ligand Repulsion

$$(4-11) \quad E_{rep} = \sum_{j=1}^n \sum_{i=1}^p \frac{A_{i,j}}{R_{i,j}^{12}}$$

$Q_{ion}$  is the ionic charge,  $Q_{i,j}$  is the charge on the  $i^{\text{th}}$  atom of the  $j^{\text{th}}$  molecule with  $p$  atoms per molecule and  $n$  molecules per cluster.  $\alpha$  is the atomic polarizability and  $\alpha_M$  the polarizability of the water molecule.  $R_{i,j}$  is the ion-atom distance and  $R_{i,j,k,l}$  is the distance between the  $i^{\text{th}}$  atoms of  $j^{\text{th}}$  molecule and  $k^{\text{th}}$  atom of the  $i^{\text{th}}$  molecule.  $S_{j,m}$  is the distance of the  $j^{\text{th}}$  molecule from the  $m^{\text{th}}$  molecule in the cluster and  $R_{ion,j}$  is the distance between the central ion and  $j^{\text{th}}$  molecule, and finally,  $\theta$  is the angle between the induced dipole and the axis of the water molecule and  $P$  is the permanent dipole moment of



water (1.84 Debye). "A" is a semi-empirical constant whose evaluation will be given in the next paragraph. The numerical factors in the above equations are adjusted to give the energy in Kcal/mole for values of Q in atomic units and R and S in  $\text{A}^\circ$ . The polarizability of oxygen, hydrogen, and the water molecule were taken as 0.60, 0.44, and  $1.44\text{A}^\circ{}^3$  respectively (35). The ionization potentials of the negative ions were taken as the electron affinities of the parent atom and are 3.57 eV for fluoride, 3.76 eV for chloride, 3.54 eV for bromide, and 3.29 eV for iodide ion (48). The value 12.56 eV was used for the ionization potential of water (43). The calculation of potential energy was done by means of an IBM 360 computer. The program used was taken from the work of S. K. Searles (35) and adapted for the negative ions calculation by Dr. R. Yamdagni, Department of Chemistry, University of Alberta.

For determination of values of the constant "A", the following procedure was adapted. The values of "A" for repulsion between two atoms of inert gases Ne, Ar, Kr and Xe were calculated by the equation

$$(4-12) \quad A = 4\epsilon\sigma^{12}$$

$\epsilon$  is the depth of potential well and  $\sigma$  is the inter-atomic distance for zero potential energy. The values of  $\epsilon$  and  $\sigma$  taken from literature (39), (40) as well as values of "A" calculated from the equation (4-12) are presented in table



(4-5). The square root of these values of "A" for the inert gases were plotted versus the atomic radii, figure (4-23) obtained from reference (46). Using the experimental radii of the negative ions obtained by Gourary and Adrian (48) and the Bohr hydrogen radius, values of  $A^{1/2}$  for halide negative ions as well as hydrogen atom were obtained from the plot of figure (4-23). The constant "A" for repulsion between individual halide negative ions and the hydrogen atom of the water molecule was then assumed to be:

$$A_{X^-}, H = A_H^{1/2} \cdot A_{X^-}^{1/2}$$

For the clusters with more than one water molecules many different structures are possible. For the purpose of these calculations, the most symmetrical ligands arrangements were assumed. In other words, the clusters with two water molecules were assumed to be linear with negative ions placed equidistant between two water molecules. Three molecular clusters were assumed to have trigonal structure with negative ions in the centre, four molecular clusters have tetrahedral structure, clusters with five water molecules were considered to have bipyramidal and those with six water molecules were assumed to be octahedral. The final results of the classical electrostatic calculations for different halide negative ions and for two different arrangements, symmetric  $X^- \text{---} \begin{array}{c} \text{H} \\ | \\ \text{O} \\ | \\ \text{H} \end{array}$  and asymmetric  $X^- \text{---} \begin{array}{c} \text{H} \\ \diagup \\ \text{O} \end{array}$ , are given in table (4-6).



Table 4-5

The Coefficient "A" for Repulsion Term ( $A/R^{12}$ ) between  
 Two atoms of the Inert Gases from Equation  $A=4\epsilon\sigma^{12}$

	$\epsilon$ Electron-Volt	$\sigma$ A°	$A$ KCal-A° <sup>12</sup>
Neon-Neon	$3.129 \times 10^{-3}$	2.82	$7.30 \times 10^5$
Argon-Argon	$1.036 \times 10^{-2}$	3.44	$2.62 \times 10^6$
Krypton-Krypton	$1.41 \times 10^{-2}$	3.827	$1.29 \times 10^7$
Xenon-Xenon	$1.84 \times 10^{-2}$	4.22	$5.93 \times 10^7$

$\epsilon$  is the depth of the potential well

$\sigma$  is the inter-atomic distance for zero potential energy



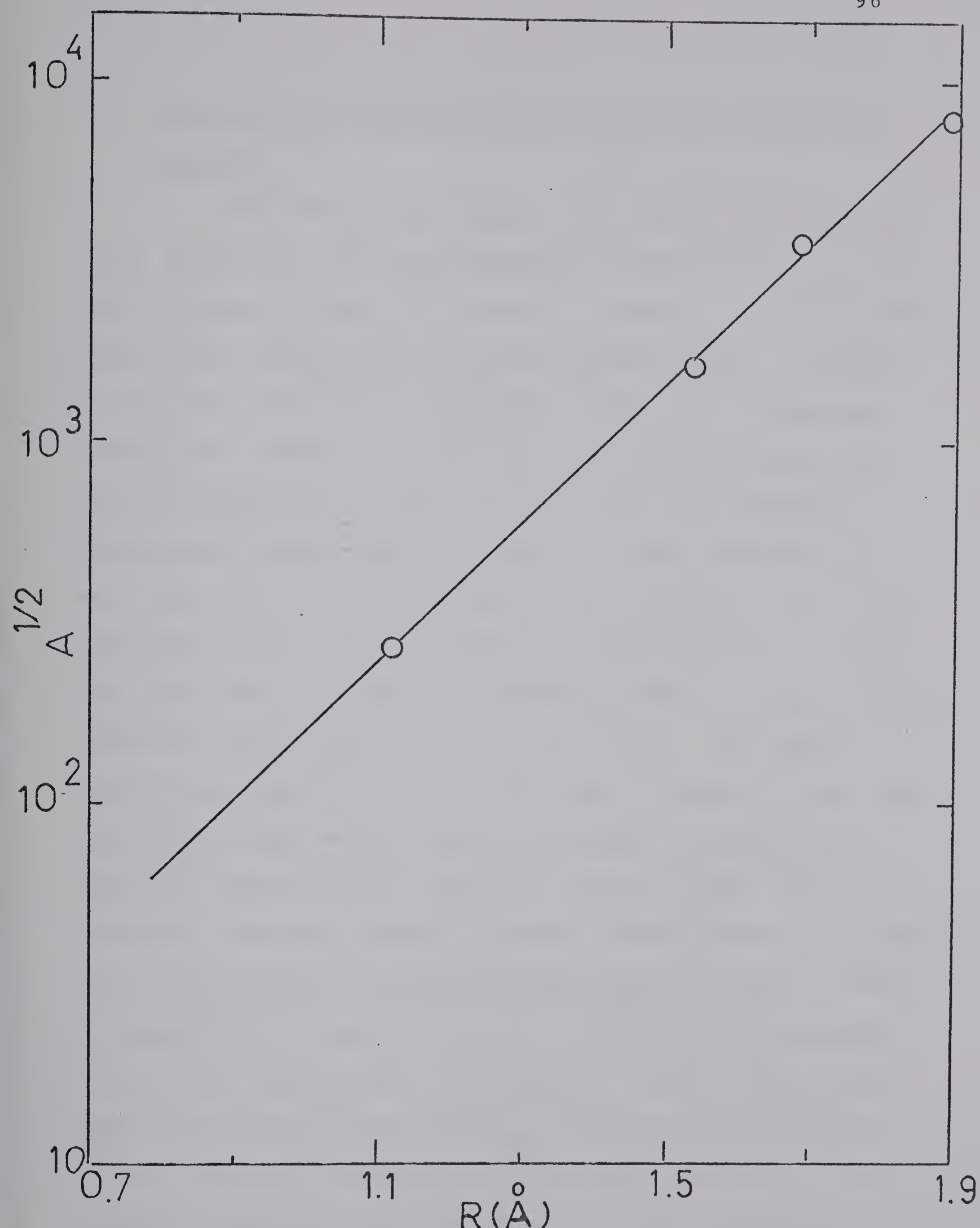


Figure 4-23: Square Root of Repulsion Coefficient 'A' for Noble Gases as a Function of Atomic Radii.



#### 4.4 Comparison of Calculated and Experimental Hydration Energies

The theoretical  $\Delta E_{n-1,n}$  calculated from equation (4-4) along with the experimentally determined  $\Delta H_{n-1,n}$  for halide negative ions are plotted in figures (4-24) to (4-31). Comparison between the calculated values of  $\Delta E_{n-1,n}$  based on the two different arrangements of the water molecules around the negative ion indicates that initially the symmetric arrangement is more favorable but the asymmetric arrangement becomes more favorable for the clusters with more than about three water molecules. This is due to the closeness of the ligand molecules in the symmetric arrangement, and thus, a larger contribution from the dipole-dipole repulsion terms (equations 4-7, 4-8, 4-9). The dipole-dipole repulsion term, of course, does not exist in the cluster  $X^-(H_2O)$ , but as more water molecules are added, the effect of dipole-dipole repulsion energy becomes more pronounced. Evidently, when the fourth water molecule is added the dipole repulsion energy becomes strong enough to cause a change from a symmetrical to an asymmetrical arrangement of the water molecules in the complex. Table (4-6) shows that the absolute values of  $\Delta E_{0,1}$  calculated on the basis of the symmetric arrangements, are higher than  $\Delta H_{0,1}$ , determined experimentally, by about 20 to 30% depending on the halogen under consideration. Of course the possibility



Table 4-6

Calculated and Experimental Values of Energy Change for Reaction



-ΔE <sub>0,1</sub> Kcal/mole	-ΔE <sub>1,2</sub> Kcal/mole		-ΔE <sub>2,3</sub> Kcal/mole		-ΔE <sub>3,4</sub> Kcal/mole		-ΔE <sub>4,5</sub> Kcal/mole		-ΔE <sub>5,6</sub> Kcal/mole	
	Cal	H								
	Sym	Asym	Expt	Sym	Asym	Expt	Sym	Asym	Expt	Sym
F <sup>-</sup>	29.8	19.1	23.3	25.4	18.6	16.6	17.8	16.1	13.7	11.9
Cl <sup>-</sup>	18.6	12.0	13.1	17.0	11.6	12.7	13.9	10.5	11.7	11.6
Br <sup>-</sup>	16.0	10.4	12.6	14.8	10.0	12.3	12.5	9.2	11.5	10.8
I <sup>-</sup>	12.3	8.0	10.2	11.5	7.9	9.85	10.2	7.3	9.40	9.12



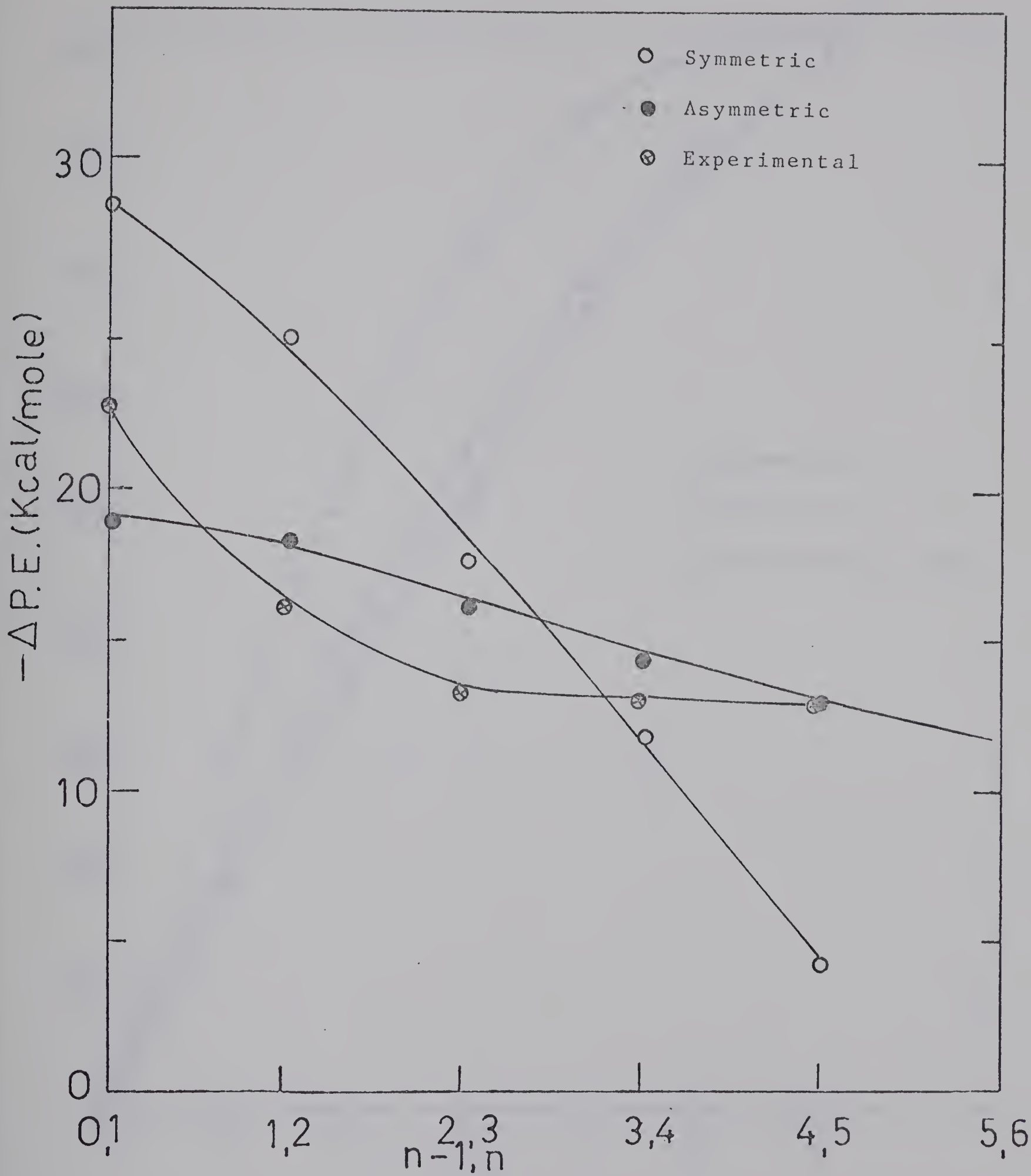


Figure 4-24: Plots of Change of Potential Energy for Cluster  $F^-(D_2O)_{n-1,n}$  Versus  $n-1,n$ .



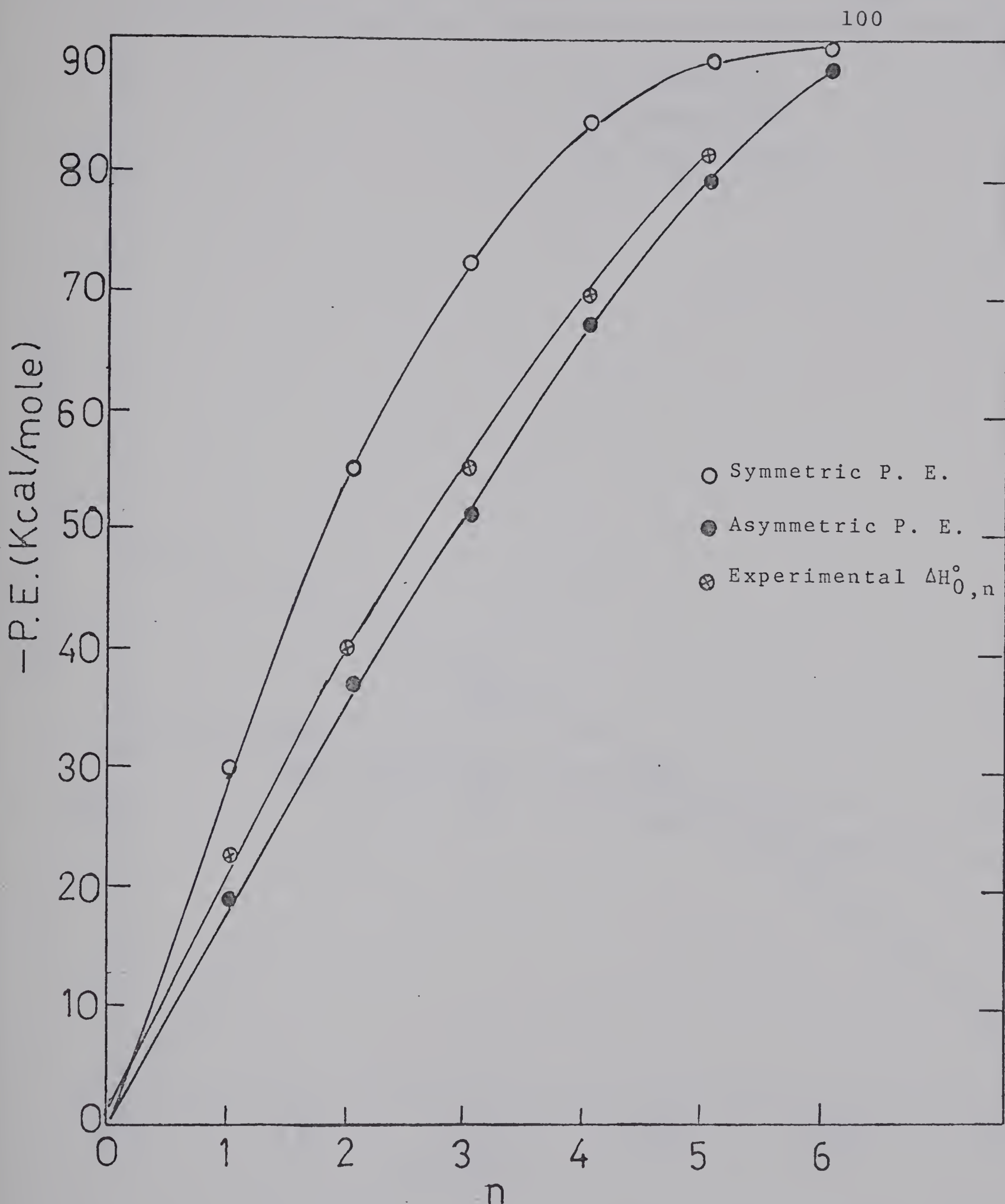


Figure 4-25: Plots of Potential Energy for Cluster  $\text{F}^-(\text{D}_2\text{O})_n$  Versus  $n$ .



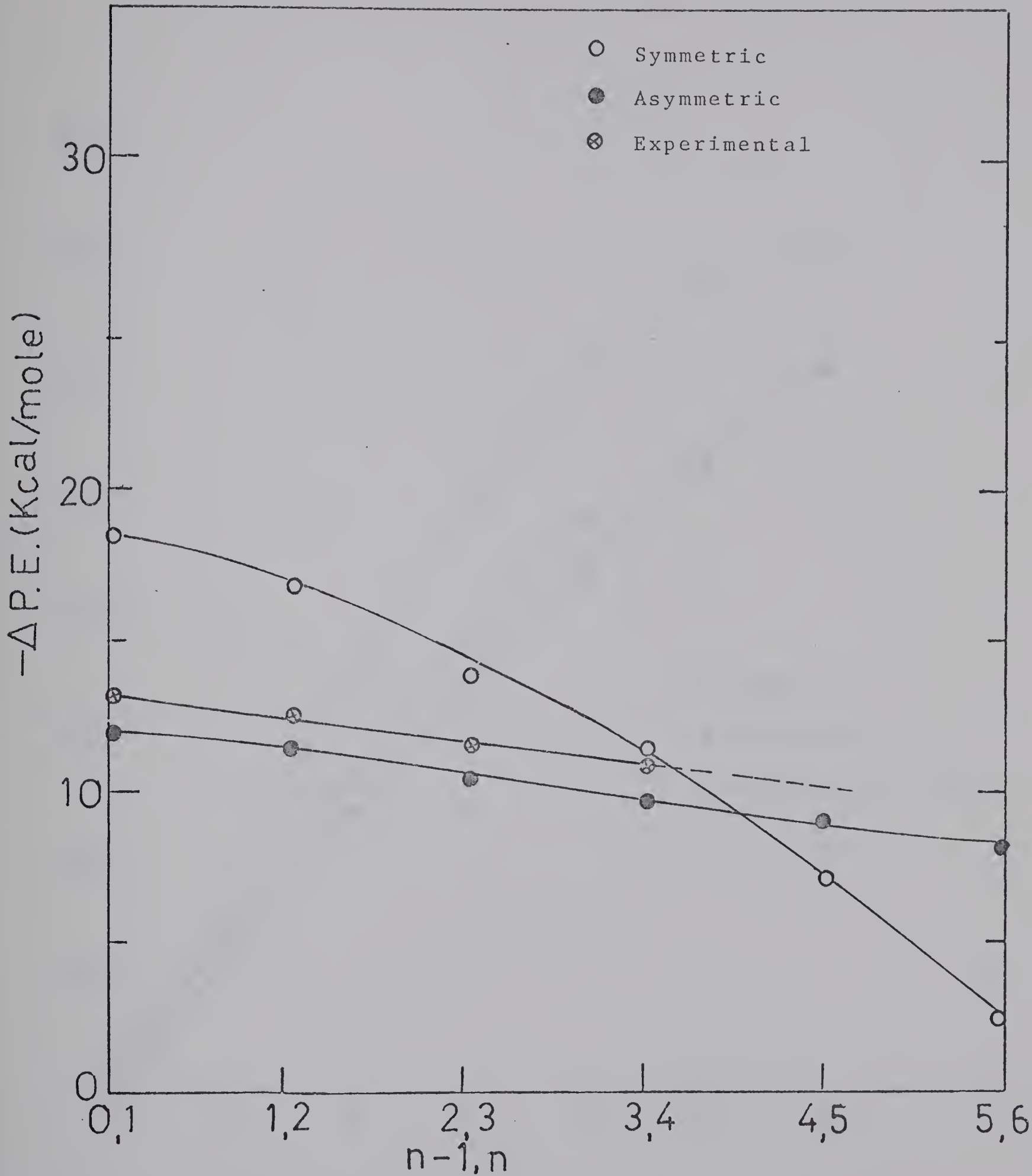


Figure 4-26: Plots of the Change of Potential Energy for Cluster  $Cl^-(H_2O)_{n-1,n}$  Versus  $n-1,n$ .



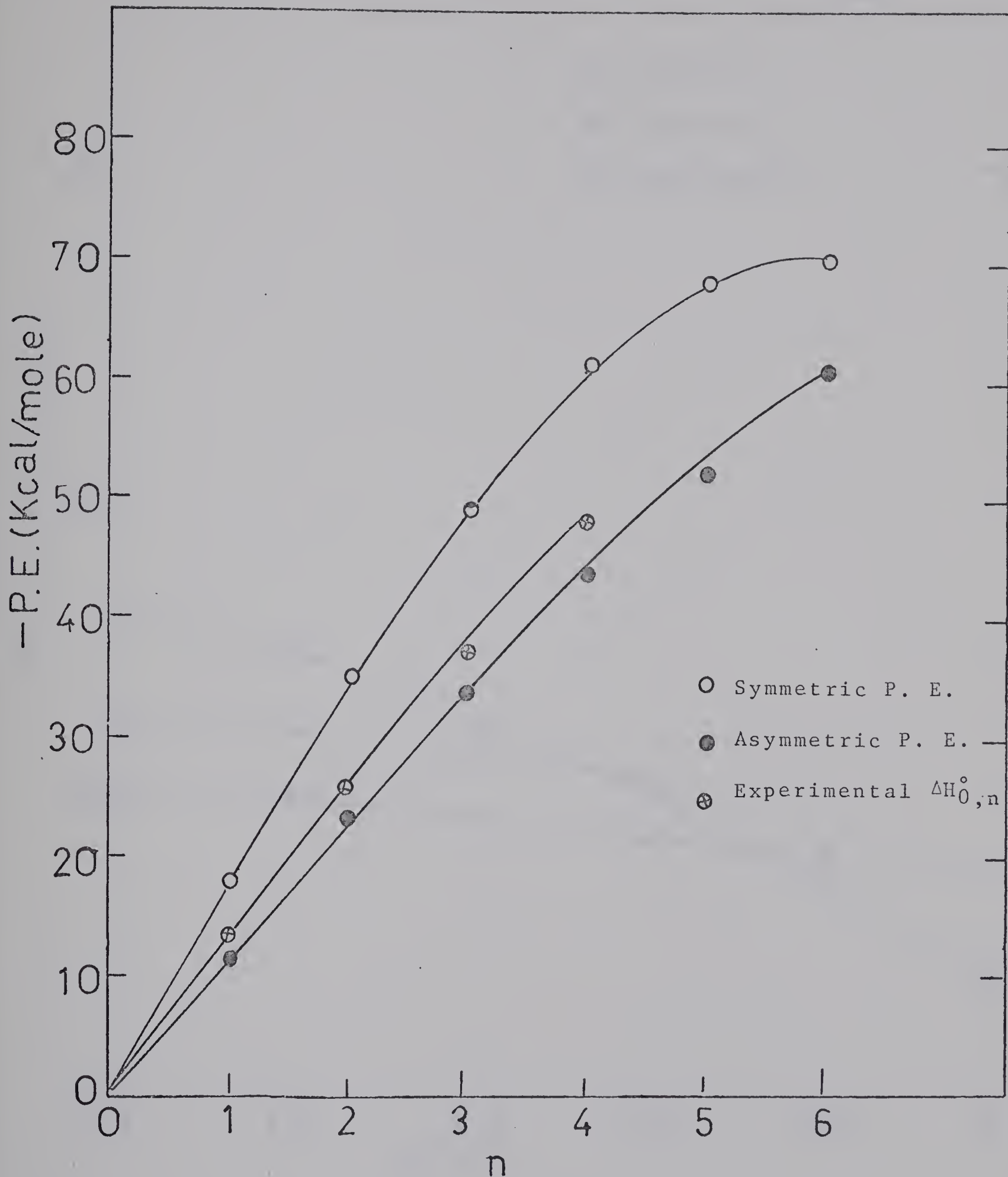


Figure 4-27: Plots of Potential Energy for Cluster  $\text{Cl}^-(\text{H}_2\text{O})_n$  Versus n.



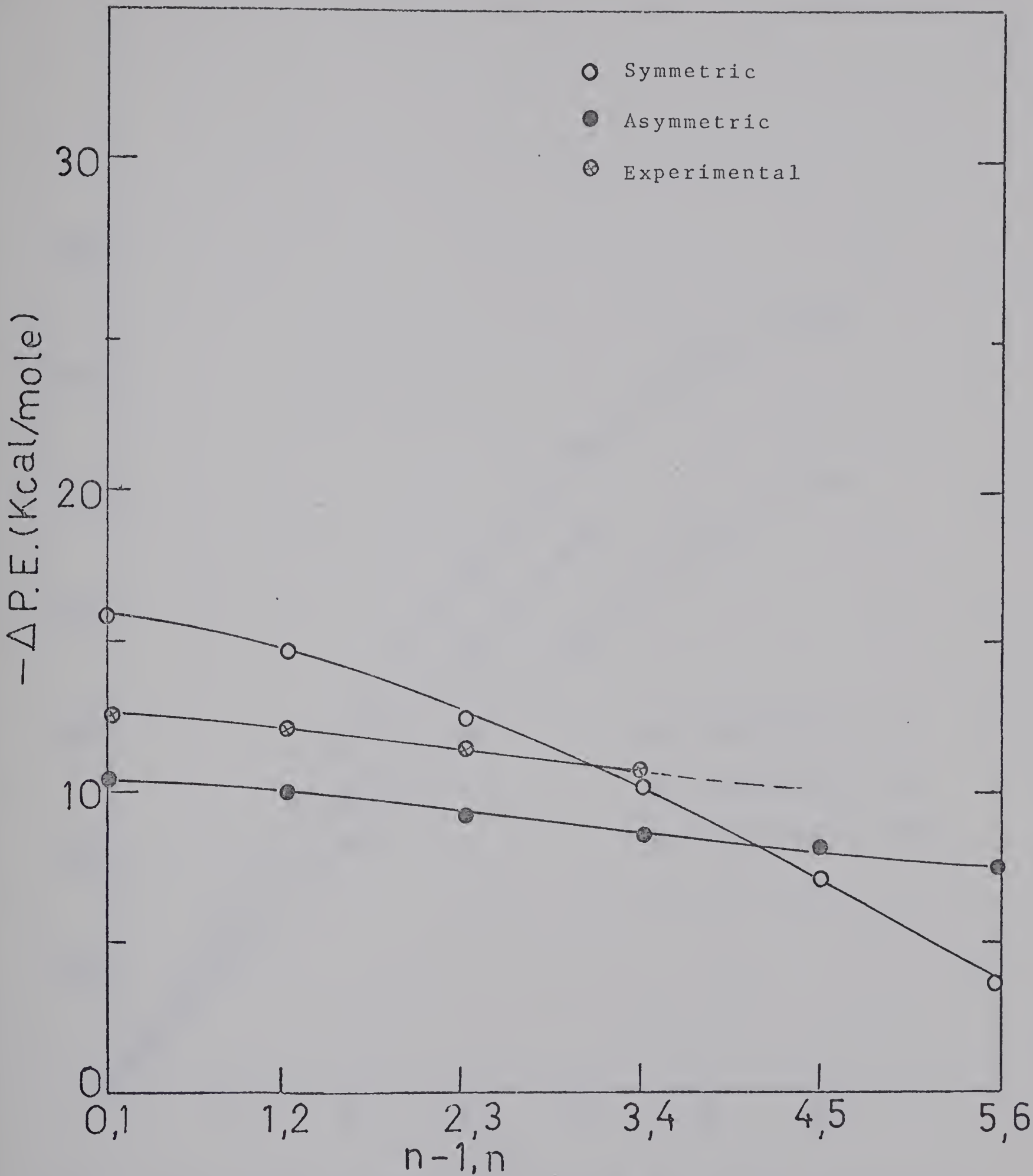


Figure 4-28: Plots of Change of Potential Energy for Cluster  $\text{Br}^-(\text{H}_2\text{O})_{n-1,n}$  versus  $n-1,n$ .



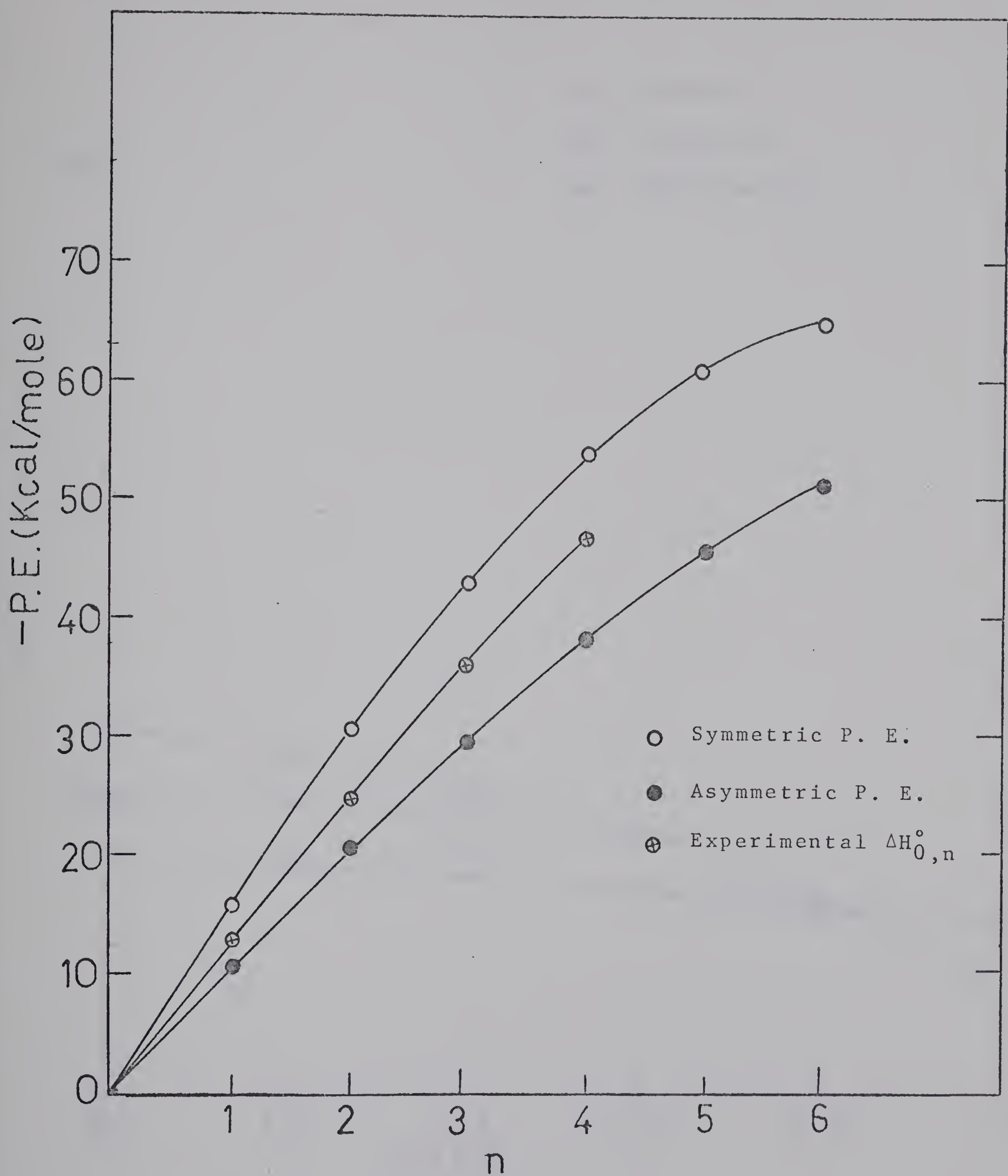


Figure 4-29: Plots of Potential Energy for Cluster  $\text{Br}^-(\text{H}_2\text{O})_n$  Versus  $n$ .



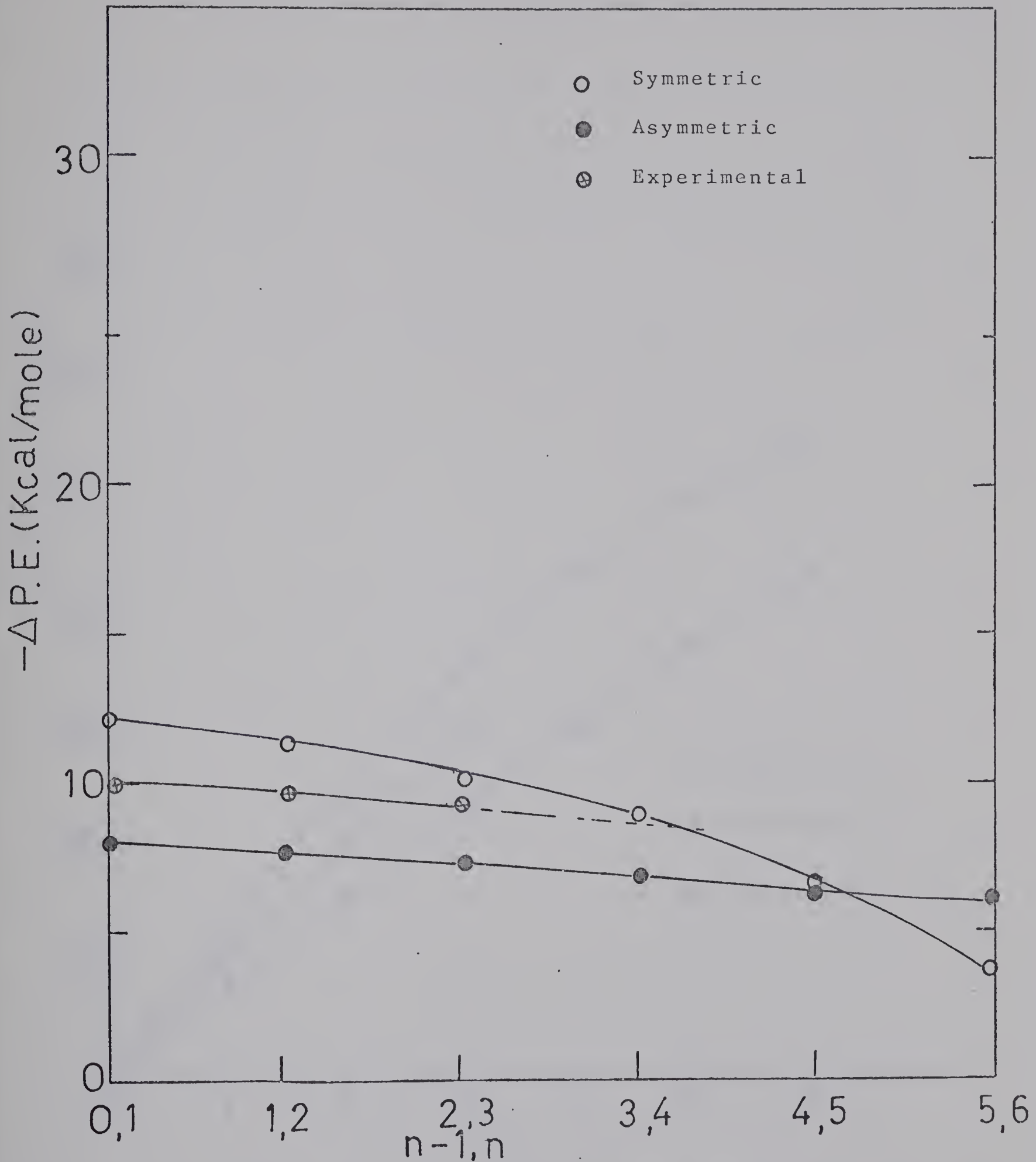


Figure 4-30: Plots of Change of Potential Energy for Cluster  $I^-(H_2O)_{n-1,n}$  Versus  $n-1,n$ .



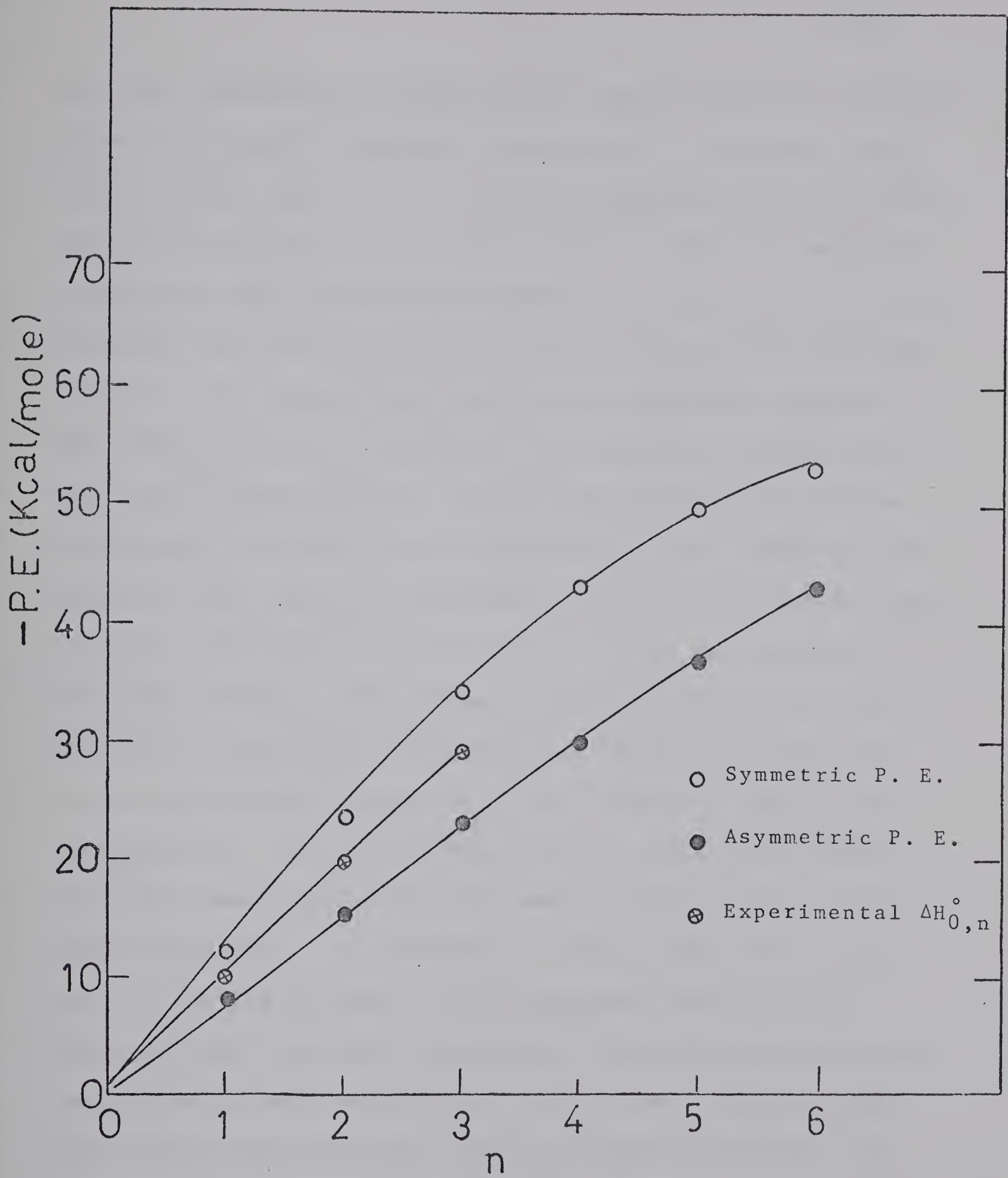


Figure 4-31: Plots of Potential Energy for Cluster  $I^-(H_2O)_n$  Versus  $n$ .



that our experimental values are in error cannot be entirely ruled out, but the internal consistency of the data represented by the Van't Hoff's plots of figures (4-17) to (4-20) makes the existence of an error of 20 to 30% very unlikely. Perhaps the most significant factor contributing to the lack of better agreement between the experimental and calculated values is the method used and the approximations made in the evaluation of the constant "A" in the ion-ligand repulsion term (equation 8-4). Aside from the question of the reliability of method, the uncertainty in the radii of the negative ions, used in evaluating "A" could be a major source of error. To illustrate the effect of the uncertainty of the ionic radii on the ultimate values of  $\Delta E_{0,1}$  the ionic radii of Gourary and Adrian were increased by 5% and the total electrostatic energies of the cluster  $X^-(H_2O)_n$  were recalculated. The new values of  $\Delta E_{0,1}$  for all the halide ions are compared with the old ones in table (4-7). This table shows that a 5% increase in ionic radii will result in a 7.4 to 14% decrease in the absolute value of  $\Delta E_{0,1}$ . Thus, one may conclude that perhaps the values of the ionic radii used in this calculation are too low. This becomes more obvious when the  $Na^+$  radius obtained by Gourary and Adrian is compared with the atomic radius of neon ( $r_{Na^+} = 1.17$  and  $r_{Ne} = 1.12 \text{ \AA}$ ). This of course is not acceptable, and shows that the Gourary and Adrian ionic radii are too low.



Table 4-7

Decrease in Absolute Values of  $(-\Delta E_{0,1})_{\text{sym}}$  as a Result of 5%

Increase in Ionic Radii of the Halide Negative Ions

Ion	$(-\Delta E_{0,1})_{\text{sym}}^{**}$	$(-\Delta E_{0,1})_{\text{sym}}^{**}$	per cent
	Based on G and A*	with 5% increase in $r_{\text{ion}}$	Decrease
$\text{F}^-$	29.8	27.6	7.4
$\text{Cl}^-$	18.6	16.9	9.2
$\text{Br}^-$	16.0	14.3	10.6
$\text{I}^-$	12.3	10.6	14.0

\*Reference (47)

\*\*Unit; Kcal/mole



for negative ions and too high for positive ions by approximately 10%.

It has been suggested (71) that the Van der Waals radii should be used, instead of the ionic radii, in electrostatic calculations such as those in this work. It would be of interest, in future studies, to make some calculations similar to the ones which were performed in this work but with values of "A" based on Van der Waals' radii.

In conclusion, it should be emphasized that in view of the approximations which had to be made and the simple models used, the calculated values could only support our experimental results qualitatively.

#### 4.5 Calculation of The Entropy Change $\Delta S^{\circ}_{0,1}$

The entropy change for a reaction such as



can be calculated theoretically by means of statistical mechanics. In such calculations, the assumption is made that the change of the entropy can be represented simply as the sum of translational, rotational, and vibration contributions

$$(4-14) \quad \Delta S = \Delta S_t + \Delta S_r + \Delta S_v$$

Each individual part of the right hand side of equation (4-14) is then evaluated separately. The translational



contribution can be calculated from Sackur-Tetrode equation (49). The application of Sackur-Tetrode equation to the chemical reaction represented by equation (4-13) is

$$\Delta S_t = \frac{3}{2} R \ln \frac{M_{X^-}(H_2O)}{(M_{X^-})(M_{H_2O})} - \frac{5}{2} R \ln T + 2.311$$

here  $M_{X^-}(H_2O)$ ,  $M_{X^-}$  and  $M_{H_2O}$  are molecular weight of  $X^-(H_2O)$ ,  $X^-$  and  $H_2O$  respectively.  $T$  is the absolute temperature in degrees K; the gas constant,  $R$ , is taken as  $1.987 \text{ cal. deg.}^{-1}$ ; and  $\Delta S_t$  comes out in entropy units, e.u. The rotational contribution to the entropy of one mole of gas is given (49) by the equation

$$(4-15) \quad S^\circ_{\text{rot}} = R(\ln Q_{\text{rot}} + 1)$$

$Q_{\text{rot}}$ , the rotational partition function is

$$(4-16) \quad Q_{\text{rot}} = \frac{(8 \pi)^{5/2} (kT)^{3/2} (I_x I_y I_z)^{1/2}}{a h^3}$$

where  $I_x$ ,  $I_y$  and  $I_z$  are the three moments of interia about the three principal axes and "a" is the symmetry number.

When the equation (4-15) is applied to calculate the change of entropy for reaction (4-13), the following equation will be obtained

$$(4-17) \quad \Delta S_{\text{rot}}^\circ = R \ln \frac{[Q_{\text{rot}}]_{X^-(H_2O)}}{[Q_{\text{rot}}]_{H_2O}}$$

When the proper values of the partition functions are substituted in equation (4-17) and the appropriate simplification has been made, the  $\Delta S_{\text{rot}}^\circ$  will be



$$(4-18) \quad \Delta S_{\text{rot}}^{\circ} = \frac{R}{2} \ln \frac{[I_x \ I_y \ I_z]_{X^-(H_2O)}}{[I_x \ I_y \ I_z]_{H_2O}}$$

For the evaluation of  $\Delta S_{\text{rot}}^{\circ}$  from equation (4-18), the moments of inertia of the cluster  $X^-(H_2O)$  as well as the moments of inertia of  $H_2O$  molecule are required. The moments of inertia of  $H_2O$  are (51):  $I_x = 1.92$ ,  $I_y = 1.02$  and  $I_z = 2.95 \times 10^{-40} \text{ g-cm}^2$ . The moments of inertia for the cluster  $X^-(H_2O)$  are based on the  $X^- - OH_2$  equilibrium distances obtained from the electrostatic calculations in the previous section and the bond distances and the bond angle of the water molecule. These moments of inertia as well as the  $X^- - OH_2$  equilibrium distances are given in table (4-8). The moments of inertia of  $D_2O$ , used for the calculation of  $F^-(D_2O)$  also taken from reference (51), are:  $I_x = 3.81$ ,  $I_y = 1.79$  and  $I_z = 5.75 \times 10^{-40} \text{ g-cm}^2$ . The principal axes of  $D_2O$  and  $F^-(D_2O)$  used to calculate the moments of inertia are shown in figure (4-32). Similar types of arrangements were used to calculate the moments of inertia of the other halide negative ion clusters  $X^-(H_2O)$ .

To calculate the vibrational contribution to the entropy change of the reaction (4-9), it was assumed that the fundamental vibrations of water molecule remain the same before and after the formation of the cluster  $X^-(H_2O)$ . Accordingly, the vibrational entropy change is due to three new vibrations in the complex. These are the stretching vibration along the oxygen, halide ion axis, and two rocking

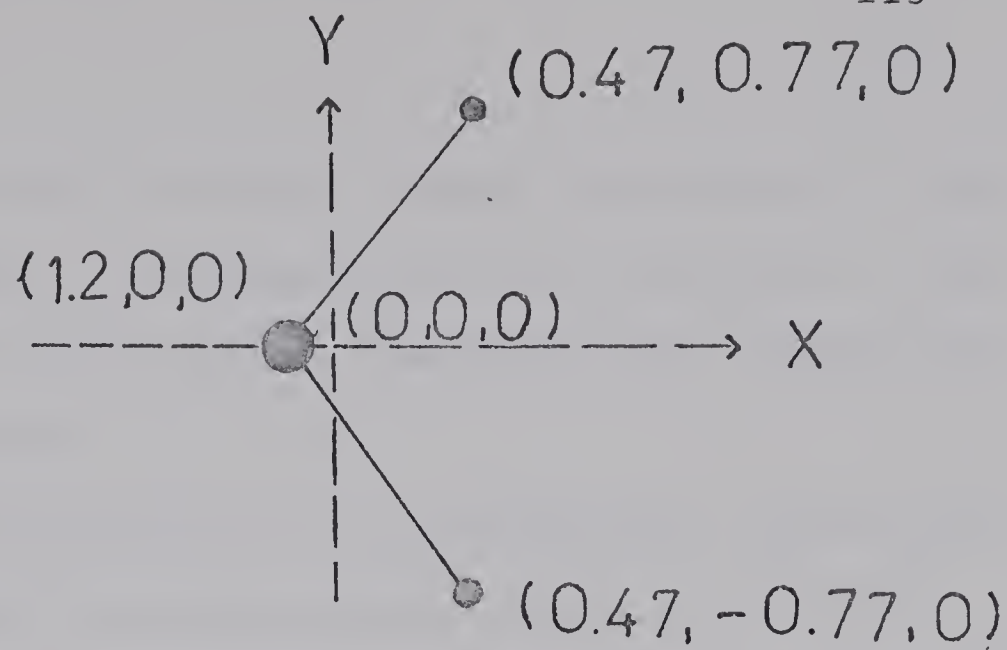


Table 4-8

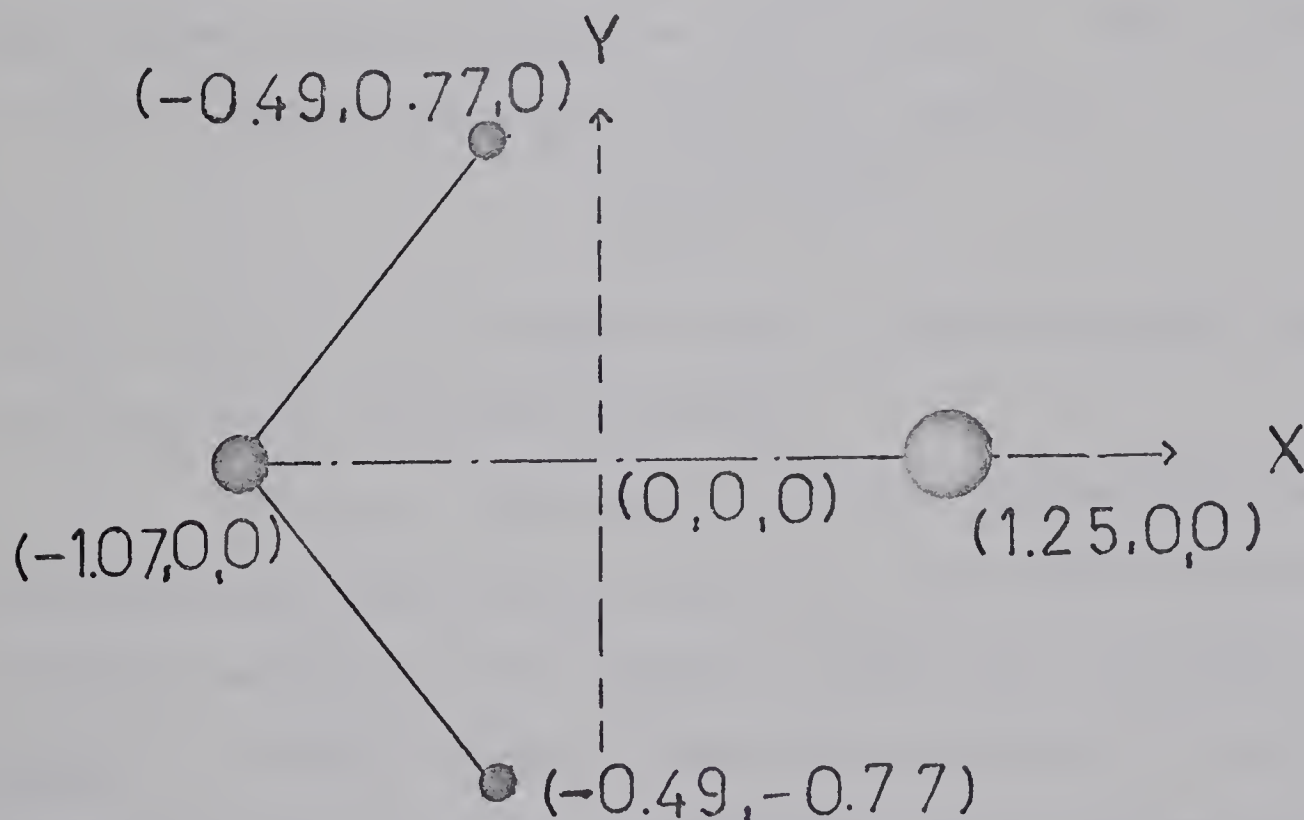
Moments of Inertia and  $X^-$ - $OH_2$  Equilibrium Distances

Cluster	$X^-$ - $OH_2$ Distance $\text{\AA}^\circ$	$\text{IX}10^{40} \text{ g-cm}^2$		
		$I_x$	$I_y$	$I_z$
$F^- (D_2O)$	2.320	3.94	80.30	83.24
$Cl^- (H_2O)$	2.810	1.97	149.7	151.7
$Br^- (H_2O)$	2.990	1.97	241.0	243.
$I^- (H_2O)$	3.330	1.97	280.0	282.0





Principal Axes of  $D_2O$ . The Z axis is  
Perpendicular to the Plane of Paper.



Principal Axes of  $F^-(D_2O)$ . The Z Axis is  
perpendicular to the Plane of Paper.

Figure 4-32: Principal Axes of  $D_2O$  and  $F^-(D_2O)$  used in the Calculation of Moments of Inertia.



vibrations of the water molecule around its centre of mass. One of these rocking vibrations occurs in the plane of the molecule  $X^-(H_2O)$ , figure (4-34), and the other one perpendicular to this plane.

In the calculation of the stretching vibrational frequency, the water molecule and the negative ion were treated as two mass points. The force constant for this vibration was estimated by fitting an equation of parabola to the bottom portion of the potential energy curves of figure (4-33). These curves were obtained by plotting the total electrostatic potential of the previous section versus water molecule-negative ion distance. The frequency,  $v$  then, can be calculated from the equation

$$v = \frac{1}{2\pi} \left( \frac{K}{u} \right)^{1/2}$$

where the  $u$  is the reduced mass of water-negative ion system and  $K$  is the force constant.

The two rocking vibrational frequencies were obtained by first calculating the total electrostatic potential energy of the complex  $X^-(H_2O)$  as a function of angle  $\theta$ , figure (4-34). Then the equation of a parabola, in the form of (4-19), was fitted to the bottom portion of the potential energy curve as in stretching frequency calculation.

$$(4-19) \quad E = \frac{1}{2} K_{roc} \theta^2$$



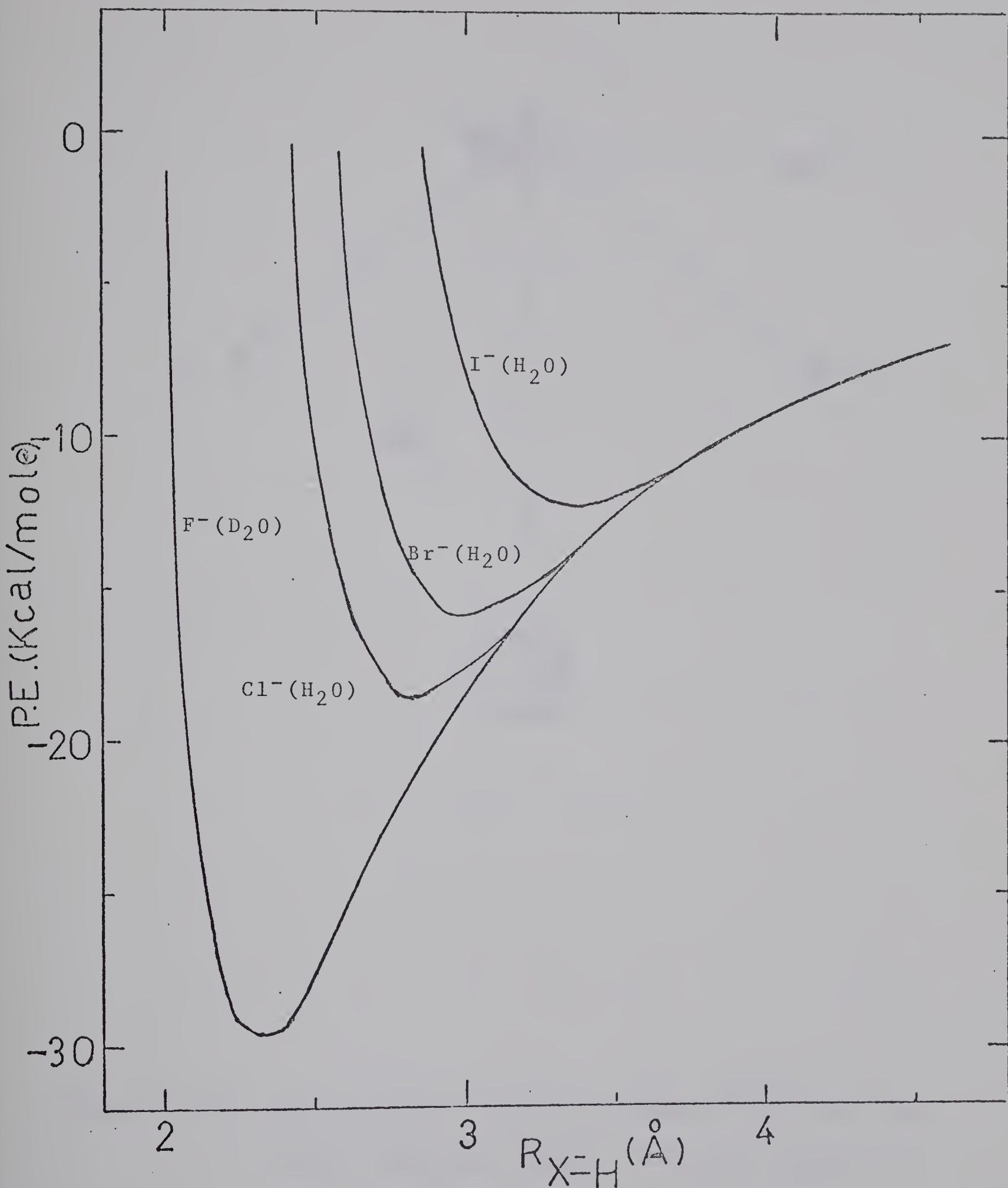


Figure 4-33: Plots of the Potential Energies of  $\text{X}^-(\text{H}_2\text{O})$  Versus  $\text{X}^--\text{H}_2\text{O}$  Distance.



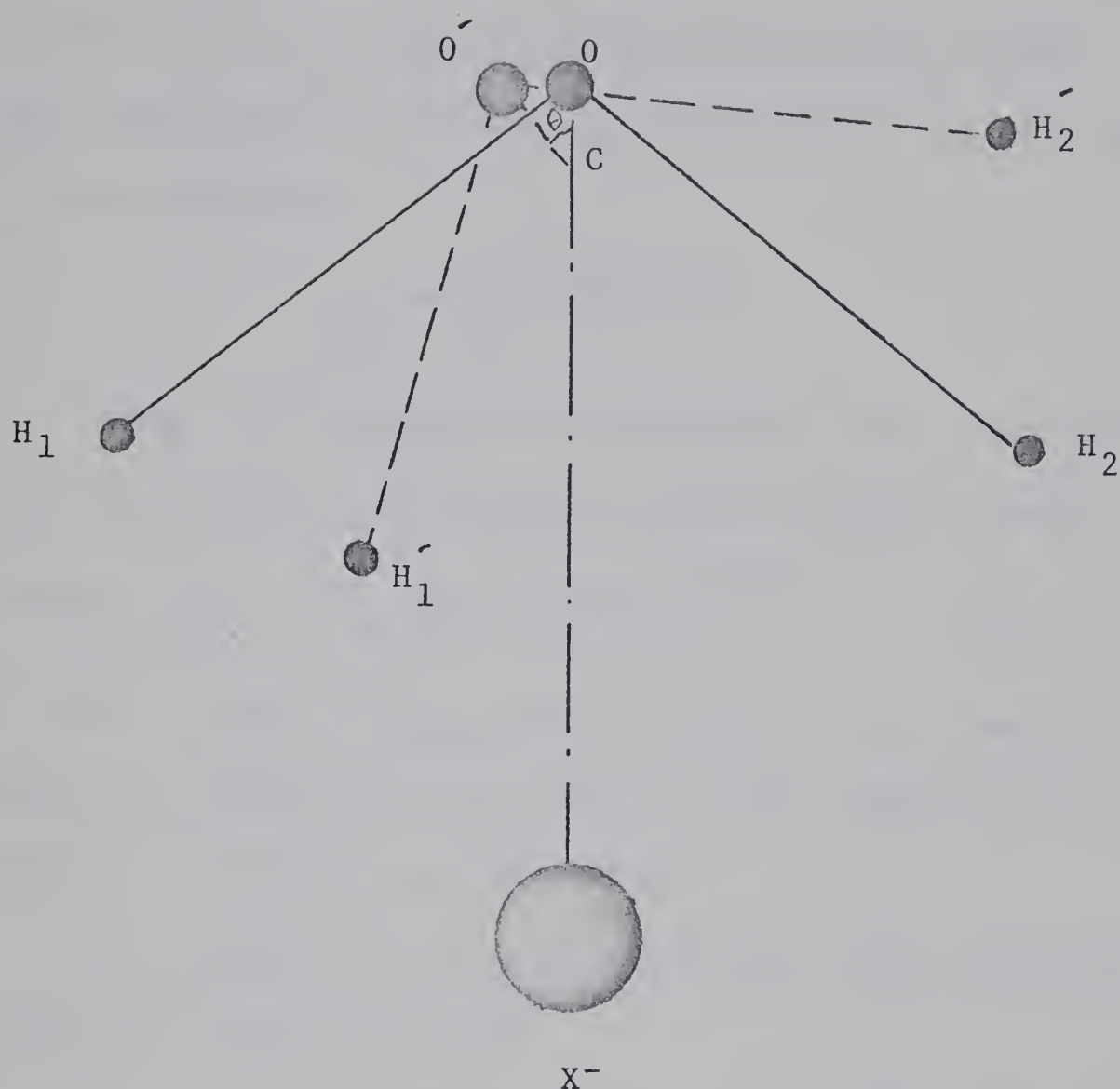


Figure 4-34: Rocking Motion of Water Molecule in the Plane of the Cluster X<sup>-</sup>(H<sub>2</sub>O). C is the centre of Mass of H<sub>2</sub>O Molecule.



$K$  is the force constant,  $\theta$  is the angle of the rocking motion of the water molecule, and  $E$  is the potential energy. Finally, the frequencies of rocking vibrations were obtained (52) by the equation

$$v_{\text{roc}} = \frac{1}{2\pi} \left( \frac{K_{\text{roc}}}{I} \right)^{1/2}$$

Once the frequencies are known, the contribution to the entropy can be determined from equation (4-20) (50)

$$(4-20) \quad S_{\text{vib}}^{\circ} = R \sum_{i=1}^3 \left[ \left( \frac{h v_i}{K T} \right) \left( e^{\frac{h v_i}{K T}} - 1 \right)^{-1} - \ln \left( 1 - e^{\frac{h v_i}{K T}} \right) \right]$$

However, the values of  $S_{\text{vib}}^{\circ}$  have already been computed and tabulated as a function of  $h v_i / K T$  or  $v'/T$ , where  $v'$  is the wave number, in various publications.

The values of  $S_{\text{vib}}^{\circ}$  in this work were obtained from reference (52) page 654

$$S_{\text{vib}}^{\circ} = \frac{E - E_{\circ}}{T} - \frac{F - E_{\circ}}{T}$$

where  $(E - E_{\circ})/T$  and  $(F - E_{\circ})/T$  are tabulated as a function of  $v'/T$ . The factors  $E$ ,  $E_{\circ}$  and  $F$  are the energy, the zero point energy and free energy, respectively, of a harmonic oscillator whose wave number is  $v'$ .

In table (4-9) the force constant  $K_i$ , the vibration frequency  $v_i$  and the entropy contribution  $S_i^{\circ}$   $\text{vib}$  are tabulated. Table (4-10) represents the various contributions to the entropy change as well as the experimental values of  $\Delta S_{298}^{\circ}$  for the clusters  $X^-(H_2O)$ .



Table 4-9

Force Constants, Vibrational Frequencies and  $S_{vib}^\circ$  for Three New  
Vibrations of  $X^-(H_2O)$

Cluster	Frequency, Sec <sup>-1</sup>			Force Constant*			$S_{vib}^\circ$ , e.u.		
	$V_1 X10^{-12}$	$V_2 X10^{-12}$	$V_3 X10^{-12}$	$K_1 X10^{12}$	$K_2 X10^{12}$	$K_3 X10^{13}$	$S_1^\circ$	$S_2^\circ$	$S_3^\circ$
$F^-(D_2O)$	11.1	8.0	13.2	7.5	1.60	12.9	1.10	1.61	0.83
$Cl^-(H_2O)$	8.5	10	13.1	5.6	1.14	7.0	1.53	1.26	0.83
$Br^-(H_2O)$	6.6	10.7	12.8	4.2	1.33	6.5	1.95	1.15	0.88
$I^-(H_2O)$	5.2	4.8	9.6	2.8	0.81	3.7	2.40	2.57	1.31

\*Unit:  $K_1$  dyne/cm,  $K_2$  and  $K_3$  erg/rad.

Subscript 1 represents stretching vibration

Subscript 2 represents rocking vibration in the plane of  $X^-(H_2O)$

Subscript 3 represents rocking vibration perpendicular to the plane  $X^-(H_2O)$



Table 4-10

Translational, Rotational and Vibrational Contributions to  
Experimentally Determined  $\Delta S^\circ_{298}$  for Ion Cluster  $X^-(H_2O)$

Cluster	Components of $\Delta S^\circ_{\text{Theo.}}$			$-\Delta S^\circ_{298}$ Theo.	$-\Delta S^\circ_{298}$ Expt.
	$\Delta S^\circ_t$	$\Delta S^\circ_r$	$\Delta S^\circ_v$		
$F^-(D_2O)$	-32.4	6.34	3.54	22.5	17.4
$Cl^-(H_2O)$	-33.2	8.81	3.47	20.9	16.5
$Br^-(H_2O)$	-33.8	9.75	3.98	20.0	18.4
$I^-(H_2O)$	-34.0	10.04	6.28	17.7	16.3

All  $\Delta S^\circ$  values are given in entropy unit, e.u.



The comparison of the experimental values with the theoretical values of  $\Delta S_{298}^\circ$  indicates that the absolute values of the experimental  $\Delta S_{298}^\circ$  are low by as much as 5 e.u. for  $F^-(D_2O)$ . The calculated values of  $\Delta S_{298}^\circ$  may involve some error due to the approximations made in the calculations. However, these approximations should not cause an error in excess of one to two e.u. Thus a major part of the difference between the experimental and calculated  $\Delta S_{298}^\circ$  for  $F^-(D_2O)$  may be due to the error in  $\Delta S_{\text{exp}}^\circ$ , which, in turn, can be contributed to the experimental uncertainty in the values of  $\Delta H^\circ$  and  $\Delta G^\circ$ . One Kcal/mole or about 5% error in the absolute value of  $\Delta H^\circ$  will cause an error of 3.3 e.u. in the absolute values of  $\Delta S_{298}^\circ$ . Furthermore,  $\Delta G_{298}^\circ$  values, for the formation of the cluster  $X^-(H_2O)$ , have been obtained from the extrapolated values of the equilibrium constants; therefore, an additional error may have been introduced by this extrapolation.

Another point which should be mentioned is that the absolute value of  $\Delta S_{\text{exp}}^\circ$  for  $Br^-(H_2O)$  is higher than those of  $Cl^-(H_2O)$  and  $F^-(D_2O)$ . The theoretical consideration, based on the argument that higher halide ion-ligand bond energy in  $F^-(D_2O)$  and  $Cl^-(H_2O)$  should give a larger decrease in entropy, would make our data look internally inconsistent, at the first glance. However, this can also be attributed to a small experimental error in the  $(\Delta H^\circ - \Delta G^\circ)$



values for  $\text{Cl}^-(\text{H}_2\text{O})$  and  $\text{F}^-(\text{D}_2\text{O})$ . Assuming that the  $\Delta S_{\text{exp}}^\circ$  of  $\text{Br}^-(\text{H}_2\text{O})$  is correct, the values of  $\Delta S_{\text{exp}}^\circ$  for  $\text{F}^-(\text{D}_2\text{O})$  and  $\text{Cl}^-(\text{H}_2\text{O})$  are low by 2 to 3 entropy units.

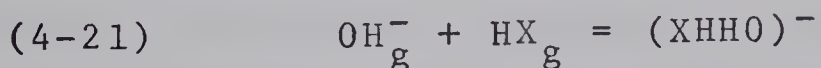
The entropy change for the reactions involving larger clusters [ $\text{X}^-(\text{H}_2\text{O})_n$  for  $n$  greater than one] can also be calculated by the above procedure, except a number of additional approximations have to be made. Therefore, such calculations were not performed.

#### 4.6 Gas Phase Solvation of $\text{OH}^-$ by Hydrogen Halides

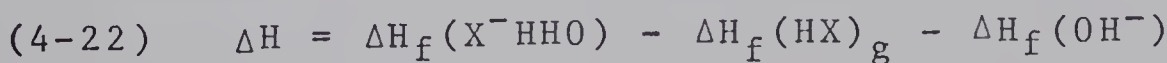
In the previous text the halide hydrates were written as  $\text{X}^-(\text{H}_2\text{O})$ . However the negative charge need not be completely localized on the halogen atom. The electronic structure is probably better represented as a hybrid of the forms:



Therefore, there should be only one heat of formation for the resonance hybrid for which we will use the notation  $(\text{XHHO})^-$ . This consideration shows that it is possible to calculate the enthalpy change for reaction (4-21).



This is given by



Thus once  $\Delta H_f(\text{XHHO})$  is determined, the enthalpy change



for the reaction (4-21) can be calculated. The heat of formation of  $(X^-HHO)$  is given by

$$\Delta H_f(X^-HHO) = \Delta H_f(X^-) + \Delta H_f(H_2O) + \Delta H_{0,1}$$

The  $\Delta H_f(H_2O)_g$  and  $\Delta H_f(HX)_g$  are well known (48) and  $\Delta H_f(X^-)$  is simply equal to  $\Delta H_f(X)$  plus the electron affinity of the halogen atom. The electron affinity of OH is taken as 1.82 eV (53), and the values of  $\Delta H_{0,1}$  are taken from table (4-1) to (4-4). The results of calculation of the enthalpy change for the solvation of  $OH^-$  by hydrogen halides are given in table (4-11).

#### 4.7 Ion-Molecule Reactions Involved in the Production of Negative Ion, $X^-$

In the previous chapter "Production of ions and sampling", it was mentioned that when oxygen was present as carrier gas, the halide negative ions were produced through ion molecule reactions of the type



The production of the halide negative ions in the absence of  $O_2$  gas, however, is probably the result of the direct capture of the thermal electron by the parent compounds followed by dissociation. In the production of  $Cl^-$  from  $CCl_4$ , for instance, the following process may have taken place.





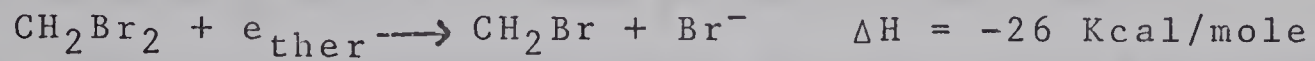
Table 4-11

Enthalpy change, for reaction  $\text{OH}^- + \text{HX} \rightarrow (\text{XHHO})^-$ 

Reaction	$-\Delta H$ Kcal/mole
$\text{OD}^- + \text{DF} = \text{OD}^- (\text{DF})$	48
$\text{OH}^- + \text{HCl} = \text{OH}^- (\text{HCl})$	77
$\text{OH}^- + \text{HBr} = \text{OH}^- (\text{HBr})$	84
$\text{OH}^- + \text{HI} = \text{OH}^- (\text{HI})$	93



The enthalpy change for the reaction (4-23) can be calculated from the available thermochemical data (48):  $EA(Cl) = 86 \text{ Kcal/mole}$ ,  $D(CCl_3-Cl) = 76 \text{ Kcal/mole}$ . This data would give a value of  $-10 \text{ Kcal/mole}$  for  $\Delta H_{rec}$  of (4-23). The probable dissociative electron capture processes for production of the other halide negative ions studied and the corresponding enthalpy changes are as follows:



As it was mentioned in previous chapter, when the hydration of fluoride ion was being studied, a series of peaks corresponding to the ions  $OD^-(D_2O)_n$  were observed. It is believed that the following process was involved in the production of  $OD^-$



Taking the values 42 and 82 Kcal/mole for electron affinities of the hydroxide radical and fluorine, respectively, and 139 and 121 Kcal/mole (48) for bond energies of (D-F) and (D-O-D) respectively, one would obtain a value of 22 Kcal/mole for the heat of reaction (4-24). Although this calculation shows that the reaction (4-24) is endothermic, the endothermicity is not large enough to rule out its occurrence in the ion source. The corresponding reactions for other halide



negative ions are



The energy requirements for these reactions to take place are three to four times larger than for reaction (4-20), thus the occurrence of reactions (4-25), (4-26) and (4-27) in the ion source would be less probable than that of (4-16). This is in accordance with the fact that the series  $\text{OH}^-(\text{H}_2\text{O})_n$  was not observed in the study of  $\text{Cl}^-$ ,  $\text{Br}^-$  and  $\text{I}^-$ .

At the end of this work some runs were made with pure  $\text{D}_2\text{O}$ , in attempt to check the production of  $\text{OD}^-(\text{D}_2\text{O})_n$ . However, in addition to  $\text{OD}^-(\text{D}_2\text{O})_n$ , the series  $\text{F}^-(\text{D}_2\text{O})_n$  was also observed. This was due to the minute traces of fluorine in the apparatus, which could not be removed even with continuous baking for three days. Consequently, no conclusive evidence for the production of  $\text{OD}^-(\text{D}_2\text{O})_n$  in pure  $\text{D}_2\text{O}$  could be obtained. To study the nature of the ion molecule reactions which take place in the production of  $\text{F}^-$  and  $\text{OD}^-$ , a pulsing system is being installed in the present instrument. Hopefully, the future study being carried out in this laboratory by other investigators will give us a better understanding of these reactions.



#### 4.8 Equilibrium Distribution of $X^-(H_2O)_n$

The equilibrium constant values, obtained in this work and presented in this chapter, can be utilized to calculate the relative equilibrium concentrations of the cluster  $X^-(H_2O)_n$  at various temperatures and partial pressures of water. As an illustration, the relative equilibrium concentrations of the clusters  $Cl^-(H_2O)_n$  are presented in figure (4-35) for a temperature of 300°K and partial pressures of water ranging from  $10^{-3}$  to 10 torr. For this calculation the equilibrium constants,  $K_{0,1}$ ,  $K_{1,2}$ ,  $K_{2,3}$  and  $K_{3,4}$ , at temperature of 300°K, were taken from figure (4-18). The equilibrium constant  $K_{4,5}$  is not given in figure (4-18); however, its value could be estimated from some of the high pressure (4 to 5 torr) runs made at room temperature. This estimated value is 0.08 torr<sup>-1</sup>. The concentration of  $Cl^-$  was arbitrarily set to unity. The concentration of the cluster  $Cl^-(H_2O)_n$ ,  $[Cl^-(H_2O)_n]$  is given by (4-28)

$$(4-28) \quad [Cl^-(H_2O)_n] = K_{0,n} P^n$$

where  $K_{0,n}$  is the product of the equilibrium constants from  $K_{0,1}$  to  $K_{n-1,n}$ , and  $P$  is the partial pressure of water. By setting the sum of the clusters  $Cl^-$  to  $Cl^-(H_2O)_n$  to 100, the relative concentration of each cluster is obtained.

#### 4.9 Comparison of Gas Phase Hydration Energies for Positive and Negative Ions

The step gas phase hydration energies for positive



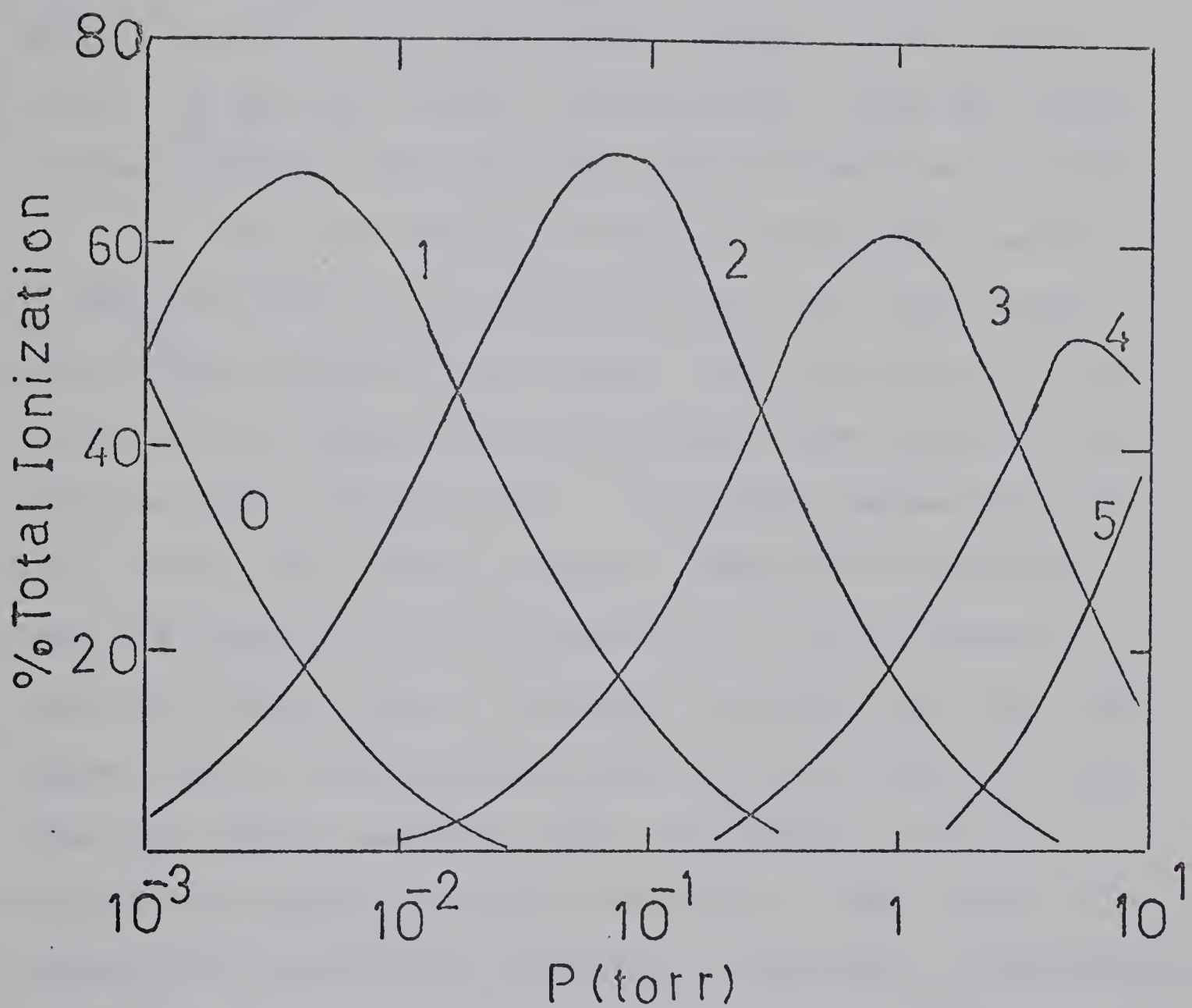


Figure 4-35: Plots of Equilibrium Distribution of  $\text{Cl}^-(\text{H}_2\text{O})_n$  at  $T=300^\circ\text{K}$ , as a Function of Water Pressure.



and negative ions are presented graphically in figures (4-36). The data for positive ions are taken from the studies of I. Dzidic (24) and S. K. Searles (35) which were made in this laboratory. For comparison, the difference of the step hydration,  $\Delta H_{0,n}^\circ$  for ion pairs,  $\text{Na}^+, \text{F}^-$ ;  $\text{Rb}^+, \text{Cl}^-$  and  $\text{Cs}^+, \text{Br}^-$  are plotted versus  $0,n$  in figures (4-37), (4-38) and (4-39), respectively. From the plots of these figures, the following observations can be made.

(i) For each ion pair chosen, the absolute values of  $\Delta H_{0,1}^\circ$  and  $\Delta H_{1,2}^\circ$  of the positive ion are higher than those of the negative ion and yet the total heats of hydration of the negative ions are higher than those of the positive ions, table (4-12). A probable explanation for this is that the initial steps of hydration of positive ions are assisted by the formation of a dative bond between the oxygen atom of the water molecule and ion. The oxygen atom in water molecule has two lone pairs of electrons and alkali positive ions, in general, do have unoccupied low energy orbitals available. Thus, there is a tendency for dative bond formation, resulting in additional strength for the bond between the positive ions and the first few water molecules.

(ii) The positive ion curves are steeper than the curves for the negative ions. This may also be a result of the existence of the dative bond, mentioned above, in



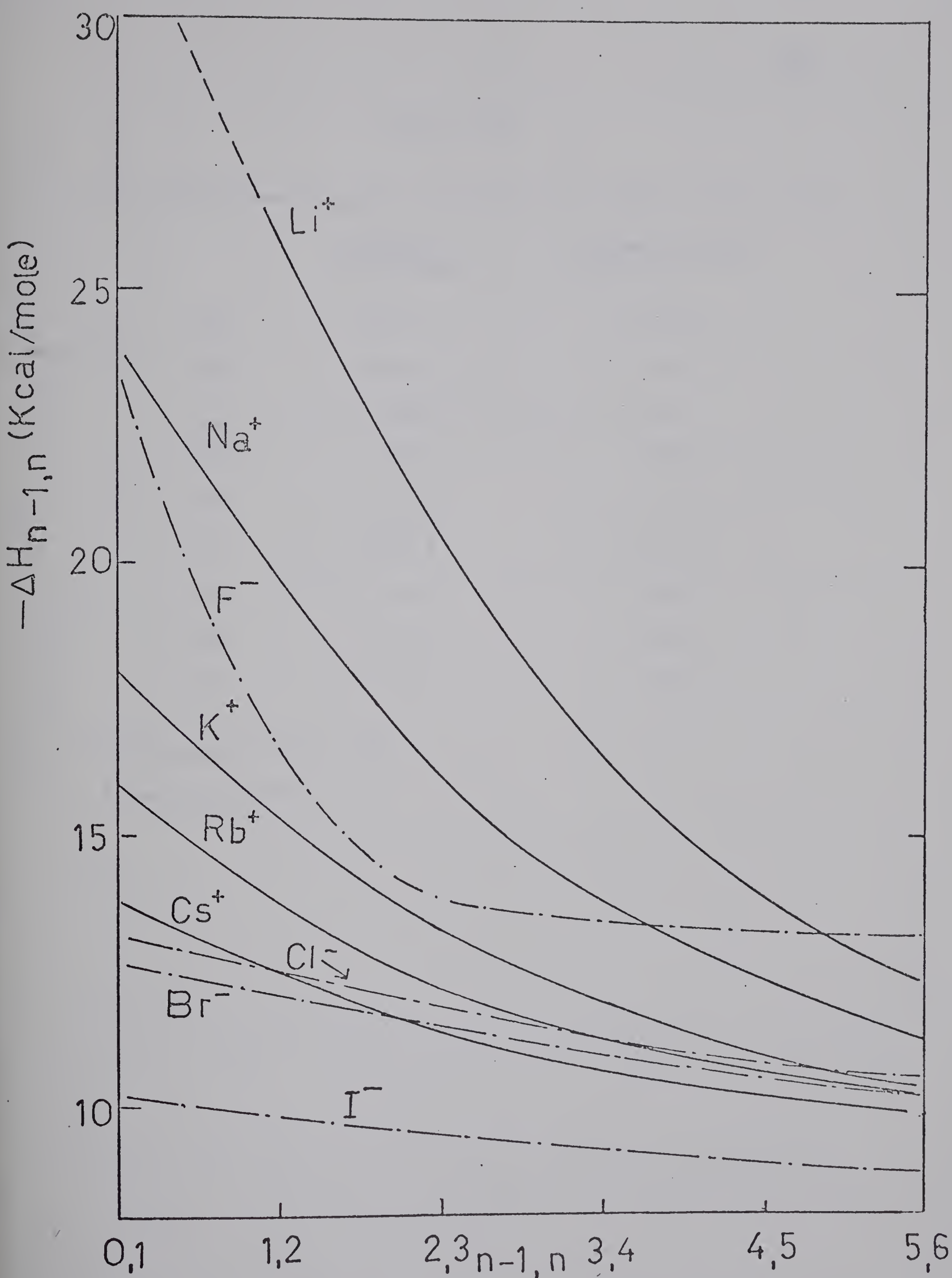


Figure 4-36: Step Hydration Energies,  $\Delta H_{n-1,n}^\circ$  Versus  $n-1,n$   
for Halide and Alkali Metals Ions.



Table 4-12

Total Hydration Energies of Halide and Alkali Metal Ions

	Randles'* Kcal/mole	Latimer <u>et</u> <u>al</u> ** Kcal/mole
Li <sup>+</sup>	-132.1	-121.2
Na <sup>+</sup>	-106.0	-94.6
K <sup>+</sup>	-85.8	75.8
Rb <sup>+</sup>	-79.8	-69.2
Cs <sup>+</sup>	-72.0	-62.0
F <sup>-</sup>	-113.3	-122.6
Cl <sup>-</sup>	-81.3	-88.7
Br <sup>-</sup>	-77.9	-81.4
I <sup>-</sup>	-64.1	-72.1

\* References (75), (76)

\*\* Reference (73)



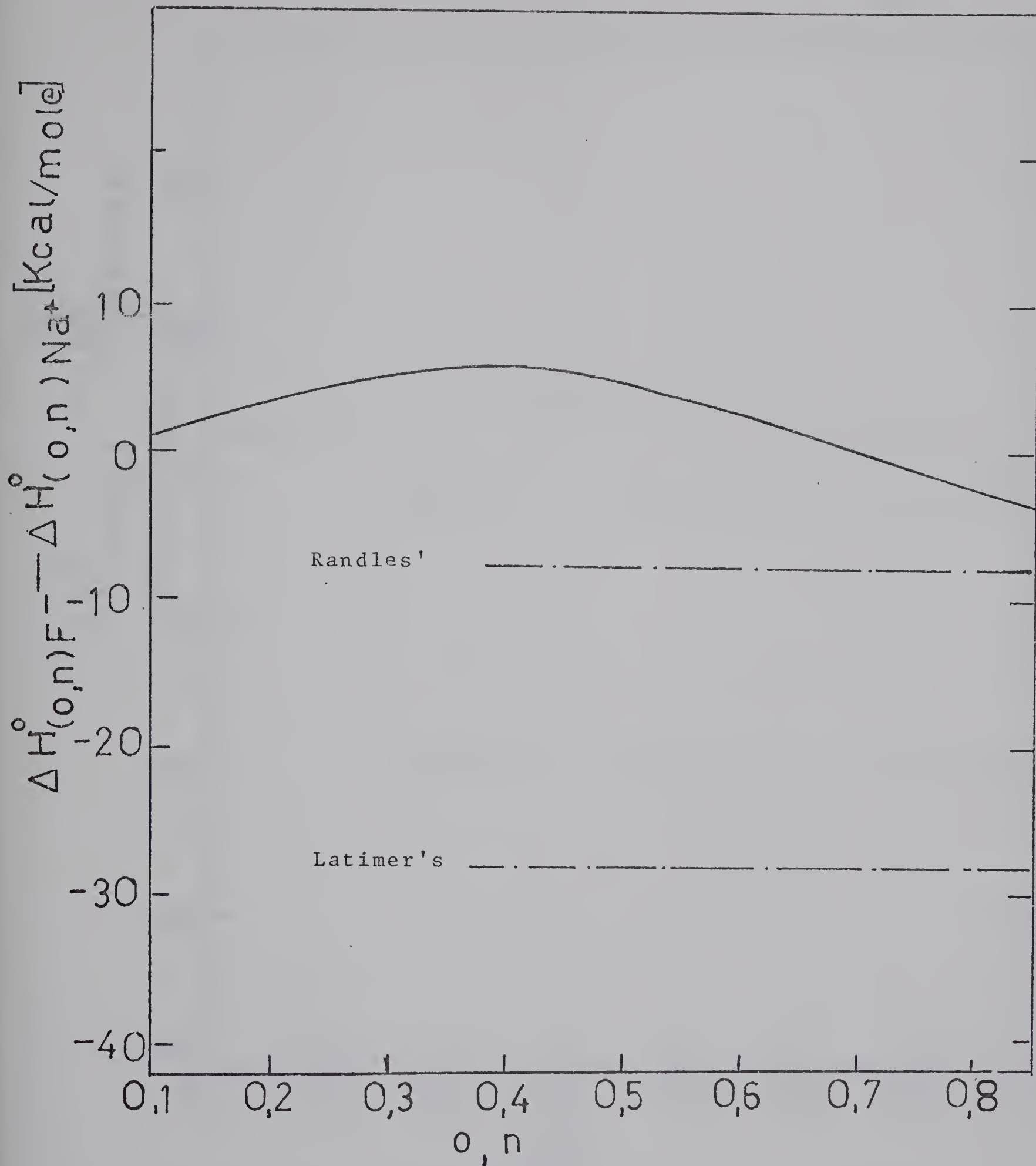


Figure 4-37: Plot of  $[\Delta H^\circ_{(0,n)}F^- = \Delta H^\circ_{(0,n)}Na^+]$  Versus  $0, n$ .

The  $\Delta H^\circ_{0,n}$  for  $n$  over 6 are extrapolated from figure (4-37).



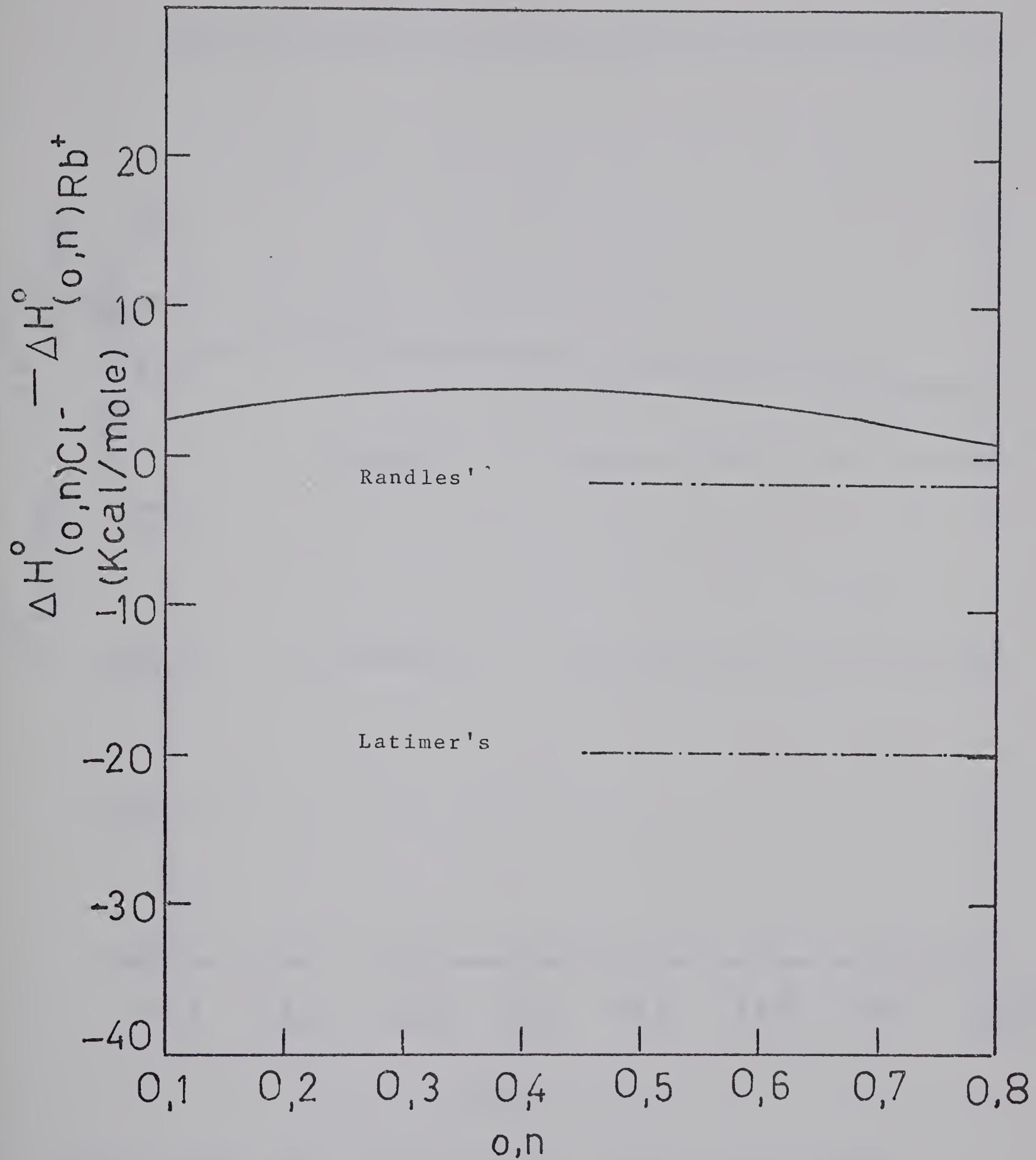


Figure 4-38: Plot of  $[\Delta H^\circ (0,n)a^- - \Delta H^\circ (0,n)Rb^+]$  Versus  $0,n$ . The  $\Delta H^\circ_{0,n}$  for  $n$  over 6 are extrapolated from figure (4-36).



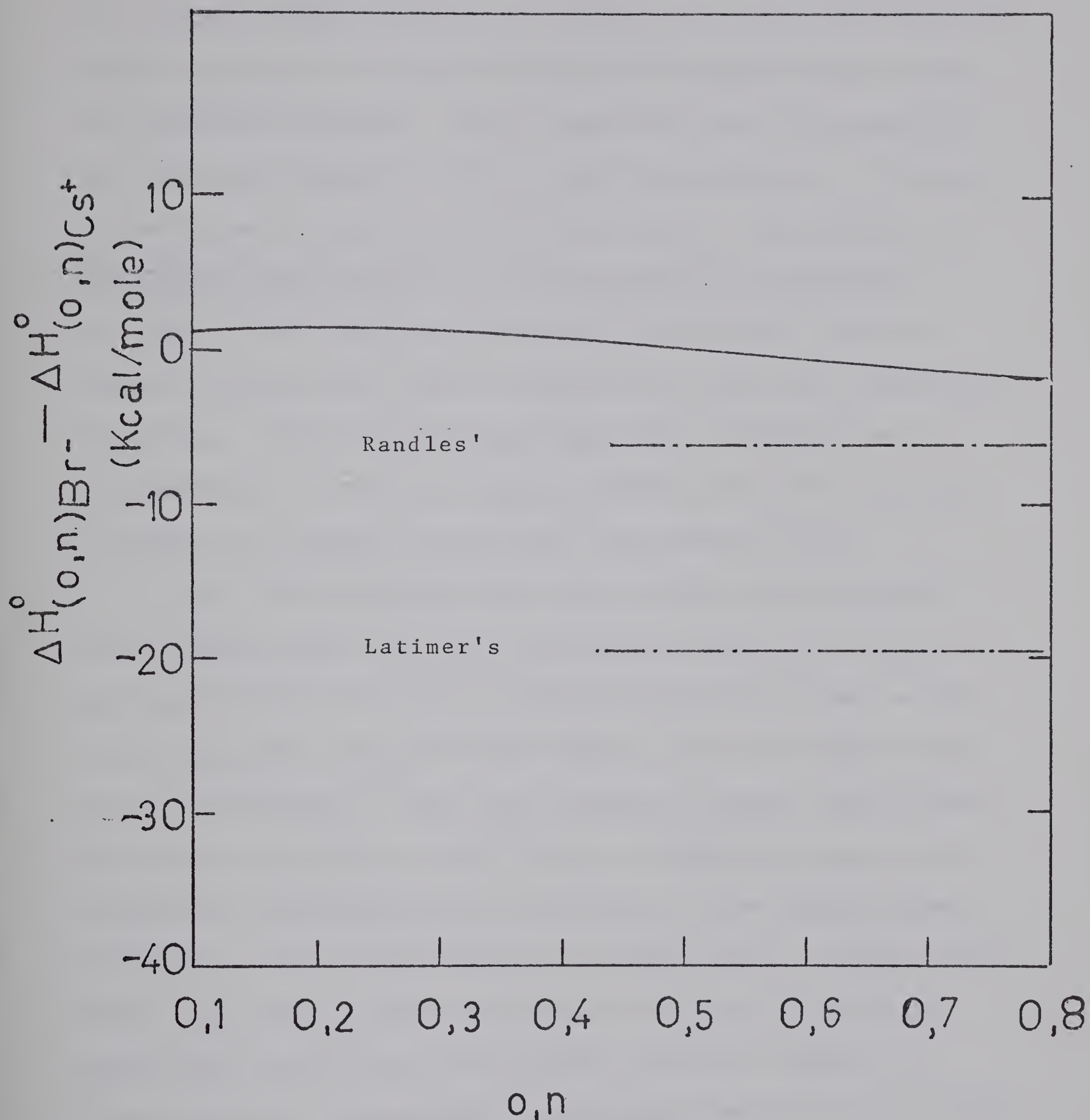


Figure 4-39: Plot of  $[\Delta H^\circ_{(0,n)} \text{Br}^- - \Delta H^\circ_{(0,n)} \text{Cs}^+]$  Versus  $0,n$ . The  $\Delta H_{0,n}$  for  $n$  over 6 are extrapolated from figure (4-36).



the positive ion cluster. In general, as more water molecules are added to an ion cluster, the ligand-ligand repulsion energy increases. Thus, there will be a decrease in the absolute values of  $\Delta H_{n-1,n}^\circ$  with increasing n. However, in addition to this positive ion cluster, the effect of the dative bond formation, which gives the additional strength to the positive ion-water bond in the initial steps of hydration, would disappear as more water molecules are added. This effect would make the difference in the two successive values of  $\Delta H_{n-1,n}^\circ$  more pronounced, thus resulting in a steeper curves for the positive ions.

(iii) The negative ion curve of the pairs selected above crosses the positive ion curve at about n=3 to n=4, and the trend in our data indicates that from then on the step hydration energies for  $X^-(H_2O)_n$  would be higher than those of  $M^+(H_2O)_n$ . Thus, the original factor, which gives the extra stability to the cluster,  $M^+(H_2O)_n$ , seems to be completely overtaken by the increase in the ligand-ligand repulsion energy for "n" greater than three. On the other hand, as it was pointed out in section (4-4), the water molecules surrounding the negative ions are capable of changing their arrangement to minimize the effect of ligand-ligand repulsion. It is interesting that this change in arrangement also take place for values of "n" somewhere between three and four.



(iv) The total single-ion hydration energies for positive and negative ions have been determined by several authors (72) to (75). In table (4-12) two sets of these values are represented. The first set is taken from the work of Latimer, Pitzer and Slanski, the second set is obtained from the review of Desnoyer (76) and is based on the values of the free energies of hydrations determined by Randles (75). Included in the figures (4-37) to (4-39) are the differences of the total hydration energies as predicted by the Latimer et al and Randles data. Examining these figures, we find that the plots of  $[\Delta H^\circ_{(0,n)X^-} - \Delta H^\circ_{(0,n)M^+}]$ , after going through a maximum, will approach the Randles line, as  $n$ , the number of water molecules around the ion increases. Although in these plots, the value of  $n$  does not go beyond eight, it is very unlikely that the difference,  $[\Delta H^\circ_{(0,n)X^-} - \Delta H^\circ_{(0,n)M^+}]$  will get as large as the values predicted by the Latimer et al data. Thus, we conclude that the data obtained in this laboratory support the values of hydration energies which are based on the Randles values of the free energies of hydration.



5 GAS PHASE HYDRATION OF OD<sup>-</sup>, O<sub>2</sub><sup>-</sup> and NO<sub>2</sub><sup>-</sup>5.1 Introduction

In addition to the halide negative ions, the gas phase hydrations of OD<sup>-</sup>, O<sub>2</sub><sup>-</sup> and NO<sub>2</sub><sup>-</sup> were also studied. The equations used to calculate the thermodynamic values of these ions are the same as those given at the beginning of the previous chapter.

Unfortunately, the study of NO<sub>2</sub><sup>-</sup> was made at a single temperature (292°K). Therefore, the evaluation of  $\Delta H_{n-1,n}^\circ$  and  $\Delta S_{n-1,n}^\circ$  is not possible for this ion. The equilibrium constants obtained for NO<sub>2</sub><sup>-</sup>(H<sub>2</sub>O)<sub>n</sub> at this temperature are given in figure (5-1) and the corresponding  $\Delta G_{n-1,n}^\circ$  are presented in table (5-1).

5.2 Hydration of OD<sup>-</sup>

The equilibrium constants obtained for the following reaction:



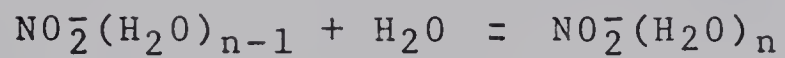
are given in figures (5-2) to (5-6). The values of the equilibrium constants at any specific ion source temperature do not show any specific trend, thus the equilibrium condition was prevailing in the ion source for the pressure range which was covered in this study.

The Van't Hoff plots of the equilibrium constants



Table 5-1

Equilibrium Constants and the Corresponding  $\Delta G^\circ_{n-1,n}$  for Reaction



$(n-1), n$	$K$ $torr^{-1}$	$-\Delta G^\circ_{n-1,n}$ $Kcal/mole$
1, 2	46	5.90
2, 3	3	4.45
3, 4	0.44	3.35



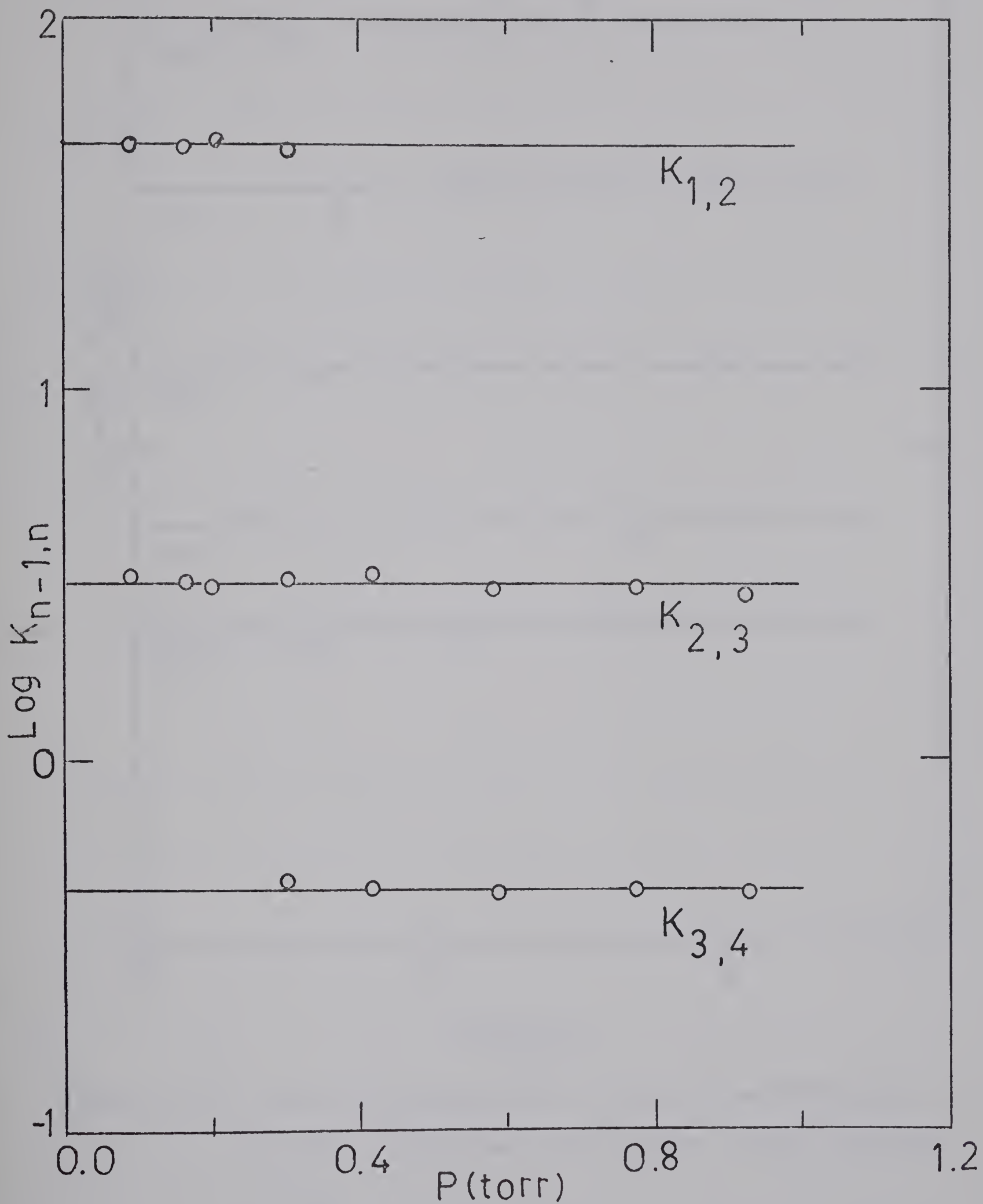


Figure 5-1: Plots of  $\text{Log } K_{n-1,n}$  for the Gas Phase Hydration of  $\text{NO}_2^-$ , at  $292^\circ\text{K}$ , Versus Pressure of  $\text{H}_2\text{O}$ .



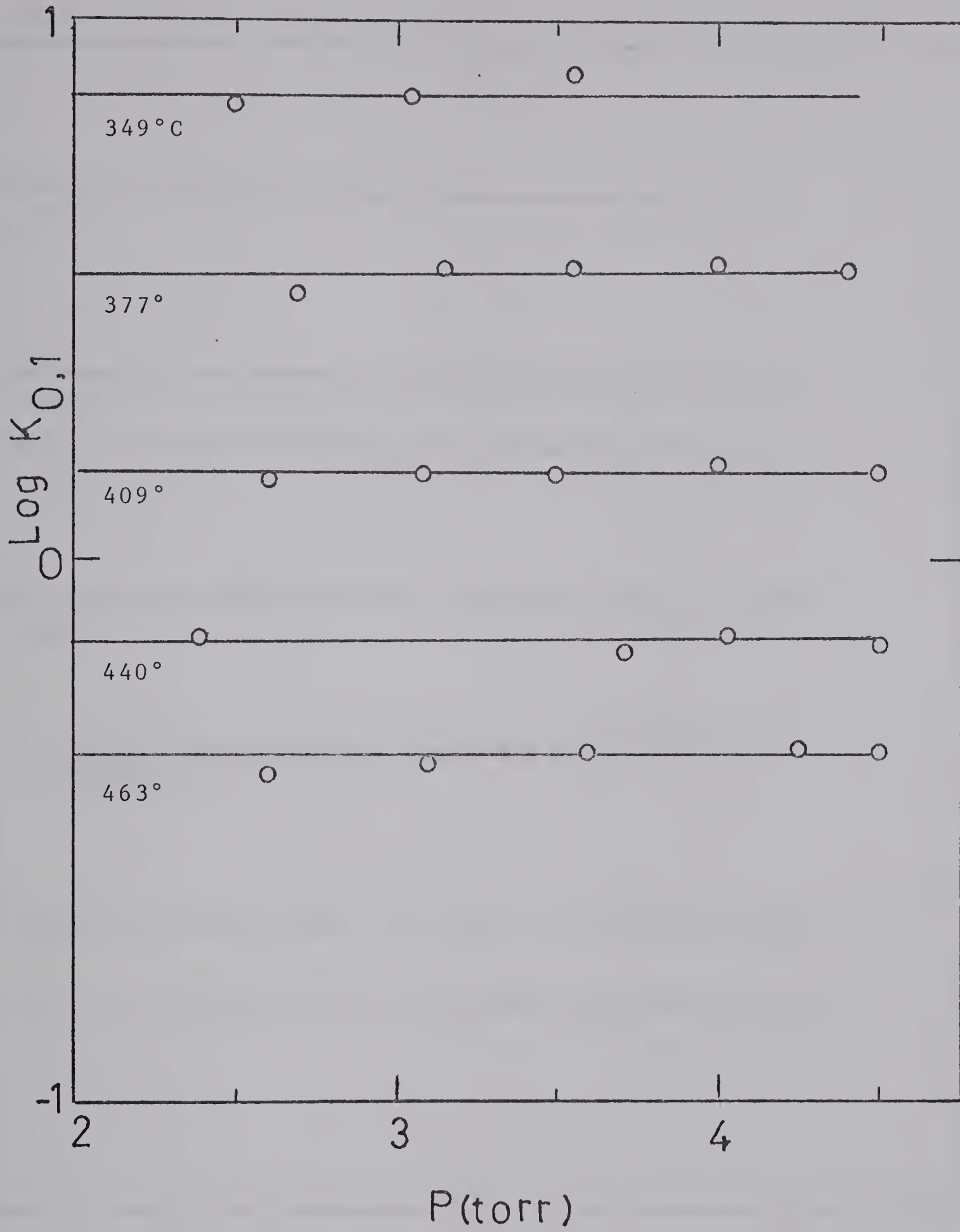


Figure 5-2: Plots of  $\text{Log } K_{0,1}$  for the Gas Phase Hydration of  $\text{OD}^-$ , at Various Temperatures, Versus Pressure of  $\text{D}_2\text{O}$ .



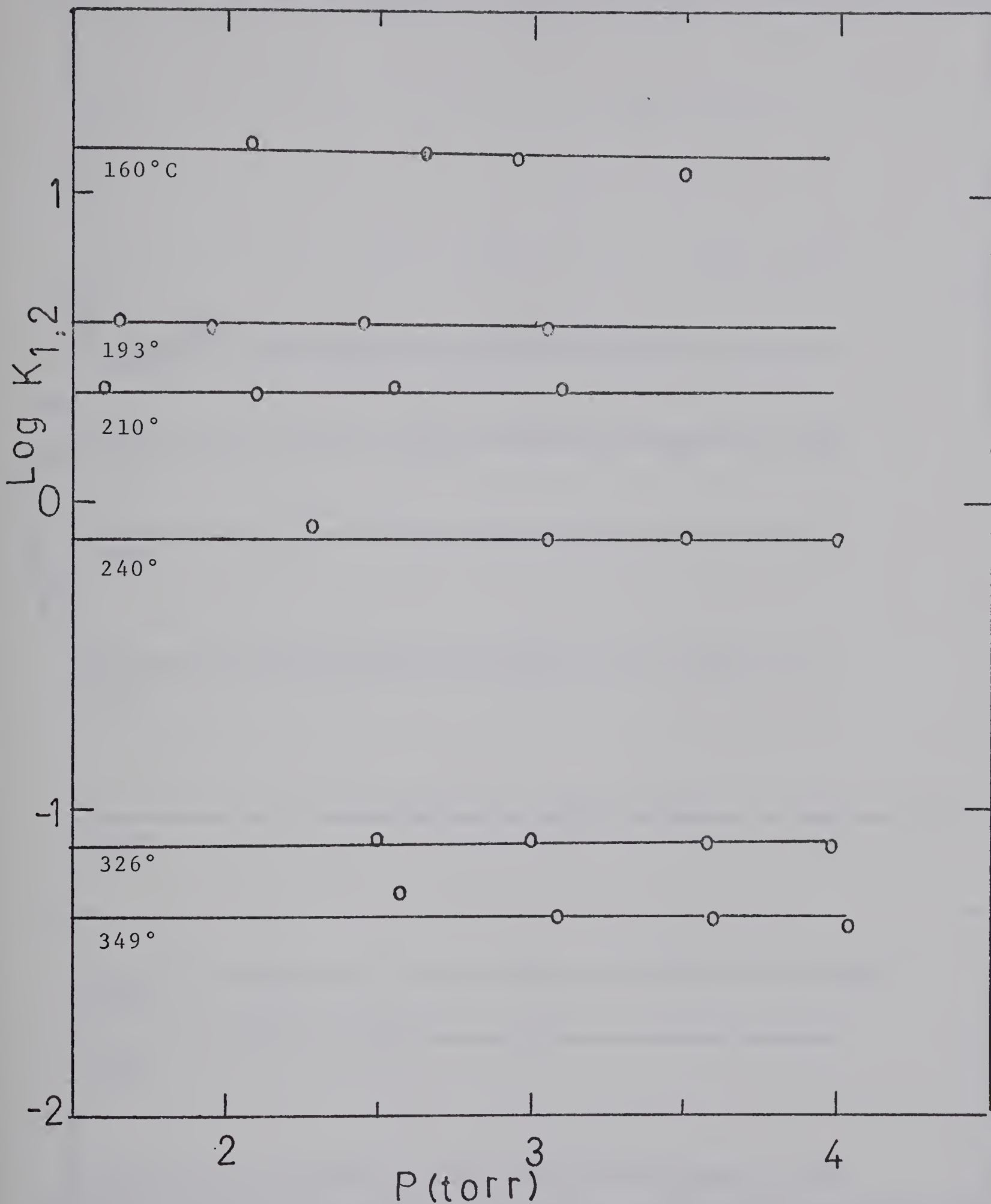


Figure 5-3: Plots of  $\log K_{1,2}$  for the Gas Phase Hydration of  $\text{OD}^-$ , at Various Temperatures, Versus Pressure of  $\text{D}_2\text{O}$ .



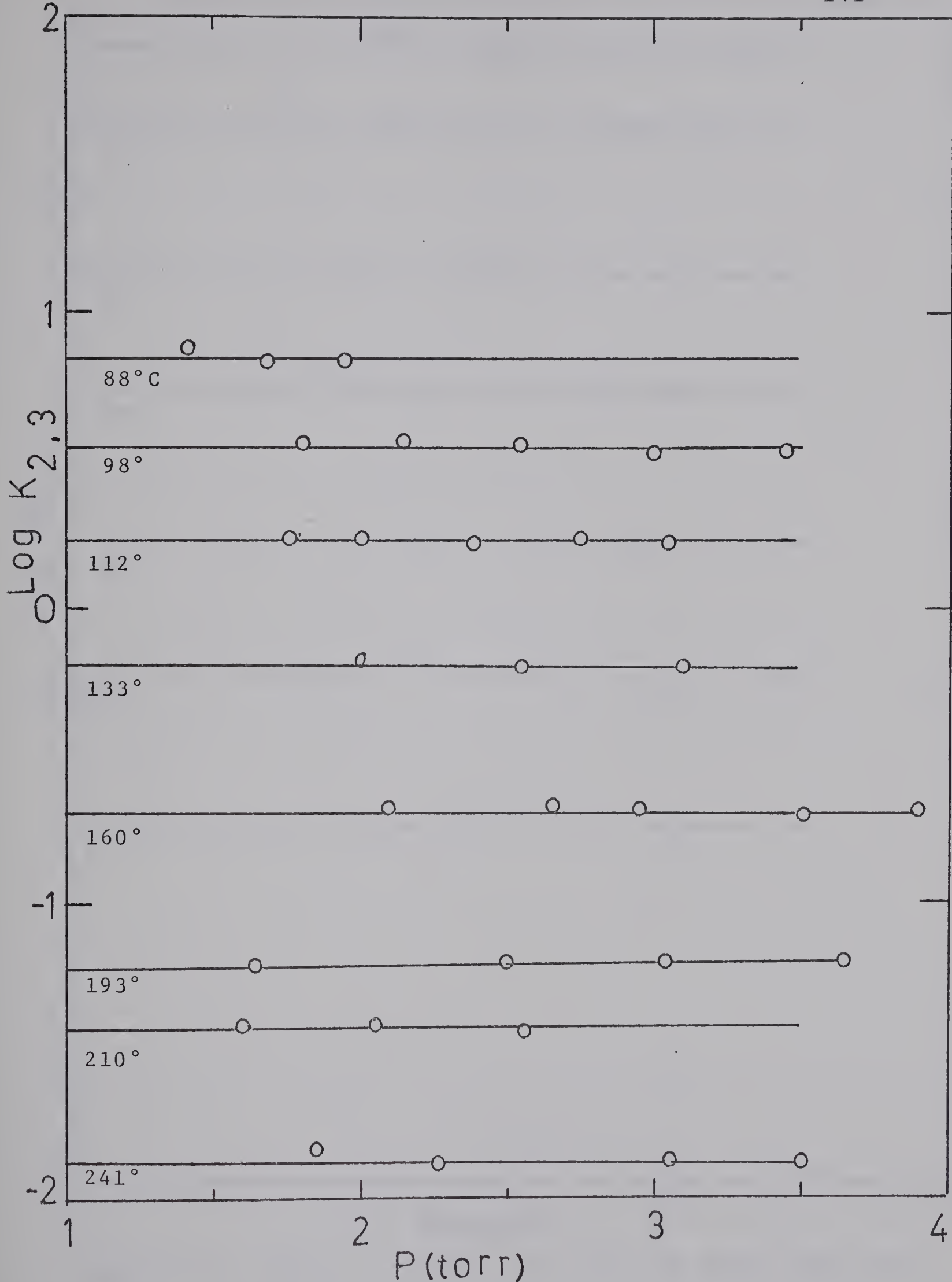


Figure 5-4: Plots of Log of K<sub>2,3</sub> for the Gas Phase Solvation of OD<sup>-</sup>, at Various Temperatures, Versus Pressure of D<sub>2</sub>O.



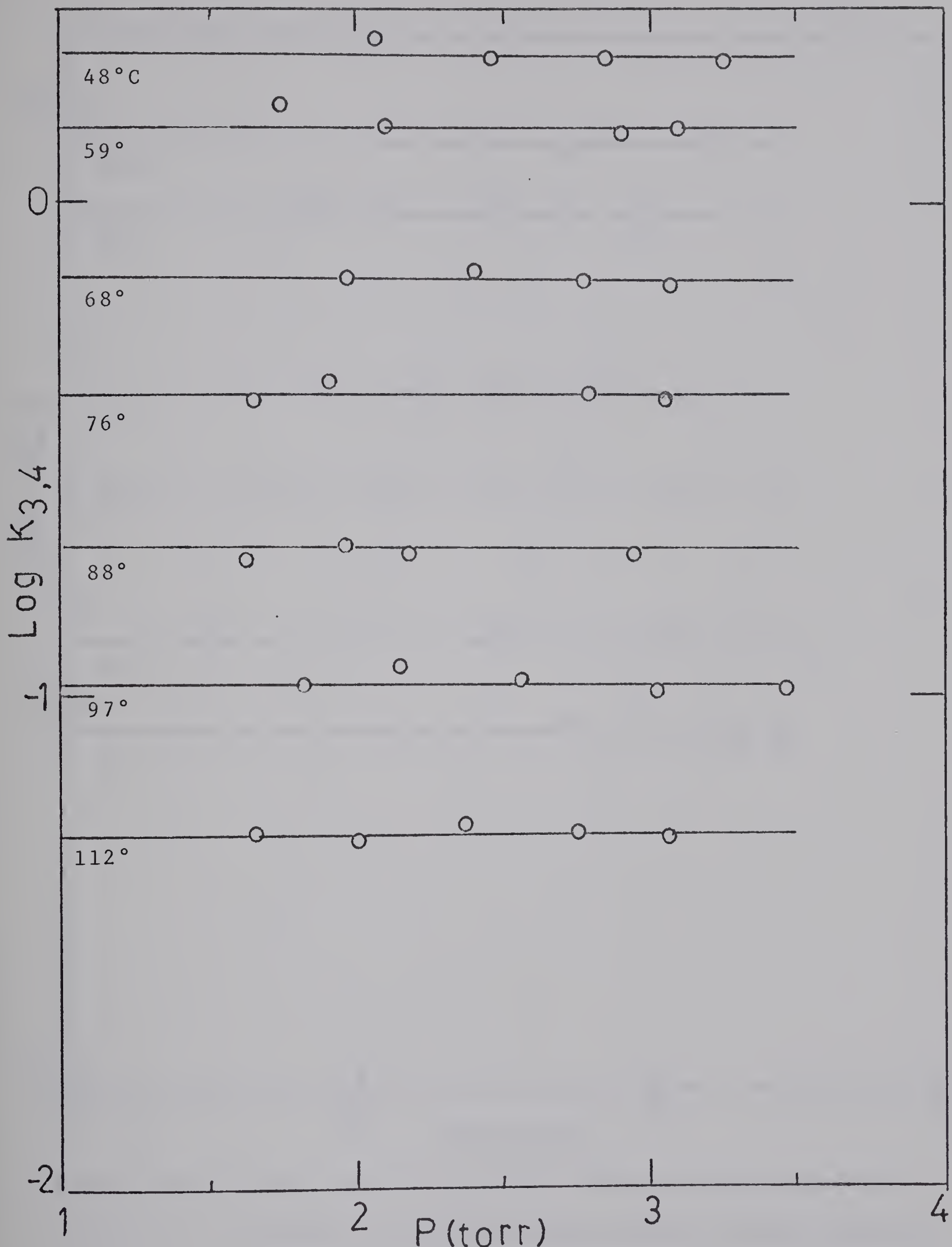


Figure 5-4: Plots of Log  $K_{3,4}$  for the Gas Phase Hydration of  $OD^-$ , at Various Temperatures, Versus Pressure of  $D_2O$ .



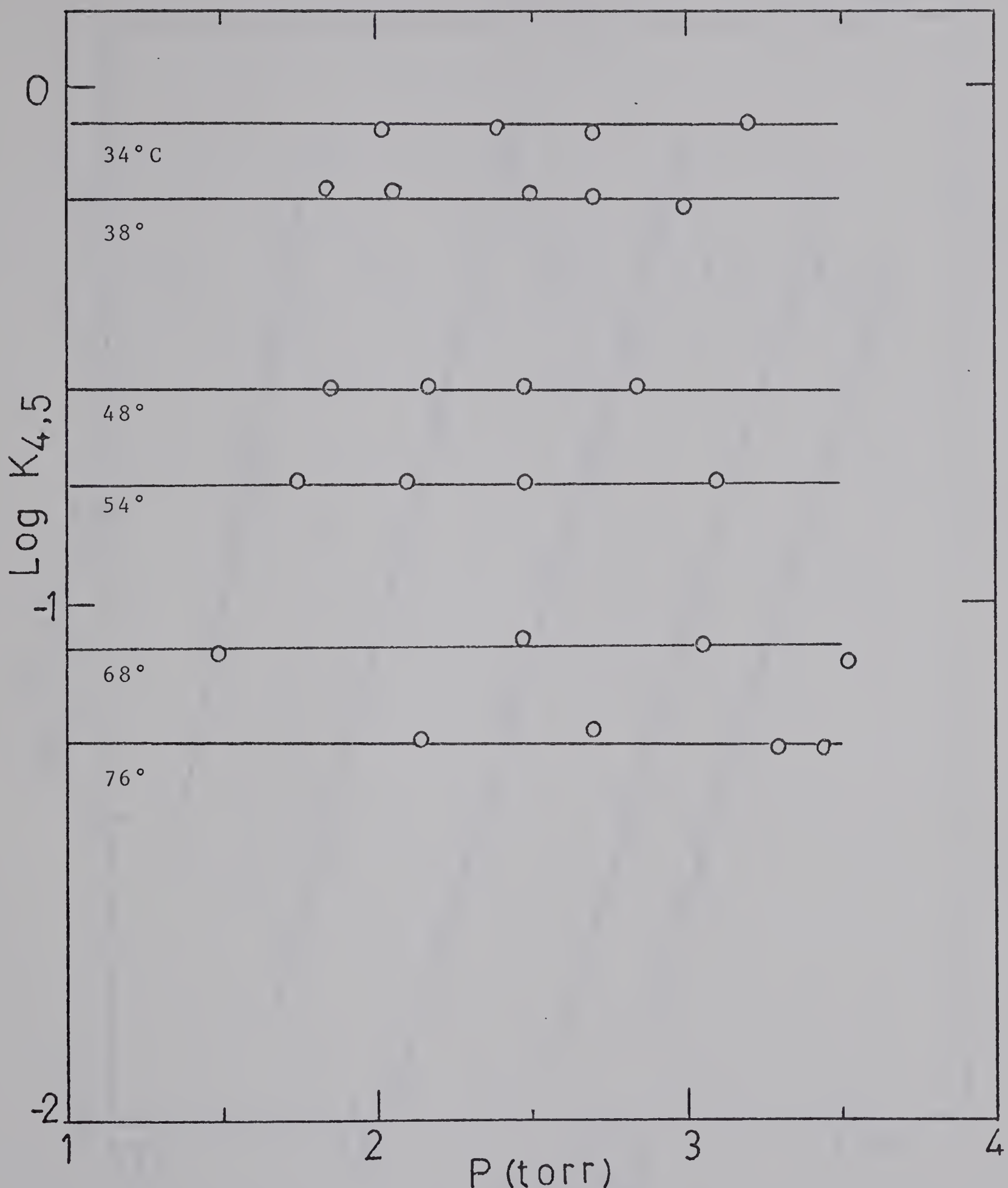


Figure 5-6: Plots of  $\text{Log } K_{4,5}$  for the Gas Phase Hydration of  $\text{OD}^-$ , at Various Temperatures, Versus Pressure of  $\text{D}_2\text{O}$ .



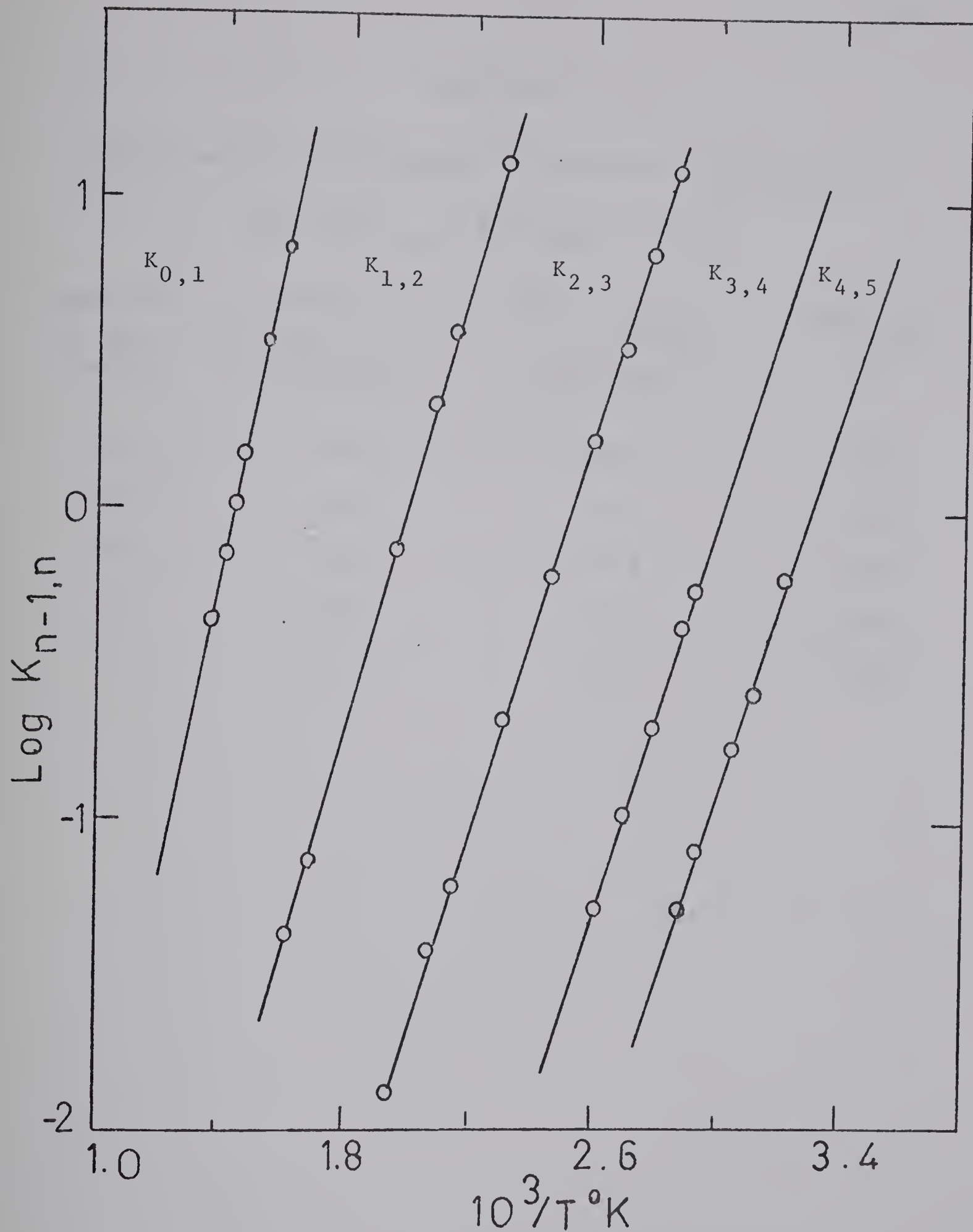


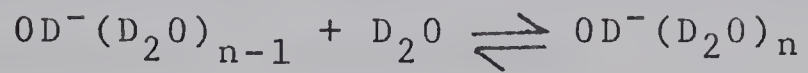
Figure 5-7: Van't Hoff-Type Plots of the Equilibrium

Constants,  $K_{n-1,n}$  for the Gas Phase Hydration  
of  $\text{OD}^-$ .



Table 5-2

Experimental Thermodynamic Values for the Reaction

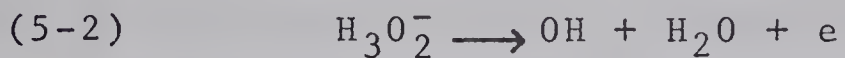


Reaction n-1, n	$-\Delta H^\circ_{n-1, n}$ Kcal/mole	$-\Delta G^\circ_{n-1, n}(298)$ Kcal/mole	$-\Delta S^\circ_{n-1, n}$ eu
0-1	22.5	16.9	19.1
1-2	16.4	10.7	19.3
2-3	15.1	7.73	24.8
3-4	14.2	5.45	29.5
4-5	14.1	4.22	33.2



are given in figure (5-7). From the slopes of these plots the  $\Delta H^\circ_{n-1,n}$  are determined;  $\Delta G^\circ_{n-1,n}$  and  $\Delta S^\circ_{n-1,n}$  were determined by equations (4-2) and (4-3) respectively. These values are presented in table (5-2).

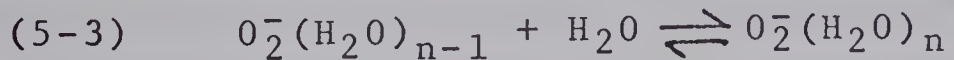
In a study of the negative ions in a hot cathode arc discharge through ammonia at an approximate pressure of 0.05 torr, Golub and Steiner have obtained a value of  $2.95 \pm 0.15$  eV as the required energy for the reaction (5-2) (54).



Based on the value of 1.8 eV for the electron affinity of OH (53), they have come up with a value of 1.2 eV for the sum of the chemical binding energy of  $\text{H}_3\text{O}_2^-$  and the kinetic energy of the separating neutral particle. Our experimental value of -22.5 Kcal/mole for  $\Delta H_{0-1}$  agrees quite well with theirs and gives approximately 0.2 eV as the kinetic energy of  $\text{H}_2\text{O}$  and OH in the reaction (5-2). Since the negative ion  $\text{OD}^-$  is not spherically symmetric and the structures of the clusters  $\text{OD}^-(\text{D}_2\text{O})_n$  are not known, no attempt was made to calculate the energy of  $\text{OD}^-(\text{D}_2\text{O})_n$  theoretically.

### 5.3 Hydration of $\text{O}_2^-$

The equilibrium constants for the reaction (5-3)



were determined for the temperature range of  $19^\circ\text{C}$  to  $251^\circ\text{C}$ .



These values are given in figures (5-8) to (5-11). The data in figure (5-11) represents the equilibrium constants obtained with the alpha source mass spectrometer at a single temperature of 19°C. The value of the equilibrium constant,  $K_{2,3}$ , obtained at this temperature is in complete agreement with the data obtained with the electron beam mass spectrometer. Unfortunately, no data was obtained for the equilibrium constants,  $K_{3,4}$  and  $K_{4,5}$  with the electron beam mass spectrometer. Therefore,  $\Delta H_{3,4}^\circ$  and  $\Delta H_{4,5}^\circ$  cannot be determined from the present work.

The Van't Hoff plots for the equilibrium constants  $K_{0,1}$ ,  $K_{1,2}$  and  $K_{2,3}$  are given in figure (5-1). Table (5-3) contains the thermodynamic values,  $\Delta H^\circ$ ,  $\Delta G^\circ$  and  $\Delta S^\circ$  for the reaction (5-3).

It is interesting to make a comparison between the relative abundances of  $O_2^-(H_2O)_n$  obtained by Moruzzi and Phelps (55) and those based on the equilibrium constants observed in this work. These two sets of data are given in table (5-4) and both were obtained at a water partial pressure of 0.44 torr and temperature 300°K. This table shows a discrepancy between the present results and those of Moruzzi and Phelps. Moruzzi and Phelps were studying the electron attachment process in a water and  $O_2$  mixture and, consequently, were not interested in equilibrium concentrations of the ion clusters  $O_2^-(H_2O)_n$ . Nevertheless, it is significant



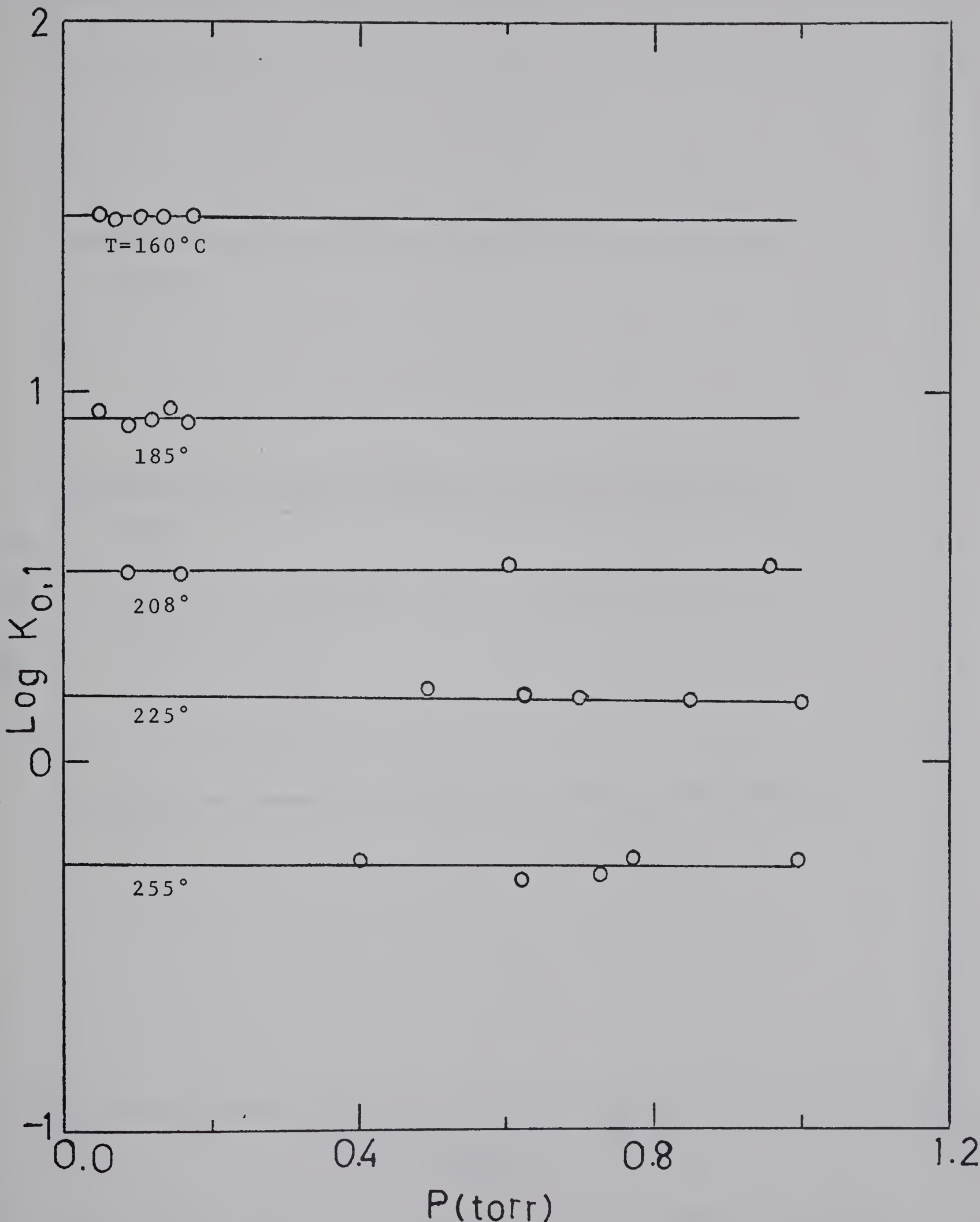


Figure 5-8: Plots of  $\log K_{0,1}$  for the Gas Phase Hydration of  $O_2$ , at Various Temperatures, Versus Pressure of  $H_2O$ .



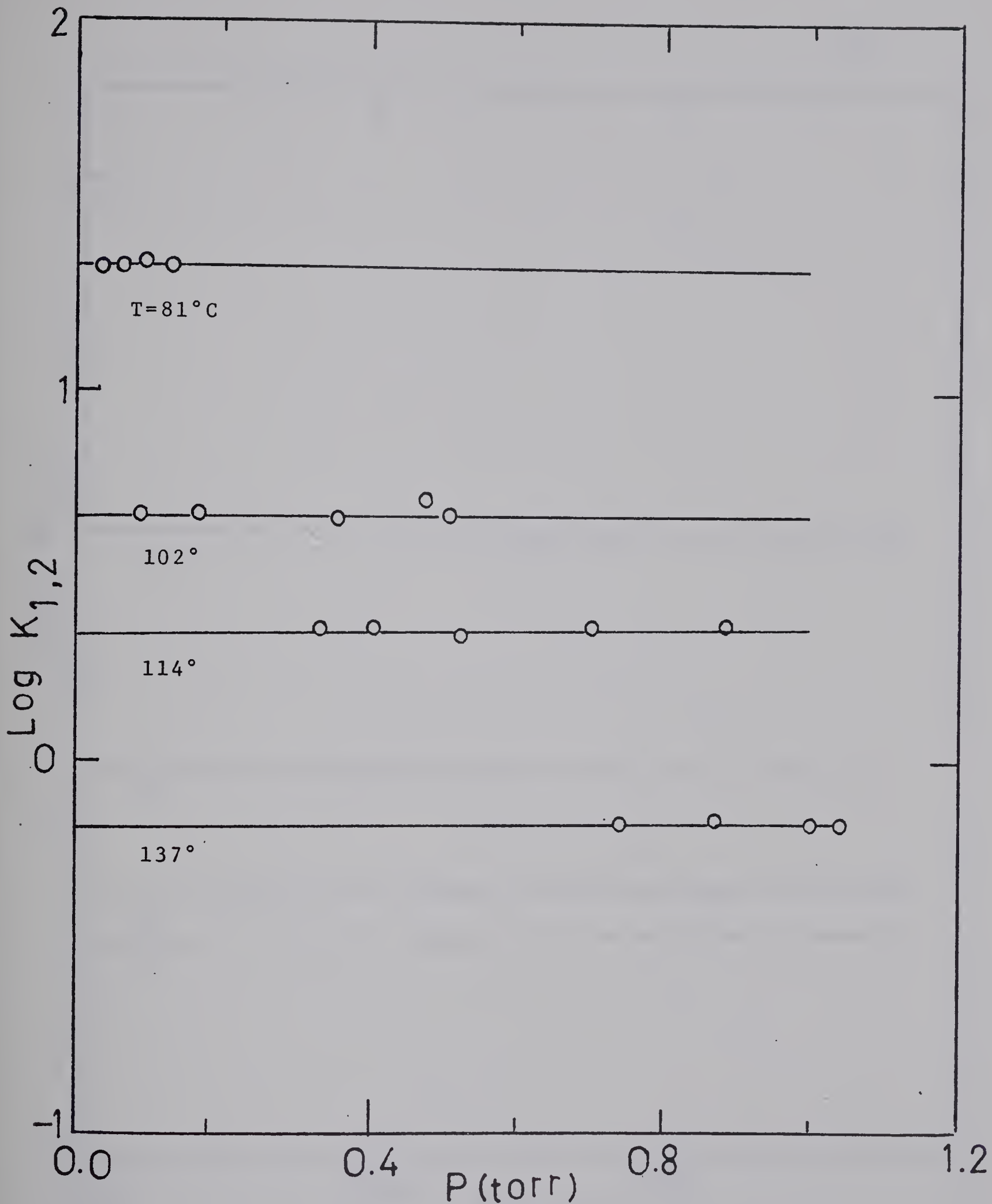


Figure 5-9: Plots of  $\text{Log } K_{1,2}$  for the Gas Phase Hydration of  $\text{O}_2^-$ , at Various Temperatures, Versus Pressure of  $\text{H}_2\text{O}$ .



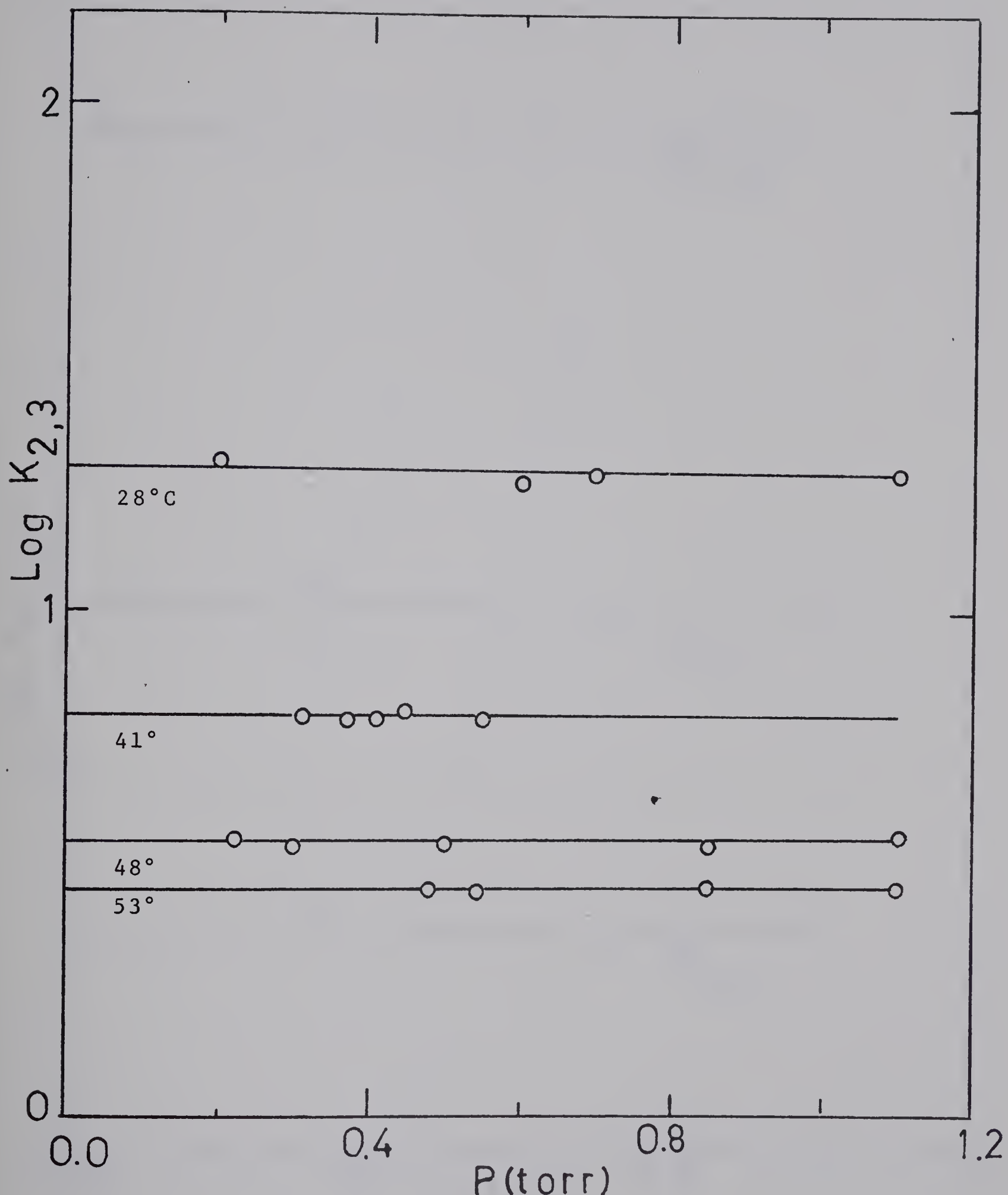


Figure 5-10: Plots of  $\text{Log } K_{2,3}$  for the Gas Phase Hydration of  $O_2$ , at Various Temperatures, Versus Pressure of  $H_2O$ .



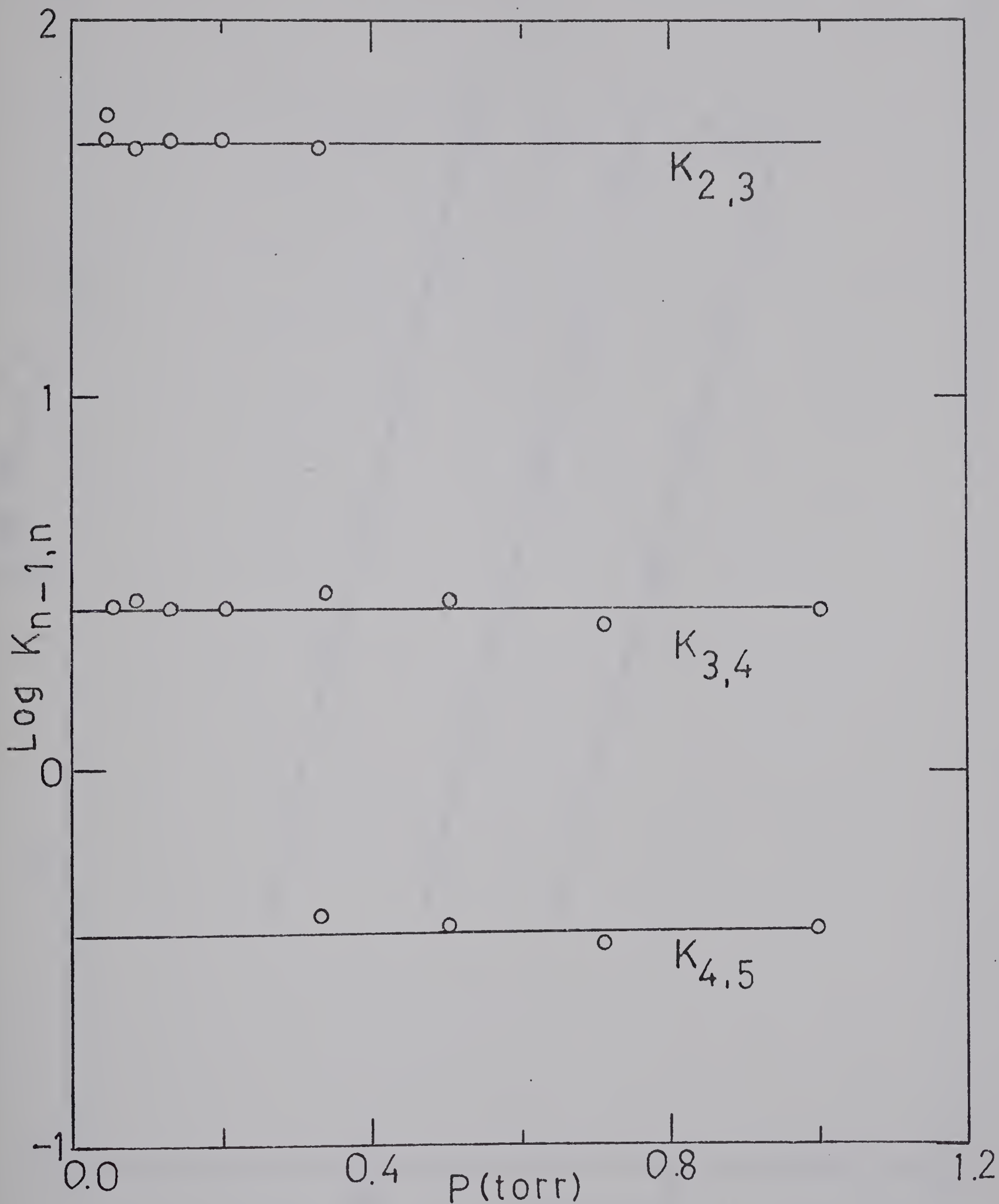


Figure 5-11: Plots of  $K_{n-1,n}$  for the Gas Phase Hydration of  $O_2^-$ , at  $292^\circ K$ , Versus Pressure of  $H_2O$ .

These Values were Obtained on the Alpha Source Mass Spectrometer.



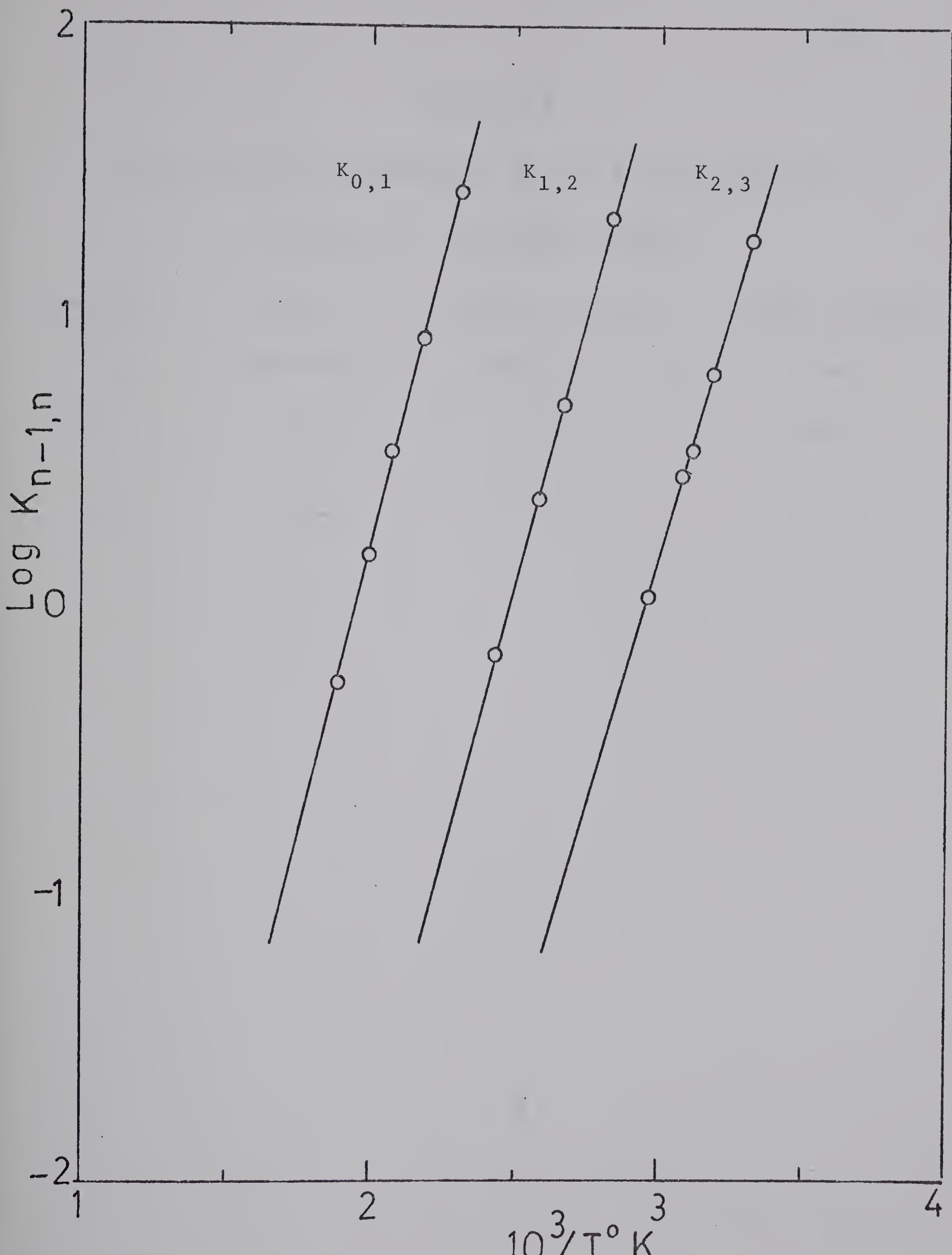
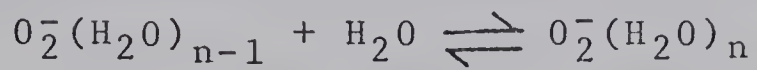


Figure 5-12: Van't Hoff-Type Plots of the Equilibrium Constants for the Gas Phase Hydration of  $O_2$ .



Table 5-3

Experimental Thermodynamic Values for the Reaction



Reaction n-1, n	$-\Delta H_{n-1, n}^\circ$ Kcal/mole	$-\Delta G_{n-1, n}^\circ (298^\circ)$ Kcal/mole	$-\Delta S_{n-1, n}^\circ (298^\circ)$ eu
0, 1	18.4	12.5	20.1
1, 2	17.2	9.71	25.1
2, 3	15.4	7.02	28.2



Table 5-4

Comparison of Relative Abundances of  $O_2^- (H_2O)_n$  Obtained From  
 This Work and Those of Moruzzi and Phelps at  
 $T = 300^\circ K$  and  $P_{H_2O} = 0.44$  torr

	This Work	M. P. *
	%	%
$O_2^-$	0	2
$O_2^- (H_2O)$	0	13
$O_2^- (H_2O)_2$	2	45
$O_2^- (H_2O)_3$	41	35
$O_2^- (H_2O)_4$	45	5
$O_2^- (H_2O)_5$	8	0

\*Reference (55)

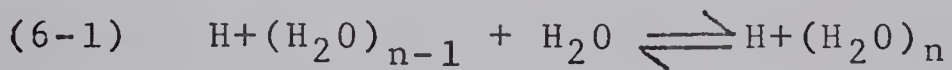


to find out the reason for this discrepancy. The Moruzzi and Phelps data shows a shift towards lower clusters and predicts a value of 2% for the relative abundance of  $O_2^-$  at 0.44 torr  $P_{H_2O}$  and 300°K, indicates that their data does not represent the actual equilibrium concentrations. One possible explanation for this is that stripping of water molecule, due to collisions outside the ion source in the accelerating region, occurred in the Moruzzi and Phelps' apparatus. Collisional induced dissociations in the region just outside of ion exit slit have been observed in this laboratory (57) and are explained in section (3-3b).



6 GAS PHASE HYDRATION OF PROTONS6.1 Introduction

The study of the gas phase hydration of proton was undertaken in this laboratory independently by two different groups on two different mass spectrometers. J. Scarborough and this author jointly studied the process (6-1)

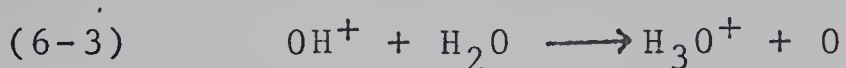
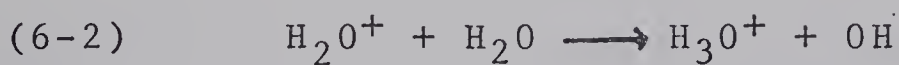


on an alpha source mass spectrometer at water partial pressures of 0.1 to .5 torr and temperatures from  $-17^{\circ}\text{C}$  to  $125^{\circ}\text{C}$ . The same process was studied by S. K. Searles and A. Zolla on another mass spectrometer, utilizing a proton beam as an ionizing medium, for the temperature range of 25 to  $600^{\circ}\text{C}$ . The reason for carrying out the two studies simultaneously was twofold: (a) the ion source of the alpha beam mass spectrometer could not be heated over  $140^{\circ}\text{C}$  and (b) since these two instruments were equipped with two entirely different types of gas handling plants, ion source, and detection systems; an extensive test of reproducibility of the data could be made.

An extensive discussion of this study has been given by S. K. Searles (35); therefore, only the results obtained by, and the points pertinent to the alpha beam mass spectrometer will be presented here.



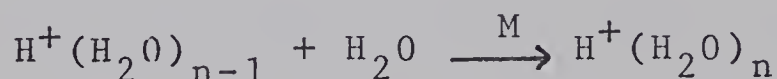
When water vapour is irradiated by some ionizing media such as electrons, protons or alpha particles; the two major primary ions produced are  $\text{H}_2\text{O}^+$  and  $\text{OH}^+$  (11). These two ions react very rapidly with water (58) (59) to yield  $\text{H}_3\text{O}^+$ .



The hydronium ion, thus produced, can undergo more reactions to yield  $\text{H}^+(\text{H}_2\text{O})_n$  according to the reactions (6-4)



(6-4)



Since the reactions (6-4) are exothermic, the third body, M, is required to deactivate the products through a "third body collision process".

## 6.2 Results and Discussions

The equilibrium constants,  $K_{n-1,n}$ , obtained with the alpha source mass spectrometer are given in figures (6-1) to (6-5). The values of the equilibrium constants for water pressures below one torr were obtained in the presence of argon as a carrier gas (total pressure of 5



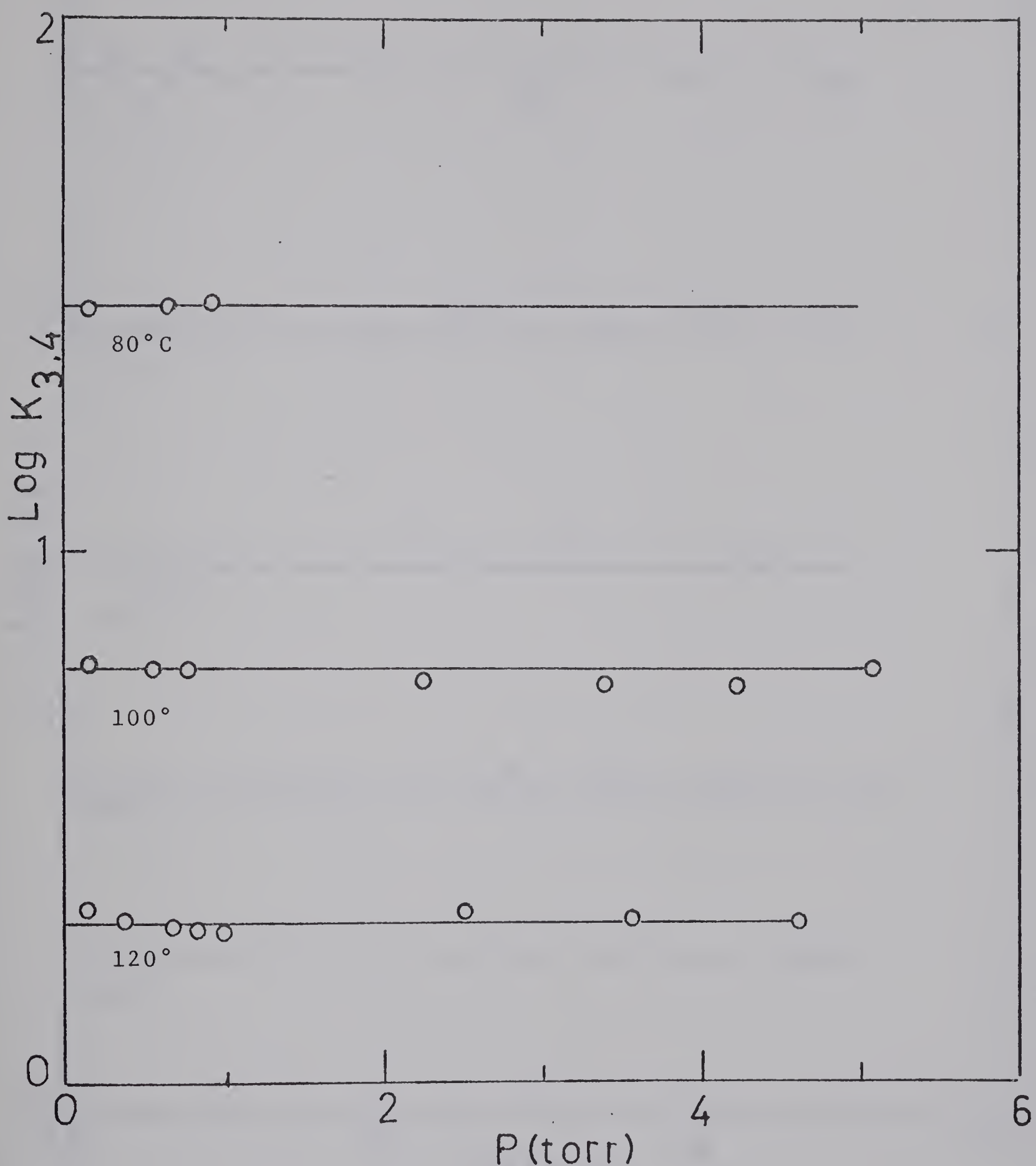


Figure 6-1: Plots of  $\log K_{3,4}$  for the Gas Phase Hydration of Proton, at Various Temperatures, Versus Pressure of  $\text{H}_2\text{O}$ .



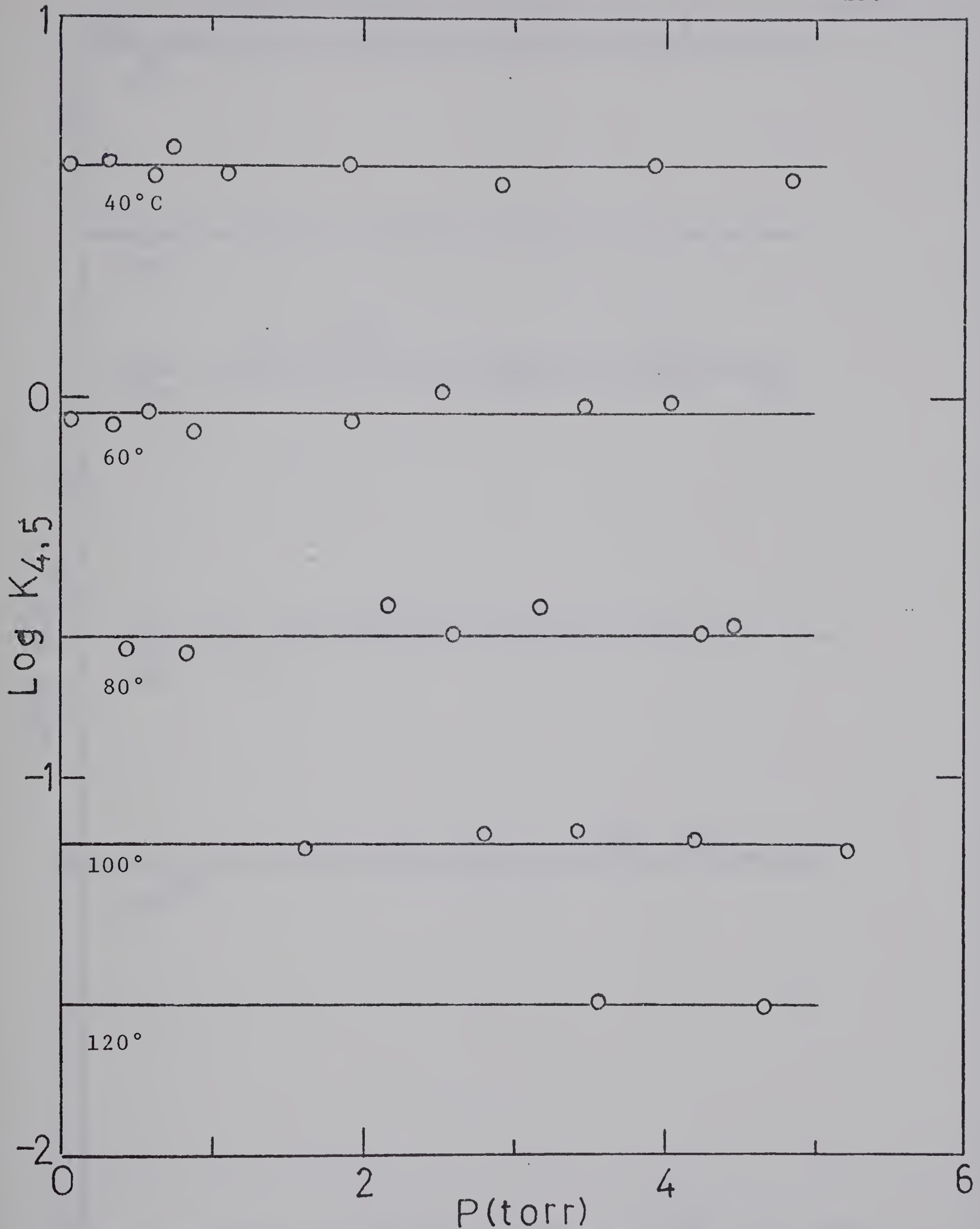


Figure 6-2: Plots of  $\log K_{4,5}$  for The Gas Phase Hydration of Proton, at Various Temperatures, Versus Pressure of  $\text{H}_2\text{O}$ .



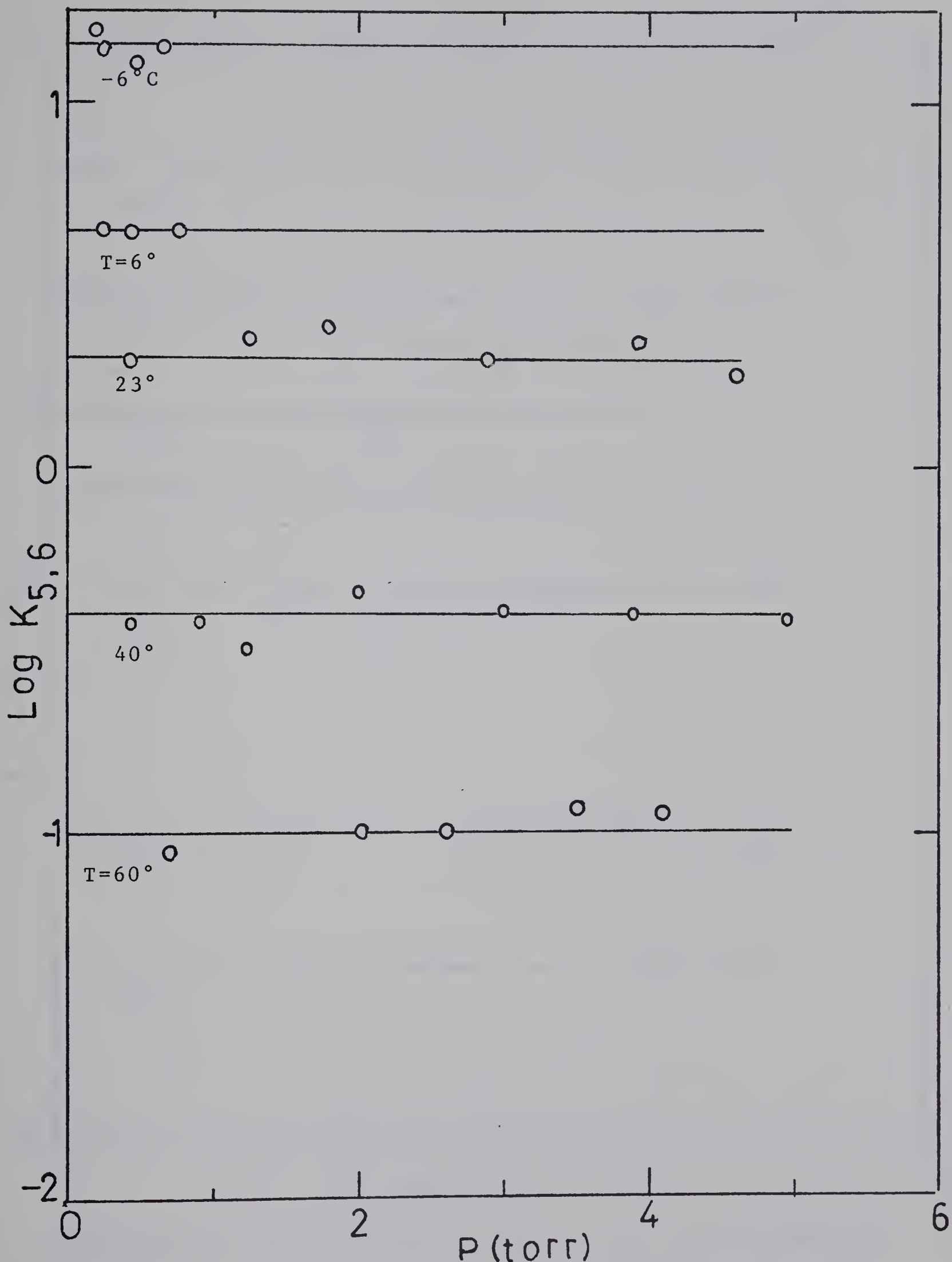


Figure 6-3: Plots of  $\text{Log } K_{5,6}$  for the Gas Phase Hydration of Proton, at Various Temperatures, Versus Pressure of  $H_2O$ .



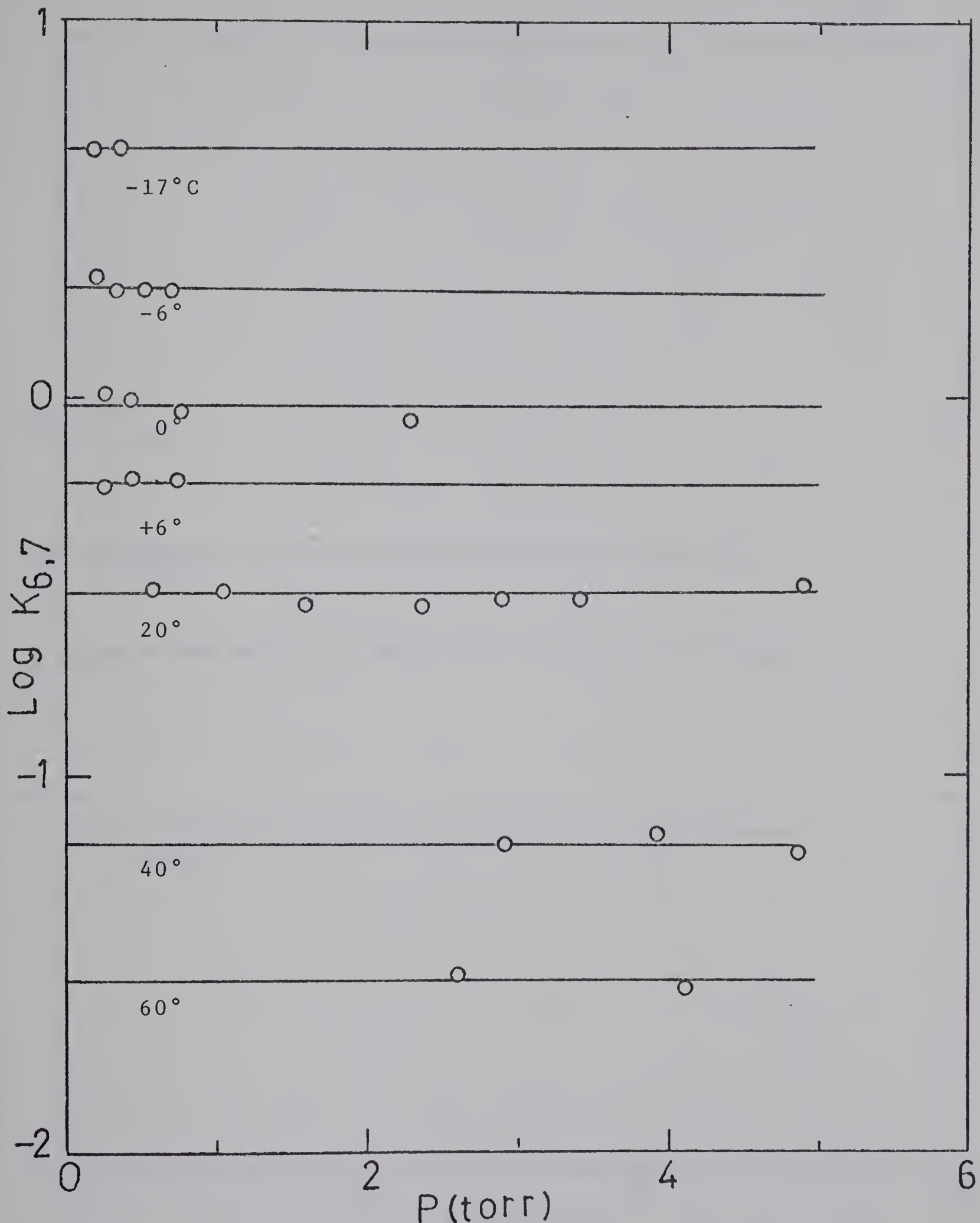


Figure 6-4: Plots of  $\text{Log } K_{6,7}$  for the Gas Phase Hydration of Proton, at Various Temperatures, Versus Pressure of  $\text{H}_2\text{O}$ .



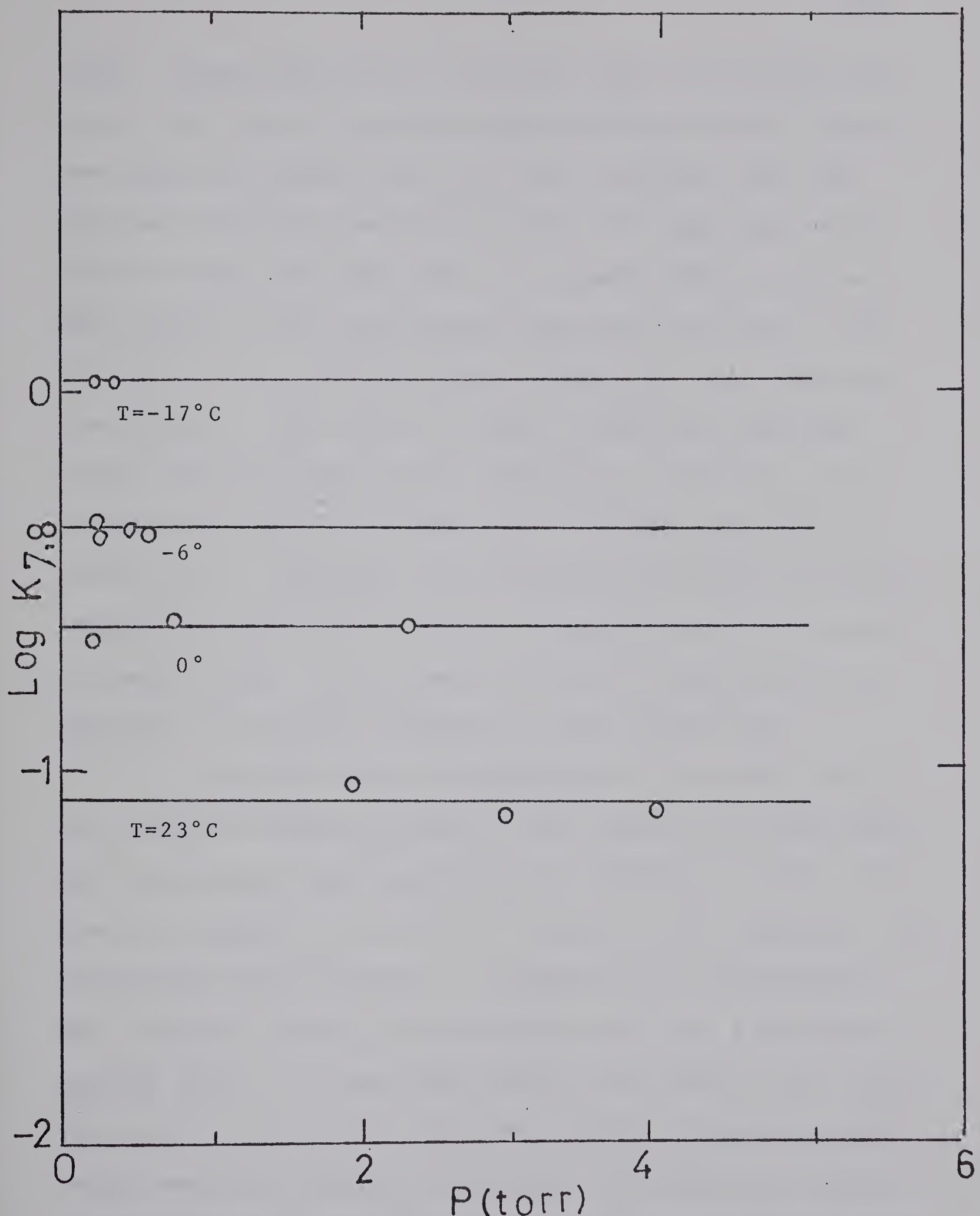


Figure 6-5: Plots of  $\text{Log } K_{7,8}$  for the Gas Phase Hydration of Proton, at Various Temperatures, Versus Pressure of  $\text{H}_2\text{O}$ .



torr). Those equilibrium constant values for water pressures over one torr were obtained with pure water vapour. The plots of figures (6-1) to (6-5) indicate that the agreement between the points taken with argon and those without argon are very good. In figure (6-6), the Van't Hoff plots of the equilibrium constants are shown. The results of S. K. Searles and A. Zolla are also shown on these plots. The values of  $\Delta H_{n-1,n}^\circ$  obtained from the slopes of Van't Hoff plots, and  $\Delta G_{n-1,n}^\circ$  and  $\Delta S_{n-1,n}^\circ$  obtained from equations (4-2) and (4-3) are summarized in table (6-1). Recently, the hydration of protons was also studied by Field (12). Field's results are also included in table (6-1). It can be seen that his results are in agreement with those obtained in this laboratory.

From the data of figure (6-6) and table (6-1), the relative concentrations of the clusters  $H^+(H_2O)_n$  have been calculated for temperatures of 300°K and 400°K. The plots of figure (6-7) show the change of the relative concentrations with pressure. The method of calculation of the relative cluster concentrations has been explained in section (4-8). As has been pointed out before (11), this data may be of interest in other fields of physical chemistry, such as radiation chemistry. The plots of figure (6-7) show that at low pressure where the low hydrates are present, the difference between the stability (free energy)



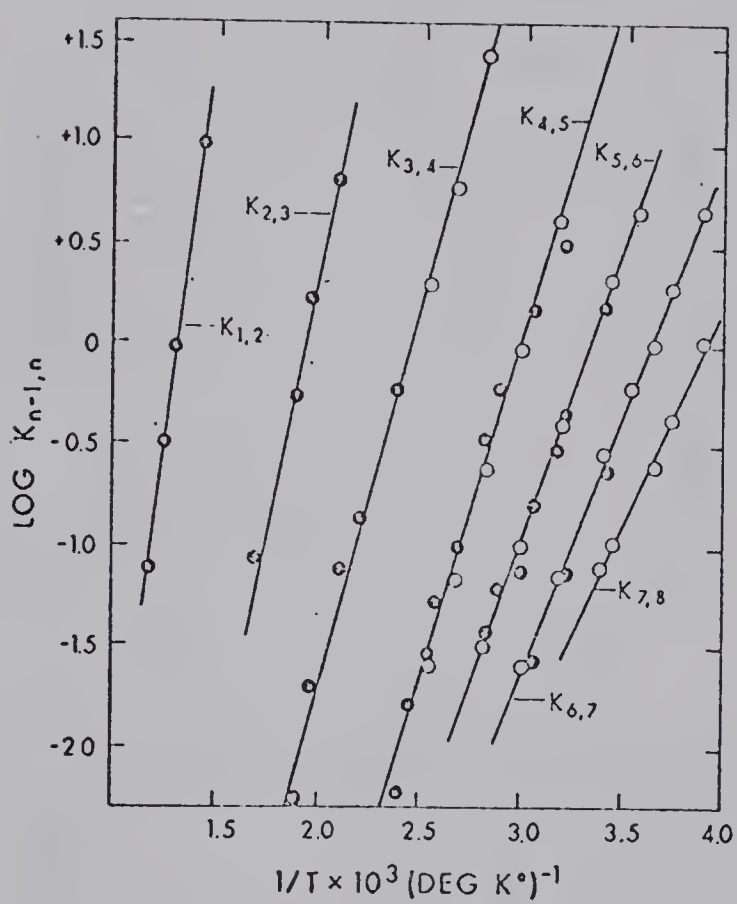


Figure 6-6: Van't Hoff-Type Plots of Equilibrium Constants,  $K_{n-1,n}$ , for the Gas Phase Hydration of Proton 0, Present work;  $\bullet$ , Proton Beam Mass Spectrometer.



Table 6-1

Values of the Thermodynamic Functions for The  
Gas Phase Hydration of Proton

n-1, n	$-\Delta H_{n-1}^{\circ}, n$ Kcal/mole			$-\Delta G_{298}^{\circ}(n-1), n$ Kcal/mole			$-\Delta S_{298}^{\circ}(n-1), n$ e.u.		
	A	B	C	A	B	C	A	B	C
0-1							33		
1-2			36						
2-3		22.3		20			29		
3-4	18.3	18.8	16.2	9.6	9.5	8.2	32		
4-5	15.7	15.3	14.8	5.6	5.5	5.2	34	33	
5-6	13.3	13.0		3.9	3.9		31	30	
6-7	11.7	11.7		2.8	2.8		30	30	
7-8	10.3			2.2			27		

A Alpha Source Mass Spectrometer Data

B Proton Beam Mass Spectrometer Data

C Field's Data (12)



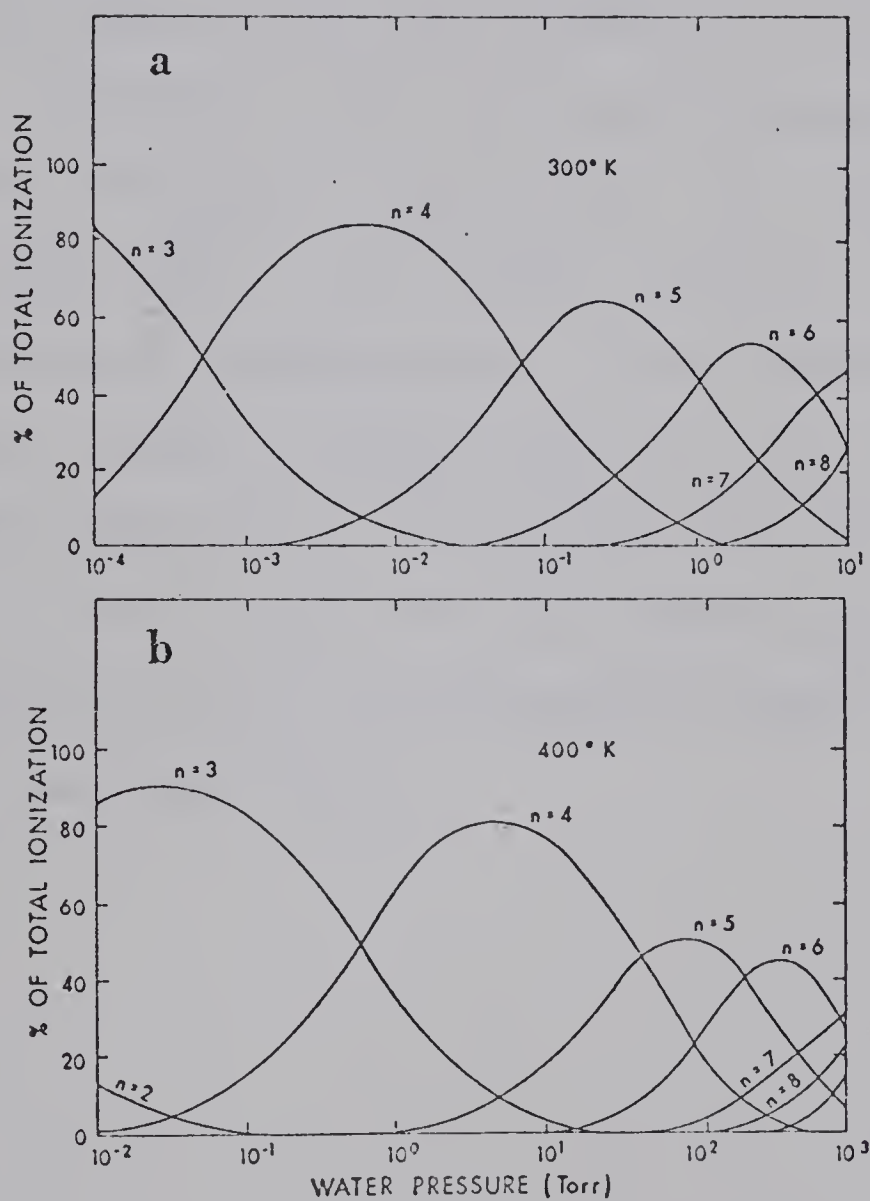


Figure 6-7: Relative Concentrations of the Cluster  $\text{H}^+(\text{H}_2\text{O})_n$ , at a)  $300^\circ\text{K}$  and b)  $400^\circ\text{K}$ , Versus Pressure of  $\text{H}_2\text{O}$ .



of the hydrates is large, thus, under these conditions the concentrations of one or two hydrates are dominant. At higher pressure where the higher hydrates become stable, differences between the free energies of the hydrate are small, and a number of hydrates are present simultaneously.

In figure (6-8) the  $\log \Delta H_{n-1,n}^\circ$  is plotted versus  $n-1,n$ . Included in this plot is the negative value of the proton affinity of water (60), -170 Kcal/mole for  $\Delta H_{0-1}^\circ$ . The  $\log \Delta H_{n-1,n}^\circ$  was chosen, so that a wide range of values could be accommodated. It is interesting to note that all values including  $\Delta H_{0,1}^\circ$  lie on a smooth curve. This suggests that step 0,1 is not too different in kind from step 1,2; 2,3; etc. Based on this observation, it has been concluded (11) that the notation  $H^+(H_2O)_n$  is more appropriate than  $H_3O^+(H_2O)_n$ .



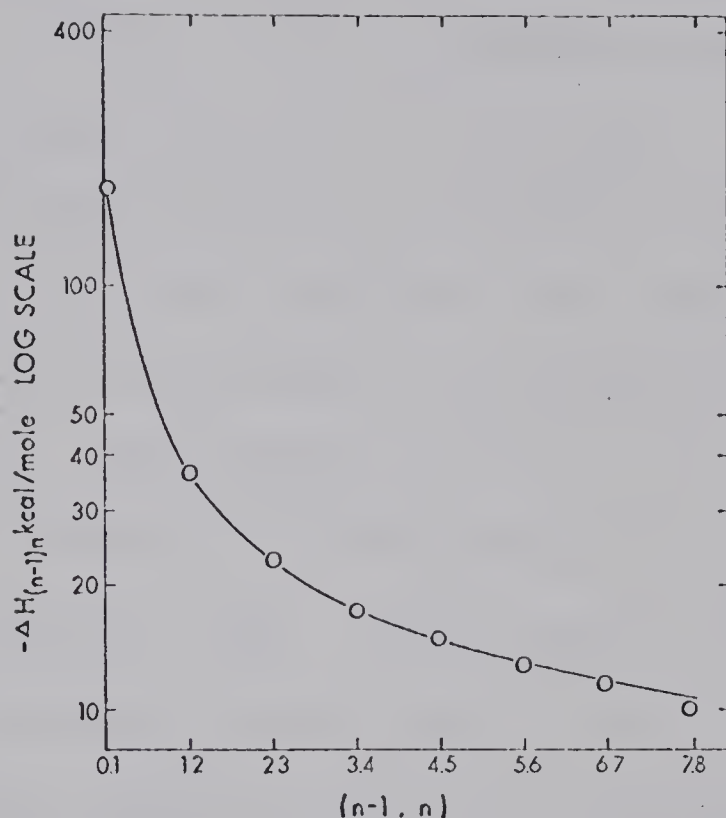


Figure 6-8: Plots of Log  $\Delta H^\circ_{n-1,n}$  Versus  $n-1, n$  for the Phase Hydration of Proton.



## 7 SUGGESTIONS FOR FURTHER RESEARCH

### 7.1 Attachment of H<sub>2</sub>O to Other Negative Ions

The study of the hydration of  $\text{NO}_2^-$  was made only at one temperature; therefore, the first suggestion would be to extend this study to other temperatures and thus determine the  $\Delta H^\circ_{n-1,n}$ ,  $\Delta G^\circ_{n-1,n}$  and  $\Delta S^\circ_{n-1,n}$ .

In addition to the ions studied in this work, there are a number of other negative ions whose attachment to water molecule is of interest in different fields of physical chemistry. One example of these ions is  $\text{CN}^-$ . Mass spectrometric studies of  $\text{CN}^-$  have been made by T. J. Herron and V. H. Dibeler (65). These authors have produced  $\text{CN}^-$  from a cyanogen halide such as  $\text{CNI}$ . The bond dissociation energy,  $D(\text{CN}-\text{I})$ , is  $67 \pm 7$  Kcal/mole (66). Therefore, the reaction (7-1)



would be exothermic by about 20 Kcal. The electron affinity of CN is higher than that of iodine by 0.4 eV (48), thus, the production of  $\text{CN}^-$  should be favored over that of  $\text{I}^-$ .

### 7.2 Competitive Solvation of Negative Ions

The mass spectrometric study of the competitive solvation of positive ions has been made in this laboratory (25), (26). The same type of study can be conducted for the negative ions. One interesting example is the



competitive solvation of halide ions by water and respective hydrogen halides. The problem may arise in accurate determination of the partial pressure of the hydrogen halide in the ion source. Hydrogen halides can be absorbed by glass, thus, a major portion of the HX added to the carrier gas, in the gas handling plant, will never reach the ion source of the mass spectrometer. One method to overcome this problem is to heat the gas handling plant and its connecting glass lines to the temperature of the ion source and assume that, after a limited period of time, the rate of absorption and desorption of HX on glass will equalize.

### 7.3 Solvation of Halide Ions by H<sub>2</sub>S

It was mentioned before, that in the study of hydration of fluoride ion, the series OD<sup>-</sup>(D<sub>2</sub>O)<sub>n</sub> was observed and was assumed to be due to the reaction (7-2)



It would be very interesting to test this assumption by the study of halide ions H<sub>2</sub>S system. In this case the corresponding reactions and their enthalpy changes are







[The bond dissociation energy,  $D(\text{HS}-\text{H})$  is 92 Kcal/mole (48) and the electron affinity of HS is 2.6 eV. Other thermochemical data are taken given in section (4-6)]. According to equations (7-5) and (7-6), the ions  $\text{HS}^-(\text{H}_2\text{S})_n$  should be the major species in the  $\text{NF}_3$ ,  $\text{H}_2\text{S}$  system and should be seen in the  $\text{CCl}_4$ ,  $\text{H}_2\text{S}$  system.



BIBLIOGRAPHY

1. H. S. W. Massey and E. H. S. Burhop, Electronic and Ionic Impact Phenomena, Oxford University Press, 1952, p. 227.
2. L. B. Loeb, Phys. Rev., 32, 81 (1928).
3. L. B. Loeb, Kinetic Theory of Gases, Third edition, Dover Publication Inc., New York (1961), p. 560.
4. E. W. McDaniel, Collision Phenomena in Ionized Gases John Wiley and Sons, Inc., New York (1964), p. 432.
5. R. J. Munson and K. Hoselitz, Proc. Roy. Soc. A-172, 43 (1939).
6. R. J. Munson and A. M. Tyndall, Proc. Roy. Soc. A-172, 28 (1939).
7. O. Luhr, Phys. Rev., 38, 1730 (1931); Phys. Rev., 44, 459 (1933).
8. H. D. Beckey, Z. Naturforsch. 15a, 822 (1960).
9. P. F. Knewstubb and T. M. Sugden Proc. Roy. Soc. A255, 520 (1960).
10. P. F. Knewstubb and A. W. Tickner, J. Chem. Phys. 38, 464, (1963).
11. P. Kebarle, S. K. Searels, A. Zolla, J. Scarborough and M. Arshadi, J. Am. Chem. Soc., 89, 6393 (1967).
12. F. H. Field, J. Am. Chem. Soc., 91, 2827 (1969).
13. A. Good, D. Durden and P. Kebarle (Submitted for publication).
14. J. H. Yang and D. C. Conway, J. Chem Phys., 40, 1729 (1964).
15. D. C. Conway, J. H. Yang, J. Chem. Phys., 43, 2900 (1965).
16. D. A. Durden, P. Kebarle and A. Good, J. Chem. Phys., 50, No. 2, 805 (1969).
17. M. Saporoschenko, Phys. Rev., 139, 351 (1965).



18. W. L. Fite, J. A. Rutherford, W. R. Snow and V. A. J. Van Lint, Disc. Farad. Soc., 33, 264 (1962).
19. R. N. Varney, J. Chem. Phys., 31, No. 5, 1314 (1959).
20. G. S. Janik and D. C. Conway, J. Phys. Chem., 71, 823 (1967).
21. D. C. Conway and L. S. Nesbitt, J. Chem. Phys., 48, 509 (1968).
22. R. E. Voshall, J. L. Pack and A. V. Phelps, J. Chem. Phys., 43, 1990 (1965).
23. S. K. Searles, P. Kebarle (Submitted for publication).
24. I. Dzidic, P. Kebarle (To be published).
25. A. M. Hogg and P. Kebarle, J. Chem. Phys., 43, 449 (1965).
26. P. Kebarle, R. N. Haynes and J. G. Collins, J. Am. Chem. Soc., 89, 5753 (1967).
27. S. C. Lind, Radiation Chemistry of Gases, Reinhold Publishing Corp. New York, 1961, p. 8.
28. H. Eyring, J. O. Hirschfelder and H. S. Taylor, J. Chem. Phys., 4, 479, 570 (1936).
29. D. P. Stevenson and D. O. Schissler, J. Chem. Phys., 29, 282 (1958).
30. K. M. Bansal and G. R. Freeman, J. Am. Chem. Soc., 90, 71, 83 (1968).
31. R. S. Narcisi and D. Bailey, J. Geophys. Res., 71, No. 15, 3687 (1965).
32. D. K. Bohme Can. J. Chem. 47, 1809 (1969).
33. R. E. Lenier and L. M. Branscomb, J. Geophys. Res. 73, 27 (1968).
34. G. J. Doyle and R. G. Caldwell, Report AD635552, Stanford Research Institute, South Pasadena, California (1966).
35. S. K. Searles, Ph. D. Thesis, University of Alberta, (1968).



36. C. E. Melton, Mass Spectrometry of Organic Ions, ed. by F. W. McLafferty, Academic Press, New York, 1963, p. 164.
37. R. M. Reese and V. Dibeler, *J. Chem. Phys.*, 24, 1175 (1955).
38. J. L. Pack and A. V. Phelps *J. Chem. Phys.* 44, 1870 (1966).
39. L. B. Loeb, Basic Processes of Gaseous Electronics, University of California Press, Berkley, 1961, chapter 2.
40. H. E. Stanton, W. A. Chupka and M. G. Inghram, *Rev. Sci. Instr.*, 27, 109 (1956).
41. J. M. Beynon, Mass Spectrometry and its Applications to Organic Chemistry, Elsevier Publishing Co., New York, 1960, p. 212.
42. F. J. Carrick, *Phil. Mag.*, 9, 131 (1930); 10, 76 (1930).
43. J. S. Muirhead-Gould and K. J. Laidler *Trans. Farad. Soc.*, 63, 944 (1967).
44. A. E. Sherwood and J. M. Prausnitz, *J. Chem. Phys.*, 41, 429 (1964).
45. D. Ter Haar, W. M. Nicol and P. Barnett, *Physica* 22, 911 (1956).
46. C. F. Bell and K. A. K. Lott, Modern Approaches to Inorganic Chemistry, Butterworth, London, 1961, p. 87.
47. B. S. Gourary and F. J. Adrian *Solid State Phys.*, 10, 127 (1960).
48. V. I. Vedeneyev, L. V. Gurvich, V. N. Kondratyev, V. A. Medvedev and Ye. L. Frankevich, Bond Energies, Ionization Potentials and Electron Affinities, Translated from Russian, Edward Arnold, London, 1962.
49. S. Glasstone, Textbook of Physical Chemistry, second edition, D. Van Nostrand Co., Inc., New York, 1946, Chapter XI.
50. E. A. Moelwyn-Hughes, Physical Chemistry, second edition Pergamon Press, Oxford, 1961, p. 509.



51. W. J. Moore, Physical Chemistry, third edition, Prentice-Hall, Inc., Englewood Cliffs, N. J., 1964, p. 605.
52. H. S. Taylor and S. Glasstone, A Treatise on Physical Chemistry, Vol. I, D. Van Nostrand Co., Inc., New York, 1947, p. 602.
53. L. M. Branscomb, Phys. Rev., 148, 11, (1966).
54. S. Golub and B. Steiner, J. Chem. Phys., 49, 5191 (1968).
55. J. L. Moruzzi and A. V. Phelps, J. Chem. Phys., 45, 4617, (1966).
56. P. Kebarle, M. Arshadi, and J. Scarborough, J. Chem. Phys., 49, 817, (1968).
57. J. G. Collins, Ph. D. Thesis, University of Alberta (1967).
58. F. W. Lampe, F. W. Field and J. L. Franklin, J. Am. Chem. Soc., 79, 6132, (1957).
59. M. M. Mann, A. Hustrulid and J. T. Tate, Phys. Rev., 58, 340, (1940).
60. M. S. Munson, J. Am. Chem. Soc., 87, 2332, (1965).
61. L. Pauling, The Nature of the Chemical Bond, Cornell University Press Ithaca, N. Y., 1948.
62. V. M. Goldschmidt Skrifter Norske Videnskaps-Akad. Oslo Mat. Naturv. Kl., 8, 1 (1926).
63. M. J. Blandamer and M. C. R. Symons, J. Phys. Chem., 67, 1304 (1963).
64. D. F. C. Morris, Structure and Bonding, 4, 63, (1968).
65. J. T. Herron and V. H. Dibeler, J. Am. Chem. Soc., 82, 1555 (1960).
66. G. Lord and A. A. Woolf, J. Chem. Soc., 2546, (1954).
67. D. A. Durden, Ph. D. Thesis, University of Alberta (1969).
68. S. Dushman, Scientific Foundation of Vacuum Technique, John Wiley and Sons, Inc., New York, 1949, p. 92.
69. A. Guthrie, Vacuum Technology, John Wiley and Sons, Inc., New York, 1963, p. 58.



70. T. C. Weddington, Trans. Farad. Soc., 62, 1482 (1966).
71. R. H. Stokes, J. Am. Chem. Soc. 86, 979 (1964).
72. D. R. Rosseinsky, Chem. Rev., 65, 467 (1955).
73. W. M. Latimer, K. S. Pitzer and C. M. Slanski, J. Chem. Phys., 7, 108 (1939).
74. E. T. Verwey, Chem. Rec. Trav. Chim., 61, 127 (1942).
75. J. E. B. Randles, Trans. Farad Soc., 52, 1573 (1956).
76. J. E. Desnoyers, "Hydration Effects and Thermodynamic Properties of ions", Modern Aspect of Electrochemistry Vol. 5, Ed. by J. O. M. Bockris.





**B29930**